

AD-754 792

RESEARCH ON MOLECULAR LASERS

George J. Wolga, et al

Cornell University

Prepared for:

Office of Naval Research  
Advanced Research Projects Agency

30 September 1972

DISTRIBUTED BY:

**NTIS**

National Technical Information Service  
U. S. DEPARTMENT OF COMMERCE  
5285 Port Royal Road, Springfield Va. 22151

# DISCLAIMER NOTICE

THIS DOCUMENT IS THE BEST  
QUALITY AVAILABLE.

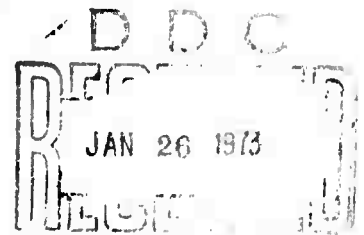
COPY FURNISHED CONTAINED  
A SIGNIFICANT NUMBER OF  
PAGES WHICH DO NOT  
REPRODUCE LEGIBLY.

AD754792

# LABORATORY OF PLASMA STUDIES



Reproduced by  
**NATIONAL TECHNICAL  
INFORMATION SERVICE**  
U S Department of Commerce  
Springfield VA 22151



**CORNELL UNIVERSITY**  
ITHACA, NEW YORK

15

Unclassified

Security Classification

DOCUMENT CONTROL DATA - R & D

(Security classification of title, body of abstract and indexing annotation must be entered when the overall report is classified)

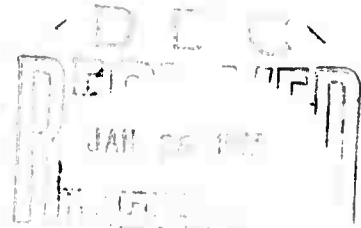
1. ORIGINATING ACTIVITY (Corporate author)  Cornell University Ithaca, NY 14850		2a. REPORT SECURITY CLASSIFICATION  Unclassified	
		2b. GROUP NA	
3. REPORT TITLE  Study of Molecular Lasers			
4. DESCRIPTIVE NOTES (Type of report and, inclusive dates) Annual Report - 1972			
5. AUTHOR(S) (First name, middle initial, last name)  George J. Wolga                      Ross A. McFarlane                      T. A. Cool Simon H. Bauer                      Donald Turcotte			
6. REPORT DATE September 30, 1972		7a. TOTAL NO. OF PAGES 148	7b. NO. OF REFS 2
8a. CONTRACT OR GRANT NO. N00014-67-A-0077-0006		9a. ORIGINATOR'S REPORT NUMBER(S) NA	
b. PROJECT NO.		9b. OTHER REPORT NO(S) (Any other numbers that may be assigned this report) NA	
c.			
d.			
10. DISTRIBUTION STATEMENT			
11. SUPPLEMENTARY NOTES		12. SPONSORING MILITARY ACTIVITY Office of Naval Research	
13. ABSTRACT Research concerning molecular and chemical lasers was conducted in the following areas:			
<ol style="list-style-type: none"> <li>1. Measurement of V→V and V→R,T rates among hydrogen halide molecules and the temperature dependence of the energy transfer rates previously determined for HF, DF, HF/CO<sub>2</sub> DF/CO<sub>2</sub> systems.</li> <li>2. Studies on rapid subsonic gas mixing with emphasis on turbulence to enhance rapid mixing,</li> <li>3. Vibrational relaxation studies of CO<sub>2</sub>(00<sup>0</sup>1) in the pressure range 1-100 atm.</li> <li>4. TEA HBr chemical laser studies,</li> <li>5. EPR study of reaction rates in the NO + F<sub>2</sub> dissociative reaction,</li> <li>6. Chemical laser studies of the reaction of atomic oxygen and acetylene including the determination of V→V energy transfer probabilities,</li> <li>7. Studies of the partition of exothermicity in the CS<sub>2</sub>-O<sub>2</sub> chemical laser system,</li> <li>8. Experimental study of the relaxation of CO<sub>2</sub>(020) and HF(v = 1) by collisions with H and F atoms.</li> </ol>			

**RESEARCH ON MOLECULAR LASERS**

**Annual Report - November 1, 1972**

**Cornell University**

**Ithaca, New York 14850**



**Sponsored by:**

**Advanced Research Projects Agency**

**ARPA Order No. 660**

KEY WORDS	LINK A		LINK B		LINK C	
	ROLE	WT	ROLE	WT	ROLE	WT
Molecular Lasers						
Chemical Lasers						
Vibrational Relaxation						
Energy Transfer						
Rapid Gas Mixing						
Chemical Reaction Rates						
Vibrational Energy Transfer						

## INDEX

	<u>Page</u>
Report Summary	1
I. Vibrational Energy Transfer and De-excitation in the HF-HCl, HF-HBr, HF-HI and HF-DF Systems	1
II. Rapid Gas Mixing Studies	20
Laminar Measurements	22
Turbulent Measurements	24
III. Vibrational Relaxation	32
A. High Pressure Relaxation in CO <sub>2</sub> (00°1)	32
1. HBr Chemical Laser Studies	32
B. Vibrational Relaxation and Chemical Reactions	33
IV. Chemical Laser Studies and Rate Determination	36
A. EPR Study of the NO + F <sub>2</sub> Reaction	36
B. Vibrational Excitation in the CS <sub>2</sub> -O <sub>2</sub> Laser Reaction	50
C. Studies of the O-C <sub>2</sub> H <sub>2</sub> Reaction	100
V. Molecular Relaxation via Atomic Collisions	141
A. Atomic Relaxation of HF(v = 1)	141
B. Atomic Relaxation of CO <sub>2</sub> (0n0)	147
C. Atomic Relaxation of CO <sub>2</sub> (00°1)	147

ANNUAL REPORT

Reporting Period

1 October 1971 - 30 September 1972

1. ARPA Order	660
2. Program Code Number	0173-7-006252
3. Name of Contractor	Cornell University
4. Effective Date of Contract	1 October 1968
5. Contract Expiration Date	30 September 1972
6. Amount of Contract for Current Period	\$187,500.
7. Contract Number	N00014-67-A-0077-0006
8. Principal Investigator	Prof. G. J. Wolga
9. Telephone Number	(607) 256-3962
10. Project Scientists	Prof. S. H. Bauer (607) 256-4028  Prof. T. A. Cool (607) 256-3512  Prof. R. A. McFarlane (607) 256-4075  Prof. D. L. Turcotte (607) 256-4026
11. Title of Work	RESEARCH ON MOLECULAR LASERS

Sponsored by

ADVANCED RESEARCH PROJECTS AGENCY

ARPA Order No. 660

The views and conclusions contained in this document are those of the authors and should not be interpreted as necessarily representing the official policies, either expressed or implied, of the Advanced Research Projects Agency or the U. S. Government.

## REPORT SUMMARY

During the period 1 October, 1971 - 30 September, 1972, the ongoing program concentrated on a number of research areas that were felt to be of significant and basic importance to the successful development of chemical and molecular laser technology. The principal areas of effort were: measurement of  $V \rightarrow V$  and  $V \rightarrow R,T$  rates among hydrogen halide molecules and the temperature dependence of the energy transfer rates previously determined for the HF, DF, HF/CO<sub>2</sub>, DF/CO<sub>2</sub> systems; studies in rapid subsonic mixing with emphasis on the use of turbulence to enhance rapid mixing; vibrational relaxation studies of CO<sub>2</sub>(00°1) in the pressure range 1-100 atm.; TEA HBr chemical laser studies; EPR study of reaction rates in the NO + F<sub>2</sub> dissociative reaction; chemical laser studies of the reaction of atomic oxygen and acetylene including the determination of V-V energy transfer probabilities between CO molecules; studies of the partition of exothermicity in the CS<sub>2</sub>-O<sub>2</sub> chemical laser system; experimental study of the relaxation of CO<sub>2</sub>(020) and HF(v = 1) by collisions with H and F atoms.

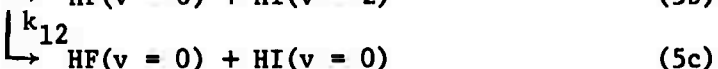
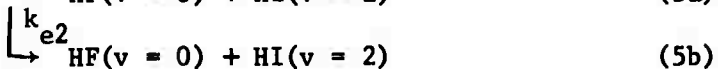
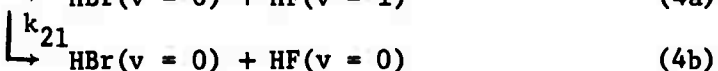
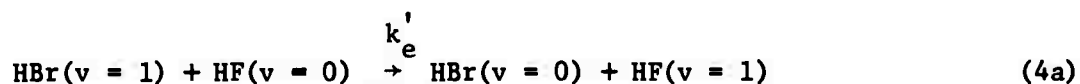
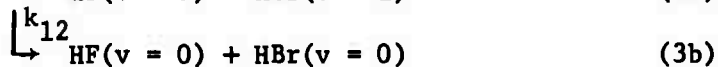
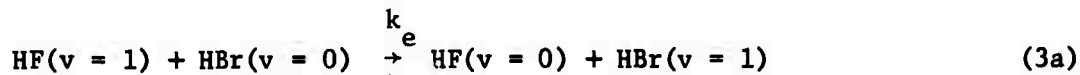
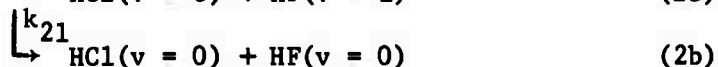
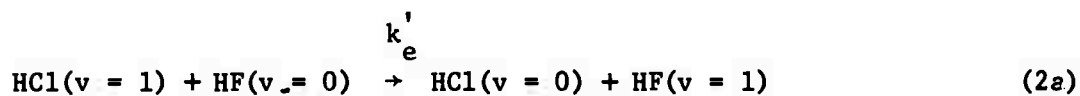
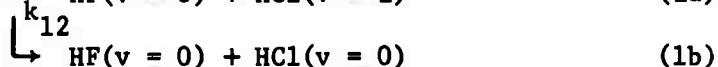
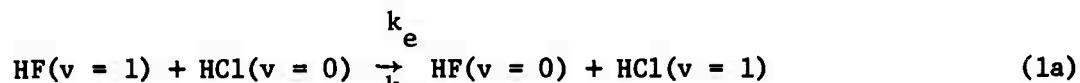
In all cases the primary method of study was the execution of laboratory experiments designed to provide quantitative results followed by appropriate integration with theory. A detailed statement of results and state of progress will be found in Sections 1 through 5 of this report.

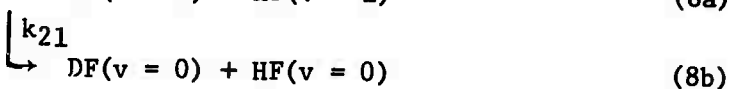
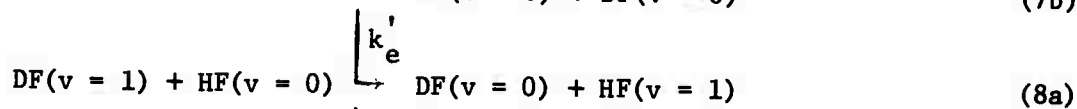
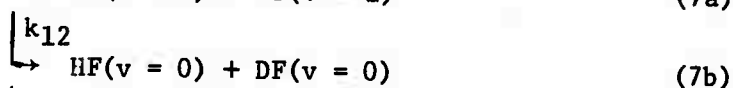
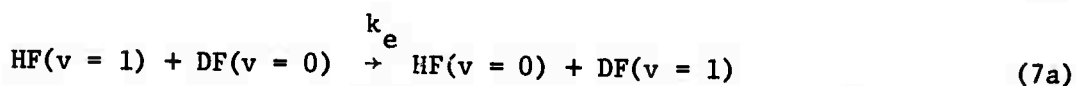
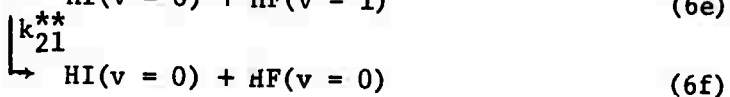
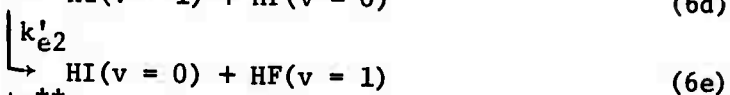
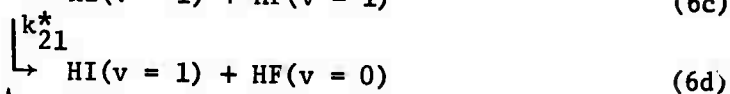
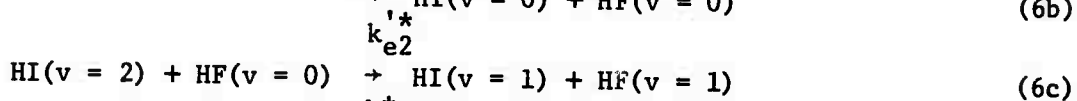
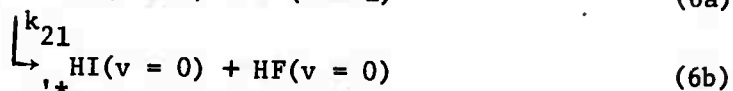
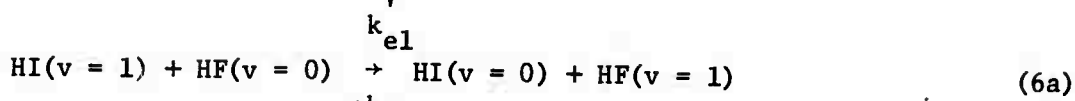
This research is motivated by the mutual interest of the sponsor and contractor in chemical lasers as efficient sources of coherent optical emission. Emphasis is placed upon the development of new and efficient lasers operating at wavelengths not previously available, and upon the

basic processes that underlie all molecular lasers. The processes quantitatively studied included vibrational energy exchange and relaxation processes, rates of chemical reactions, vibrational distributions resulting from important chemical laser reactions and rapid gas mixing processes.

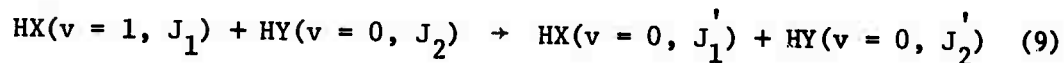
I. "Vibrational Energy Transfer and De-excitation in the HF-HCl, HF-HBr, HF-HI and HF-DF Systems" (T. A. Cool)

Several reaction schemes employed in present cw HF chemical lasers lead to the formation of vibrationally excited HF in the presence of HCl, HBr, HI and DF. We have measured several key rates for energy transfer and deactivation for such chemical laser systems at temperatures of 300 and 350°K. The large rates for these processes can be attributed to energy transfer to rotation under the influence of strong attractive (hydrogen bonding) intermolecular forces. The energy transfer processes studied during the past year are given below and the rate constants are summarized in Table I.





It is believed that all of the above processes involve large changes in rotational quantum number. This is suggested by the large values of the rate constants despite the generally large vibrational energy defects for the above processes. Moreover, it is apparent from the data that the  $k_e'$  values are too large to be explained unless energy transfer to rotation is important in minimizing the magnitude of the overall internal energy defect. Thus, the above rates are actually an aggregation of vibration rotation transitions, e.g.,



where, in general,  $J_1' \neq J_1 \pm 1$  and  $J_2' \neq J_2 \pm 1$ .

A paper concerning the above work will be presented at a forthcoming ACS meeting in January; additional work completed during the current contract year has been published [J. Chem. Phys., 56, 5863-5878 (1972)] and is included in the Appendix to this report.

TABLE I: MEASURED RATES

<u>System</u>	<u>Temperature</u> (°K)	<u>Rate Constants</u> ( $10^4 \text{ sec}^{-1} \text{ torr}^{-1}$ )
HF-HCl	300°K	$k_e + k_{12} = 2.9 \pm 0.3$
		$k'_e + k_{21} = 2.15 \pm 0.3$
	350°K	$k_e + k_{12} = 2.1 \pm 0.3$
		$k'_e + k_{21} = 1.55 \pm 0.1$
HF-HBr	300°K	$k_e + k_{12} = 0.8 \pm 0.1$
		$k'_e + k_{21} = 1.5 \pm 0.2$
	350°K	$k_e + k_{12} = 0.25 \pm 0.05$
		$k'_e + k_{21} = 1.1 \pm 0.2$
HF-HI	300°K	$k_{e1} + k_{e2} + k_{12} = 0.55 \pm .05$
		$k'_{e1} + k_{21} \lesssim 1.9 \pm .2$
	350°K	$k_{e1} + k_{e2} + k_{12} = 0.3 \pm 0.05$
		$k'_{e1} + k_{21} \lesssim 1.4 \pm 0.2$
HF-DF	300°K	$k_e + k_{12} = 13.6 \pm 0.4$
		$k'_e + k_{21} = 4.7 \pm 0.3$
	350°K	$k_e + k_{12} = 9.8 \pm 0.3$
		$k'_e + k_{21} = 3.4 \pm 0.4$

# Vibrational Energy Transfer and De-excitation in the HF, DF, HF-CO<sub>2</sub>, and DF-CO<sub>2</sub> Systems\*

RONALD R. STEPHENS† AND TERRILL A. COOL

Department of Thermal Engineering and Laboratory of Plasma Studies, Cornell University, Ithaca, New York 14850

(Received 28 December 1971)

The laser excited fluorescence method has been employed to determine the key rate constants for energy transfer and deactivation processes in the HF, DF, HF-CO<sub>2</sub>, and DF-CO<sub>2</sub> chemical laser systems at a temperature of 350°K. The self-deactivation rates for HF( $v=1$ ) and DF( $v=1$ ) molecules by ground state molecules were found to be  $k_{HF-HF} = 5.25 \pm 0.30 \times 10^4 \text{ sec}^{-1} \cdot \text{torr}^{-1}$  and  $k_{DF-DF} = 2.0 \pm 0.2 \times 10^4 \text{ sec}^{-1} \cdot \text{torr}^{-1}$ , respectively. The measured rates of  $V \rightarrow V$  transfer from HF( $v=1$ ) and DF( $v=1$ ) to the CO<sub>2</sub>(00<sup>0</sup>1) state were  $k_{HF-CO_2} = 3.7 \pm 0.3 \times 10^4 \text{ sec}^{-1} \cdot \text{torr}^{-1}$  and  $k_{DF-CO_2} = 17.5 \pm 2.5 \times 10^4 \text{ sec}^{-1} \cdot \text{torr}^{-1}$ . The respective deactivation rates of CO<sub>2</sub>(00<sup>0</sup>1) by ground state HF and DF were determined to be  $k_{CO_2-HF} = 3.6 \pm 0.3 \times 10^4 \text{ sec}^{-1} \cdot \text{torr}^{-1}$  and  $k_{CO_2-DF} = 1.9 \pm 0.4 \times 10^4 \text{ sec}^{-1} \cdot \text{torr}^{-1}$ . The large rates for these processes can be attributed to energy transfer to rotation under the influence of a sizable attractive (hydrogen bonded) intermolecular potential well and enhanced repulsion at close range.

## I. INTRODUCTION

Much progress has been achieved recently in the development of continuous-wave (cw) chemical lasers despite a serious lack of understanding of the mechanisms of those vibrational energy transfer processes which play major roles in chemical laser operation.<sup>1-5</sup> Present HF and DF cw chemical lasers have operated under conditions of partial inversion because the rate of redistribution of vibrational energy exceeds the combined rate at which gas mixing and chemical reaction proceed. Under such conditions the antecedent excitation process to stimulated emission from a given molecule is more likely to be vibrational energy transfer than direct specific excitation by chemical reaction. In the DF-CO<sub>2</sub> and HF-CO<sub>2</sub> "transfer" chemical lasers, vibrational energy transfer provides a means for the nonthermal energy release of chemical reaction to be effectively utilized as laser output from totally inverted CO<sub>2</sub>.<sup>7</sup>

Prior to the completion of the present work, reliable data were available for the self-deactivation of HF as reported by Airey and Fried,<sup>8</sup> and more recently by Solomon *et al.*<sup>9</sup> and Bott and Cohen.<sup>10</sup> No data were available, however, concerning the rate of vibrational deactivation of DF or the rates for the important processes by which vibrational energy is transferred from HF and DF to the CO<sub>2</sub>(00<sup>0</sup>1) upper laser level. Moreover, the rates for the vibrational deactivation of CO<sub>2</sub>(00<sup>0</sup>1) molecules by collisions with HF and DF molecules were unknown although the results of concurrent rate measurements are now available.<sup>11</sup>

We have used the laser excited fluorescence method<sup>12</sup> to determine the rate constants for these key processes at 350°K, a typical temperature for chemical laser operation. The experimental results for HF and DF vibrational deactivation exhibit good qualitative agreement with the vibration-rotation theory of Shin, when the effects of strong attractive interactions are considered.<sup>13a,13b</sup>

The rates of vibrational energy transfer from HF and DF to CO<sub>2</sub> are too large to be accounted for with present approximate theories. Interpretation of the results presented here suggests that the magnitude of these rates may be explained in terms of a hydrogen bonded attractive intermolecular potential well for HF-CO<sub>2</sub> and DF-CO<sub>2</sub> collision pairs which leads to enhanced repulsion at close ranges. A successful theory must necessarily allow a major portion of the difference in vibrational energy between initial and final states to be taken up as rotational motion of the collision partners.

The previously measured rate of vibration to vibration ( $V \rightarrow V$ ) transfer between D<sub>2</sub>( $v=1$ ) and CO<sub>2</sub>(00<sup>0</sup>1) states<sup>12</sup> is shown to be satisfactorily described when the vibrational energy resonance defect is converted into rotational motion of D<sub>2</sub> under the interaction of the quadrupole moment of deuterium and the asymmetric-stretching transition dipole moment of CO<sub>2</sub>.

Deactivation rates for the CO<sub>2</sub>(00<sup>0</sup>1) vibrational state by HF and DF are fast and appear to exhibit the effects of a strong attractive interaction and vibration-rotation energy transfer.

## II. EXPERIMENTAL APPARATUS AND TECHNIQUES

### A. Laser Source and Absorption Cell

The small scale transverse flow cw chemical laser and the heated absorption cell used for the present measurements have been described elsewhere.<sup>14</sup> Laser operation was based upon the continuous mixing of F atoms and F<sub>2</sub> with H<sub>2</sub> and D<sub>2</sub>.<sup>15</sup> The chopper modulated output of this device consisted of triangular pulses of 4  $\mu\text{sec}$  FWHM with a repetition frequency that was variable between 400 and 2500 Hz. The total pulse energy was typically 4  $\mu\text{J}$ ; 50% of the pulse energy was present in the 1 $\rightarrow$ 0 band transitions. The standard deviation in pulse height was less than 5%; the cw laser output was

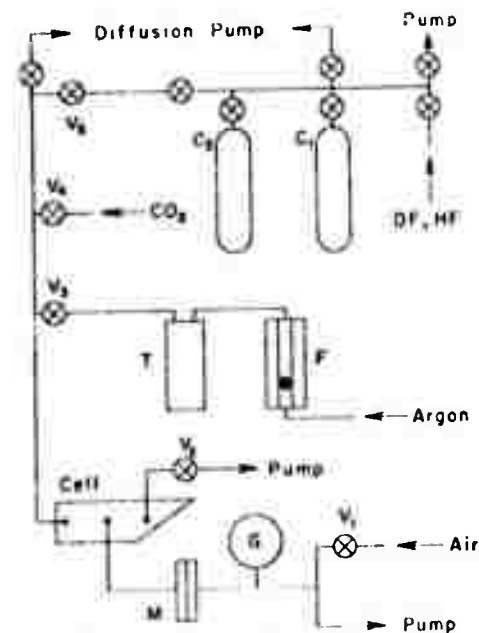


Fig. 1. Schematic diagram of gas handling apparatus.

stable to 1 part in 20 in the 2 min intervals during which fluorescence data were recorded.

A fixed cell temperature of  $350 \pm 2^\circ\text{K}$  was chosen for all of the work reported here. At the partial pressures of HF and DF used (0.05 to 1.0 torr) the dimer concentrations in HF and DF are less than 5 ppm in equilibrium at this temperature.<sup>16</sup> The cell temperature was monitored with a stainless steel jacketed thermocouple placed in direct contact with the gas within the absorption cell. The thermocouple junction was located near the center of the detector field of view about 2.5 mm outside of the path of the laser beam and about 1 mm away from the nearest wall surface.

Cell pressures were measured with a 0–10 torr MKS capacitance manometer which was accurate to within 0.1%. The calibration of the manometer electronics package supplied by the manufacturer was confirmed with a digital voltmeter capable of an accuracy of 1 part in  $10^5$ . The total cell pressure was always greater than 10 torr to prevent excessive diffusion of vibrationally excited species to the cell walls.

The gas sample was mixed and preheated before entering the heated cell. This was accomplished by injecting room temperature HF (DF) and  $\text{CO}_2$  through needle valves into a heated argon flow. The combined flow passed along a 1 m length of heated stainless steel tube of 4 mm bore with a mean residence time exceeding 1.5 sec to provide adequate mixing and equilibration before entering the cell. The heated cell was designed to provide a laminar flow without recirculation or separation in the cell region within the detector field of view. Typical gas flow rates through the cell were 0.020 mM/sec. A mean residence time within the cell was 0.2 sec. Mean cell flow velocities were 20 cm/sec.

These flow rates were sufficient to minimize the effects of surface reactions in causing adsorption or contamination of the HF or DF gas samples at the cell pressures and temperatures employed in these studies. The flow velocities were low enough, however, to avoid convective effects which would lead to an apparent shortening of the fluorescence lifetime because of the sweeping of excited molecules outside of the detector field of view.

The field of view of the detector included a sample region extending approximately 2 cm along the laser optical axis from the beam entrance window (most of the signal originated from the region nearest the entrance window). Narrow band interference filters were placed between the detector and cell to eliminate the scattered *P*-branch HF or DF laser radiation. Filters for DF with a peak transmission of 60% for a pass band located between the 1% transmission limits of 3.228 and 3.423 microns were used; for HF, filters with a peak transmission of 75% at 2.47  $\mu$  and 1% transmission limits at 2.27 and 2.64 microns were used. These filters passed most of the fluorescence on the *R* branches for the ( $v=1 \rightarrow 0$ ) HF and DF bands. Fluorescence from the  $\text{CO}_2(00^01)$  level was sampled through filters with 75% peak transmission at 4.3  $\mu$  and a FWHM of 0.4  $\mu$ .

The absorbed laser pulse energies were about three orders of magnitude below the values reported by other investigators in single pulse experiments.<sup>8,17</sup> The fraction of HF (DF) molecules excited did not exceed 0.01 and thus no special precautions were necessary to prevent excessive sample heating or excitation of the second vibrational level of HF (DF) by the laser pulses.

### B. Gas Handling and Impurities

The present gas handling system shown schematically in Fig. 1 was similar to that employed by Airey and Fried.<sup>8</sup> Those portions of the system exposed to HF were of stainless steel (except the aluminum absorption cell) and were carefully passivated to insure reproducible results. The absorption cell and HF handling system were exposed to 100 torr of HF for 24 h. The distillation cylinders ( $C_1$  and  $C_2$ ) were additionally exposed to 900 torr of HF for one week. The entire system (including argon and  $\text{CO}_2$  handling portions) was pumped down to well below  $10^{-3}$  torr and baked out at  $90^\circ\text{C}$  for several days. After this the leak rate at room temperature for the entire system of 1.5 liter volume was not detectable (less than  $10^{-3}$  torr/h). A leak rate of  $5 \times 10^{-3}$  torr/h was measured for the 0.1 liter volume absorption cell and connecting lines.

The absorption cell and connecting lines were then brought up to the operating temperature of  $350^\circ\text{K}$  and a flow of 10 torr argon and 1 torr of HF was maintained for several hours. This resulted in an increased outgassing rate which stabilized at a value of about 0.01 torr/min. No further significant change from this out-

gassing rate was observed in the entire series of experiments on HF. When all HF data were recorded, the system was prepared again according to the above procedures before any DF data were taken; similar leak/outgassing rates were measured for DF.

The major impurities (in parts per million) of the gases used in this study were as follows: argon: Matheson UHP ( $O_2 < 2$ ,  $N_2 < 4$ ,  $CO_2 < 1$ ,  $H_2O < 3$ );  $CO_2$ : Air Products Research Grade ( $O_2 + N_2 = 10$ ,  $CO < 10$ ,  $CH_4 = 1.4$ ,  $H_2O < 1.5$ ); HF: Air Products CP Grade, typical analysis ( $H_2SiF_6 = 30$ ,  $SO_2 = 40$ ,  $H_2 = 300$ ); DF: Matheson CP grade, typical analysis (98% minimum purity,  $HF < 2\%$ ). The HF and DF as actually supplied contained about 20%  $H_2$  and  $D_2$ , respectively.

Additional purification of gases was accomplished as follows. A dry-ice cold trap (see Fig. 1) was employed in the argon flow to minimize the water vapor impurity. The HF and DF were purified to remove  $H_2$  ( $D_2$ ) and  $H_2O$  ( $D_2O$ ) according to the method of Airey and Fried.<sup>8</sup> With this procedure a 5 liter sample of HF(DF) gas was admitted to the distillation cylinder ( $C_1$  of Fig. 1) and was solidified at 77°K. Gaseous  $H_2$  ( $D_2$ ) was then removed by pumping the distillation cylinder to below 0.010 torr. The cylinder was then allowed to warm to 195°K and a trap to trap distillation between cylinder  $C_1$  and a second cylinder  $C_2$  cooled to 77°K was performed at least twice before data were taken. In each stage of the distillation the last 5% of the original sample was discarded; the empty cylinder was baked out under vacuum at 90°C for 24 h before the next distillation. No detectable difference was observed between fluorescence traces taken after six distillations and those taken after two distillations.

The procedure used for establishing a given absorption cell gas composition was as follows. First the argon flow rate was set to give the desired argon cell pressure (usually 10 torr) as indicated by the capacitance manometer M. Under these conditions choked flow existed through both valves  $V_2$  and  $V_3$ ; the pressure ratio across these valves always exceeded 10:1 and 15:1, respectively. The manometer was then balanced by opening valve  $V_1$  to admit a reference air flow and by adjustment of  $V_1$  until the null position for the manometer diaphragm was established. This balance was stable to within  $\pm 10\mu$  during the 3-4 min period of a typical run. Absolute argon pressures were obtained to within 1% with pressure gauge G (Wallace and Tiernan, 0-20, or 0-100 torr) after corrections for any capacitance manometer imbalance were made.

A given partial pressure of  $CO_2$  was then established within the cell when  $V_4$  was opened and adjusted to give the desired pressure increase as indicated by the manometer M. In a similar fashion a desired pressure of HF (DF) was finally admitted by means of valve  $V_5$ . The flows through valves  $V_4$  and  $V_5$  were always choked. The partial pressure of  $CO_2$  could be maintained to within  $\pm 10\mu$  at the lower range of

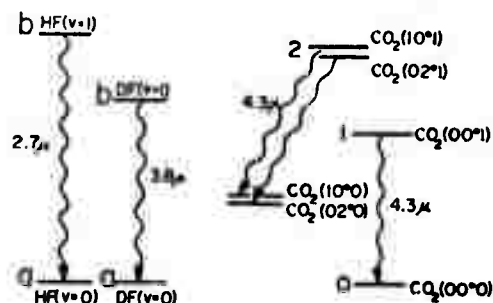


FIG. 2. Vibrational energy level diagram which illustrates the laser excited fluorescence transitions in HF, DF, and  $CO_2$ .

pressures employed or  $\pm 2\%$  at the higher pressures used. For HF(DF) the corresponding accuracies of partial pressure settings were  $\pm 20\mu$  or  $\pm 5\%$ .

After the run, valves  $V_4$  and  $V_5$  were turned off separately and the pressure changes indicated by the manometer were recorded. These values were in agreement with the initially recorded pressures to the accuracies stated above; an average of the initial and final values was usually used in data reduction. The sum of HF(DF) and  $CO_2$  partial pressures was monitored with the capacitance manometer throughout the run. Occasionally a drift in pressure would occur during a run which was clearly outside the above stated error limits; such runs were terminated and the fluorescence data discarded.

### C. Instrumentation for Fluorescence Detection

The electronics instrumentation employed for this work has already been described.<sup>14</sup> The output of the indium antimonide  $PV$  detector was amplified and used to drive either a P.A.R. Model CW-1 boxcar integrator, or Model TDH-9 waveform eductor. The time bases for both instruments were determined to within 0.5% with a 100 kHz crystal calibrator. The scanning circuits of the boxcar integrator/waveform eductor were triggered by a phototransistor synchronized to the laser pulse. The time origin for the fluorescence traces coincided with the peak of the laser pulse and could be determined to within  $\pm 0.5 \mu\text{sec}$ .

Each fluorescence trace represented the average of as many as 300 000 separate events. Before signal averaging, the signal to noise (S/N) ratios ranged from a high of 3/1 for  $CO_2$  fluorescence from the DF- $CO_2$  system to about 1/30 for DF fluorescence from the DF and DF- $CO_2$  systems. All of the HF data and most of the DF data were taken with the boxcar integrator, which provided an improvement in the S/N ratio by factors ranging from 30 to 80. The weaker DF fluorescence from the DF and DF- $CO_2$  systems (owing to the relatively long spontaneous emission lifetime of DF compared with both HF and  $CO_2$ )<sup>15</sup> usually required use of the waveform eductor which gave an improvement in S/N ratio by a factor exceeding 350. After signal

averaging, the S/N ratio of these data generally ranged from 10/1 to 100/1.

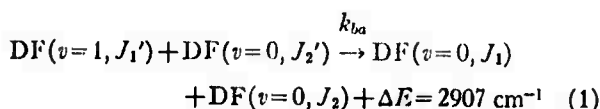
During the 2 min time period of a typical run, the base line of the fluorescence trace was usually constant to within 3%; all data which exhibited base line shifts of more than 5% were discarded. The observation that data taken with the waveform eductor were in excellent agreement with those data taken with the boxcar integrator confirmed that the stability of the laser output during a given run was adequate for the present measurements.

### III. EXPERIMENTAL RESULTS

#### A. Vibrational Energy Transfer Processes

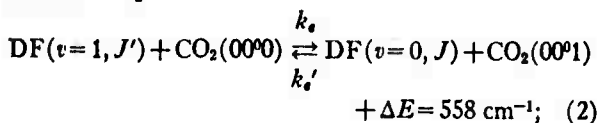
The processes of importance in describing the present measurements of vibrational relaxation in DF and mixtures of DF and CO<sub>2</sub> are the following (refer to the energy level diagram of Fig. 2):

vibration to rotation ( $V \rightarrow R$ ) energy transfer in DF:

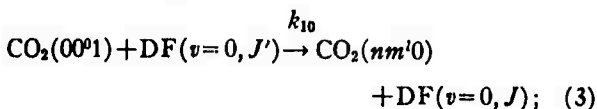


(where  $\Delta E$  is the vibrational energy difference between initial and final states);

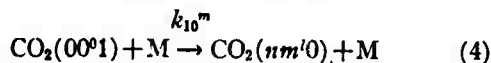
vibration to vibration ( $V \rightarrow V$ ) transfer between DF and CO<sub>2</sub>:



de-excitation of the upper CO<sub>2</sub> laser level by DF through intramolecular vibrational energy transfer in CO<sub>2</sub> and energy transfer to rotation in DF:

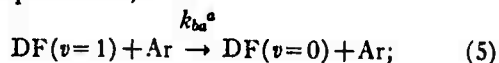


intramolecular energy transfer in CO<sub>2</sub>:

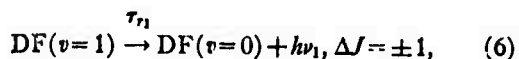


(where the species M is either CO<sub>2</sub> or argon, with the respective rate constants  $k_{10}^a$  and  $k_{10}^m$ );

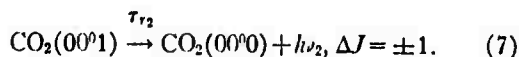
vibration to translation ( $V \rightarrow T$ ) deactivation of DF by argon ( $V \rightarrow T$  deactivation of DF and HF by CO<sub>2</sub> is assumed negligible under the conditions of the present experiments.):



fluorescence from the DF( $v=1 \rightarrow 0$ ) fundamental band

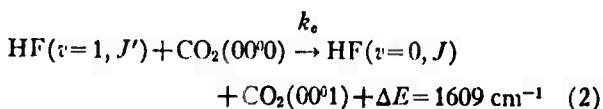


and fluorescence from the CO<sub>2</sub>[(00<sup>1</sup>)  $\rightarrow$  (00<sup>0</sup>)] 4.3 $\mu$  band

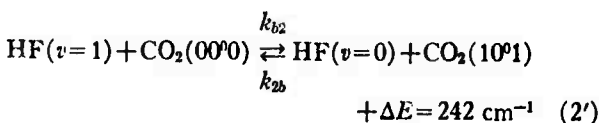


In Processes (1)–(3) only certain assignments of the rotational quantum numbers will not require a large energy transfer to translational motion. For present purposes we will consider the above rate constants as total rates summed over all rotational quantum number combinations which provide an appreciable contribution. It is assumed that equilibrium exists for rotational states within a given vibrational level.

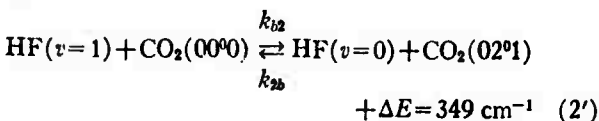
It has been proposed<sup>7</sup> that the coupling of vibrational energy between HF( $v=1$ ) and CO<sub>2</sub>(00<sup>1</sup>) levels may involve the participation of an intermediate CO<sub>2</sub> state in contrast to the direct coupling of Process (2) indicated for the DF–CO<sub>2</sub> system by the present experimental results.<sup>19</sup> Therefore, in the HF–CO<sub>2</sub> case one must consider both the direct coupling processes



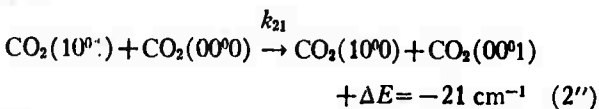
and the alternate processes



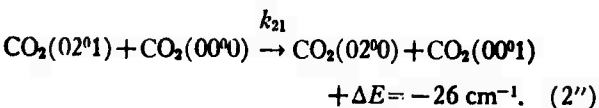
or



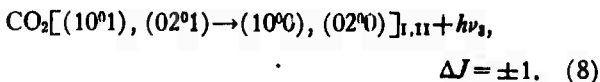
and



or



Processes analogous to those of Eqs. (1) and (3)–(7) also apply to the HF and HF–CO<sub>2</sub> systems. For the HF–CO<sub>2</sub> system we must consider the additional fluorescences of the "hot" bands<sup>20</sup>



Processes (8) present a major experimental difficulty in the determination of which of the coupling mechanisms (2) or (2') and (2'') gives rise to the observed fluorescence in the 4.3 $\mu$  region. Recent high resolution absorption measurements<sup>20</sup> indicate that the matrix elements for these bands are at least as large as that

for the CO<sub>2</sub>[(00<sup>0</sup>1)→(00<sup>0</sup>0)] band of Process (7). Thus, since fluorescence from the bands associated with both Processes (7) and (8) would lie within the pass band of the 4.3μ interference filter used here, we have no means in the present experiments to distinguish between the alternate coupling mechanisms.

**B. Self-Deactivation of HF and DF**

**1. Vibrational Deactivation of DF(v=1) by DF(v=0)**

Fluorescence from the fundamental v=1→0 band of DF was observed from mixtures of DF with argon. The intensity of this fluorescence was proportional to the

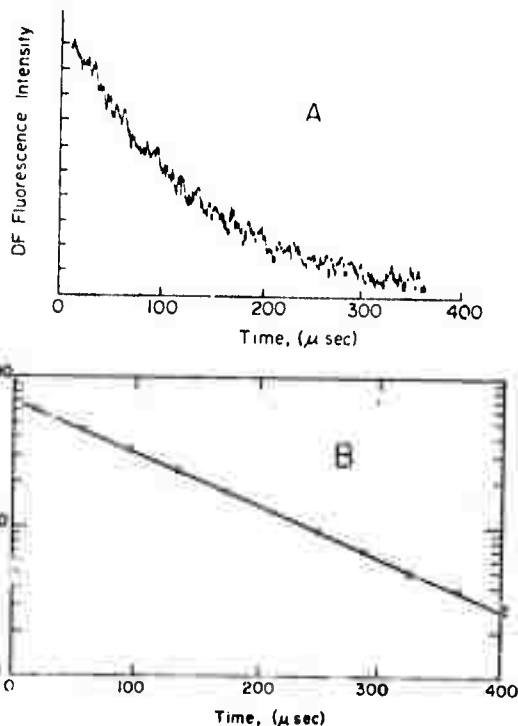


FIG. 3. A: Decay of DF(v=1)→DF(v=0) fluorescence from the mixture: DF=0.305 torr, argon=9.97 torr, at 349°K. B: Semilogarithmic graph of a smooth curve fitted to the data of Fig. 3A.

DF(v=1) concentration given by the expression

$$[DF(v=1)]/[DF]_0 = \exp(-t/\tau), \quad (9)$$

where [DF]<sub>0</sub> is the initial DF(v=1) population produced by absorption from the DF laser pulse, and

$$(p\tau)^{-1} = k_{DF-DF}X_{DF} + k_{DF-Ar}X_{Ar} + (p\tau_{r1})^{-1}. \quad (10)$$

Here p is the total pressure of the gas mixture; τ is the relaxation time, τ<sub>r1</sub> is the total radiative lifetime of the v=1 state of DF<sup>18</sup> and X<sub>DF</sub> and X<sub>Ar</sub> are the respective mole fractions of DF and argon.

Figure 3A shows a typical DF fluorescence trace; such DF relaxation data always exhibited a single exponential time constant as is illustrated for the data of Fig. 3A by the semilogarithmic plot of Fig. 3B.

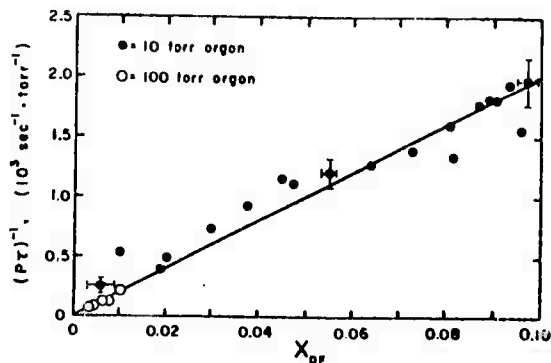


FIG. 4. Observed DF fluorescence decay rates for DF-argon mixtures at 350°K as a function of DF mole fraction.

Figure 4 contains all of the fluorescence decay data taken for mixtures of DF and argon. Here values of (pτ)<sup>-1</sup> obtained from the slopes of semilogarithmic plots of the data for each run are plotted against the mole fraction of DF in the conventional manner. Most of the data were taken for an argon partial pressure of 10 torr; however, a few points were taken at an argon pressure of 100 torr to establish the location of the intercept of the data with the ordinate. Since the intercept of Fig. 4 is at the origin within experimental uncertainty,<sup>21</sup> the neglect of the last two terms of Eq. (10) is justifiable in agreement with analogous findings from other studies of hydrogen halides.<sup>8,17,22</sup> The DF partial pressures of Fig. 4 range from 0.05 torr to 1.05 torr. This range was selected because fluorescence

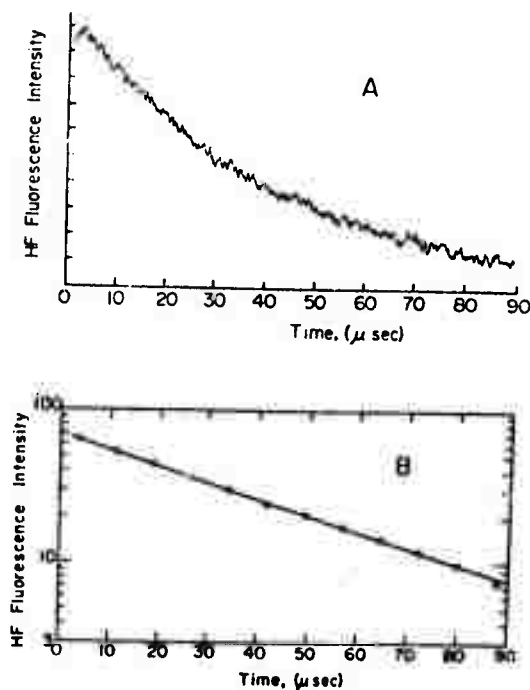


FIG. 5. A: Decay of HF(v=1)→HF(v=0) fluorescence from the mixture: HF=0.465 torr, argon=9.75 torr, at 351°K. B: Semilogarithmic graph of a smooth curve fitted to the data of Fig. 5A.

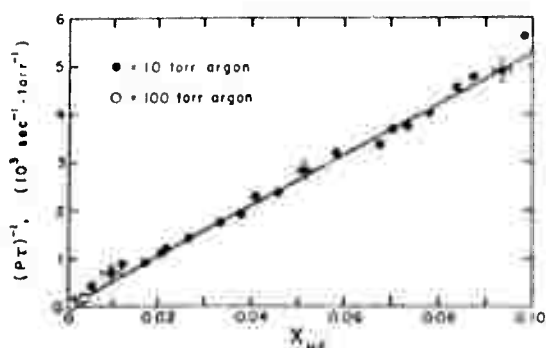


Fig. 6. Observed HF fluorescence decay rates for HF-argon mixtures at 350°K as a function of HF mole fraction.

signals were significantly weaker at higher and lower pressures. In addition, at somewhat higher pressures the accuracy of measurement would be limited by the time response of our apparatus; at lower pressures the partial pressure determinations would be less certain. The data of Fig. 4 give  $k_{ba} \equiv k_{DF-DF} = 2.0 \pm 0.2 \times 10^4 \text{ sec}^{-1} \cdot \text{torr}^{-1}$  at 350°K.

## 2. Vibrational Deactivation of HF( $v=1$ ) by HF( $v=0$ )

Fluorescence from the  $2.7\mu v=1 \rightarrow 0$  band of HF was observed and analyzed for mixtures of HF with argon in a manner similar to that discussed for DF. Single exponential decays such as shown in Figs. 5A and 5B were observed for all data. Figure 6 shows the relaxation times for all of the HF fluorescence data as a function of the mole fraction of HF. The smaller scatter of these data compared to those of Fig. 4 probably reflects the shorter radiative lifetime of HF<sup>18</sup> which affords a better fluorescence S/N ratio than was achieved for DF (compare Figs. 3A and 5A). Most of the data were taken at a 10 torr argon pressure with HF partial pressures ranging from 0.05 to 1.06 torr; a few additional traces were recorded for 100 torr of argon and HF pressures from 0.10 to 0.35 torr to confirm the negligible effect of Process (5) compared with Process (1) as was demonstrated for DF with Fig. 4.<sup>21</sup> The slope of the linear fit to the data of Fig. 6 gives the self-deactivation rate of HF as  $k_{ba} \equiv k_{HF-HF} = 5.25 \pm .30 \times 10^4 \text{ sec}^{-1} \cdot \text{torr}^{-1}$  at 350°K. Our rate constant is about 44% below the deactivation rate for HF previously measured by Airey and Fried.<sup>8</sup> Since the gas handling and purification procedures followed by the two groups were virtually identical, it is difficult to account for this discrepancy which is somewhat outside our assigned error limits.

## C. Measurements of Vibrational Energy Transfer in the HF-CO<sub>2</sub> and DF-CO<sub>2</sub> Systems

### 1. Energy Transfer in DF-CO<sub>2</sub> Mixtures

Fluorescence was observed from mixtures of DF and CO<sub>2</sub> in argon on both the ( $v=1 \rightarrow 0$ ) band of DF and

from the  $4.3\mu (00^01 \rightarrow 00^00)$  band of CO<sub>2</sub>. It was thus possible to monitor the concentrations of both the DF( $v=1$ ) and CO<sub>2</sub>( $00^01$ ) molecules following the DF laser pulse. The time dependence of these concentrations is given by the solutions of the rate equations corresponding to the processes of Eqs. (1)-(7). The solutions are given by the sum of two exponential terms<sup>12</sup>:

$$[\text{DF}(v=1)]/[\text{DF}]_0 = [(\lambda_1 - a_1)/(\lambda_1 - \lambda_2)] \times \exp(-\lambda_2 t) + [(a_1 - \lambda_2)/(\lambda_1 - \lambda_2)] \exp(-\lambda_1 t), \quad (11)$$

$$[\text{CO}_2(00^01)]/[\text{DF}]_0 = [(\lambda_1 - a_1)(a_1 - \lambda_2)/b_1(\lambda_1 - \lambda_2)] \times [\exp(-\lambda_2 t) - \exp(-\lambda_1 t)], \quad (12)$$

where  $a_1/p = k_{ba}X_{DF} + k_cX_{CO_2} + k_{ba}^aX_{Ar} + (p\tau_{11})^{-1}$ , and  $b_1/p = k_e'X_{DF}$ , and

$$(\lambda_{1,2})/p = \frac{1}{2} \{ a_1 + b_1 \pm [(a_1 - b_1)^2 + 4a_2b_1]^{1/2} \}, \quad (13)$$

where

$$a_2/p = k_eX_{CO_2}$$

and

$$b_2/p = (k_e' + k_{10})X_{DF} + k_{10}^cX_{CO_2} + k_{10}^aX_{Ar} + (p\tau_{10})^{-1}.$$

In Eq. (13) the square root term is always positive and  $\lambda_1$  corresponds to the + sign. It can readily be seen that  $\lambda_1$  and  $\lambda_2$  are positive;  $\lambda_1 > a_1$  and  $\lambda_2 < a_1$ .<sup>12</sup>

The rate constant  $k_e$  for the transfer of vibrational energy from DF to CO<sub>2</sub> by Process (2) can be determined most easily from observations of DF( $v=1$ ) fluorescence under conditions of small concentrations of DF. In the limiting case when the concentration of DF is sufficiently small, Eq. (11) reduces to the simple form of Eq. (9), where now the relaxation time is given by the expression

$$(p\tau)^{-1} = k_{ba}X_{DF} + k_eX_{CO_2} + k_{ba}^aX_{Ar} + (p\tau_{11})^{-1}. \quad (14)$$

Only the first two terms on the rhs of (14) are needed to interpret the data since, as before, the last two terms are of negligible magnitude (thus, in the discussion of the DF-CO<sub>2</sub> and HF-CO<sub>2</sub> systems, the reference

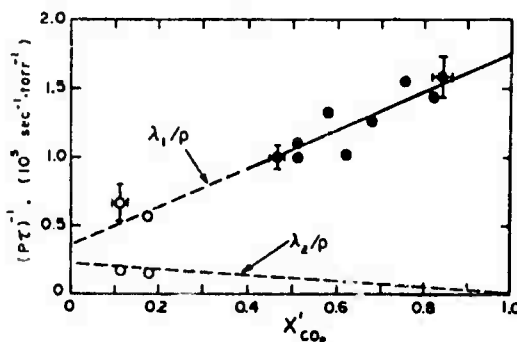


Fig. 7. Observed DF fluorescence decay rates for DF-CO<sub>2</sub>-argon mixtures at 350°K at a function of the reduced mole fraction of CO<sub>2</sub>;  $X'_{CO_2} = X_{CO_2}/(X_{DF} + X_{CO_2})$ .

pressure  $p$  is the sum of only the CO<sub>2</sub> and DF (HF partial pressures). Figure 7 shows relaxation rate data (solid points) for various values of  $X_{CO_2}' \equiv (X_{CO_2}) / (X_{DF} + X_{CO_2})$  ranging from 0.46 to 0.84 (the open data points and the dashed lines of Fig. 7 are discussed at the end of this section). These data exhibited a well defined single exponential behavior and  $(pr)^{-1}$  values were obtained from semilogarithmic plots in a manner similar to that discussed in connection with Figs. 3A and 3B. Extrapolation of these data with the solid line of Fig. 7 to the value  $X_{CO_2}' = 1$  yields a value for the rate constant for  $V \rightarrow V$  transfer from DF ( $v=1$ ) to CO<sub>2</sub>(00<sup>0</sup>1) of  $k_i = 1.75 \pm 0.25 \times 10^5 \text{ sec}^{-1} \cdot \text{torr}^{-1}$ . [The solid line of Fig. 7 is not simply a reasonable fit to the data shown, but also has a slope constrained by the values of  $k_e'$  and  $k_{10}$  as will become apparent after some further discussion.]

Equation (12) describes the rise and subsequent decay of CO<sub>2</sub>(00<sup>0</sup>1) concentration. The rate constant  $k_{10}$  for the de-excitation of CO<sub>2</sub>(00<sup>0</sup>1) by DF ( $v=0$ ) was measured from examination of CO<sub>2</sub>(00<sup>0</sup>1) fluorescence for times sufficiently long after the initiating laser pulse that the decay of CO<sub>2</sub>(00<sup>0</sup>1) population could be accurately described by the single exponential term  $\exp(-\lambda_2 t)$  appearing in Eq. (12). That is, when  $\exp(-\lambda_2 t) \gg \exp(-\lambda_1 t)$ , then  $(pr)^{-1} = \lambda_2/p$ . When  $\lambda_2$

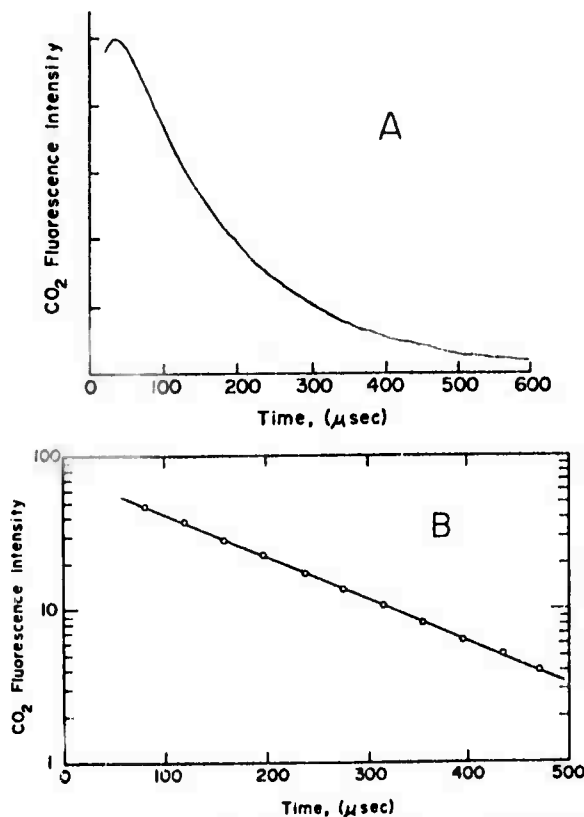


FIG. 8. A: Decay of CO<sub>2</sub>[(00<sup>0</sup>1) → (00<sup>0</sup>0)] fluorescence during the latter stages of relaxation for the mixture: DF=0.340 torr, CO<sub>2</sub>=0.720 torr, argon=9.91 torr, at 351°K. B: Semilogarithmic graph of a smooth curve fitted to the data of Fig. 8A.

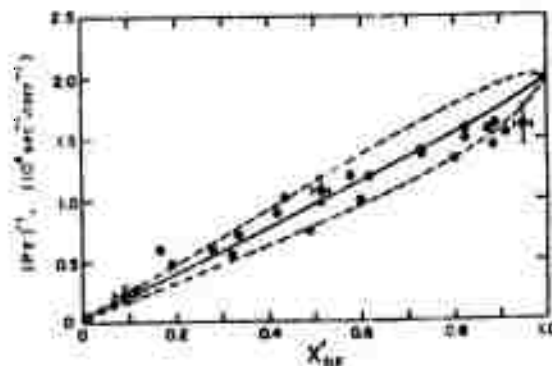


FIG. 9. Observed CO<sub>2</sub> fluorescence decay rates for the latter stages of relaxation for DF-CO<sub>2</sub>-argon mixtures at 350°K as a function of the reduced mole fraction of DF;  $X_{DF}' = X_{DF} / (X_{DF} + X_{CO_2})$ .

was computed with the Eqs. (13), the terms  $k_{bo}^*$  and  $(pr_{r1})^{-1}$  were again dropped; the term  $k_{10}^*$  has a small value<sup>23</sup> of  $50 \text{ sec}^{-1} \cdot \text{torr}^{-1}$  and was also neglected; the value of  $\tau_{r2}$  is long enough<sup>18</sup> that the last term appearing in the expression for  $b_2$  can usually be neglected without appreciable error.<sup>24</sup>

A representative CO<sub>2</sub>(00<sup>0</sup>1) fluorescence trace (Fig. 8A) was used to construct Fig. 8B, which illustrates the linear time dependence of the logarithm of fluorescence intensity observed for all DF-CO<sub>2</sub> mixtures during the latter stages of relaxation. Figure 9 shows the observed dependence of  $(pr)^{-1}$  values determined from such plots upon the ratio  $X_{DF}'$ , where  $X_{DF}' \equiv (X_{DF}) / (X_{DF} + X_{CO_2})$ , for all of the CO<sub>2</sub> fluorescence data. The cell compositions were systematically chosen to cover the partial pressure ranges for DF from 0.05 to 1.0 torr, for CO<sub>2</sub> from 0.05 to 10.0 torr, and for argon from 10 to 20 torr.

The value for the rate constant  $k_{10}$  may be deduced from the data of Fig. 9. In Eqs. (13) the rate constant  $k_{10}^*$  is known to be  $335 \text{ sec}^{-1} \cdot \text{torr}^{-1}$  at 350°K<sup>25</sup>; the values of  $k_{bo}$  and  $k_e$  have been given above. Detailed balancing provides the relationship  $k_e' = k_e \exp(-558 hc/kT)$ ; where, as has been stated,  $k_e$  and  $k_e'$  are over-all rate constants (summed on  $J$  and  $J'$ ) and rotational equilibrium at the temperature  $T$  is assumed. Use of these rate constants and the relationship,  $(pr)^{-1} = \lambda_2/p$ , for three different assumed values for  $k_{10}$  leads to the curves shown with the data of Fig. 9. The solid curve has been drawn for the value  $k_{10} = 1.9 \times 10^4 \text{ sec}^{-1} \cdot \text{torr}^{-1}$ . The upper and lower dashed curves are for  $k_{10} = 2.3 \times 10^4 \text{ sec}^{-1} \cdot \text{torr}^{-1}$  and  $1.5 \times 10^4 \text{ sec}^{-1} \cdot \text{torr}^{-1}$ , respectively; these curves represent reasonable upper and lower bounds on  $k_{10}$  when the data of Fig. 9 and the error limits on  $k_e$ ,  $k_e'$ ,  $k_{bo}$ , and  $k_{10}^*$  are considered. Thus, we find the value for the rate of de-excitation of the upper laser level of CO<sub>2</sub> by DF to be  $k_{10} = 1.9 \pm 0.4 \times 10^4 \text{ sec}^{-1} \cdot \text{torr}^{-1}$  at 350°K.

The foregoing determination of the rate constants  $k_{bo}$ ,  $k_e$ , and  $k_{10}$  for the processes of Eqs. (1)–(3) has been facilitated by the examination of certain ex-

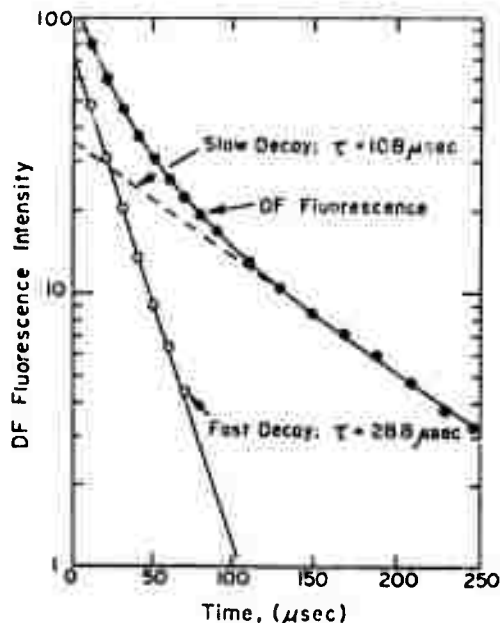


FIG. 10. Semilogarithmic graph of the DF fluorescence relaxation for the mixture: DF=0.510 torr, CO<sub>2</sub>=0.110 torr, argon=9.72 torr. The fluorescence is resolvable into the sum of two exponential decay terms. The slow decay time ( $\tau=108 \mu\text{sec}$ ) is determined from a straight line fit to the data of the latter stages of relaxation. The difference between this line and the DF fluorescence observed early in the relaxation yields a second straight line with a decay time  $\tau=28.8 \mu\text{sec}$ .

perimental conditions for which the fluorescence signals may be represented as single exponential decays. It is appropriate to now verify that the use of the rate constant values thus determined does in fact permit an accurate description of the observed fluorescence traces throughout the entire accessible range of experimental parameters. Figure 10 shows a semilogarithmic plot of DF( $\nu=1$ ) fluorescence data from a trace taken for the composition: DF: 0.51 torr, CO<sub>2</sub>: 0.11 torr, and argon: 9.72 torr. Here a double exponential behavior is clearly resolvable. From Fig. 10 we measure directly the values:  $\lambda_1/p=5.6 \times 10^4 \text{ sec}^{-1} \cdot \text{torr}^{-1}$  and  $\lambda_2/p=1.5 \times 10^4 \text{ sec}^{-1} \cdot \text{torr}^{-1}$ . These values may be compared with calculated values based upon the measured rate constants and Eq. (13) of  $\lambda_1/p=6.2 \times 10^4 \text{ sec}^{-1} \cdot \text{torr}^{-1}$  and  $\lambda_2/p=1.6 \times 10^4 \text{ sec}^{-1} \cdot \text{torr}^{-1}$ .

A further illustration of the good agreement between experimental fluorescence traces and calculated fluorescence behavior is given in Figs. 11A, 11B, and 11C. These traces were all taken for essentially the same gas composition. In order to adequately resolve both early and late time behavior of the CO<sub>2</sub> fluorescence, Figs. 11A and 11B were taken for identical conditions but were recorded with differing time bases. Figure 11C gives the corresponding DF fluorescence decay. The curves shown with the data were calculated from Eqs. (11)–(13) with the rate constants quoted above and were normalized to the experimental traces. Not all of the fluorescence traces showed the excellent

agreement with calculations illustrated in Figs. 11A–11C; however, in every case the agreement was within the uncertainty associated with the data point scatter of Figs. 4, 7, and 9.

In concluding this section, we must confirm the validity of the extrapolation made in Fig. 7 in the determination of the rate constant  $k_e$  from DF fluorescence data. The extrapolation was based on the fact that single exponential behavior was observed for the solid points of Fig. 7, and upon the observation that as  $X_{\text{CO}_2'}$  tends toward unity ( $X_{\text{DF}} \rightarrow 0$ ) the rhs of Eq. (11) approaches the single term:  $\exp(-a_1 t)$ . We are now in a position to show that the solid line of Fig. 7 is correctly drawn within narrow limits. Since the solid data points of Fig. 7 represent single exponential decays, these  $(pr)^{-1}$  values must correspond to either  $\lambda_1/p$  or  $\lambda_2/p$  of Eqs. (11) and (12). The upper and lower dashed lines of Fig. 7 show the respective variations with  $X_{\text{CO}_2'}$  of the values of  $\lambda_1/p$  and  $\lambda_2/p$  calculated from our rate constant values and Eq. (13). The right-hand portion of the upper dashed line coincides with the solid curve drawn to determine  $k_e$ . A direct comparison with experiment is provided

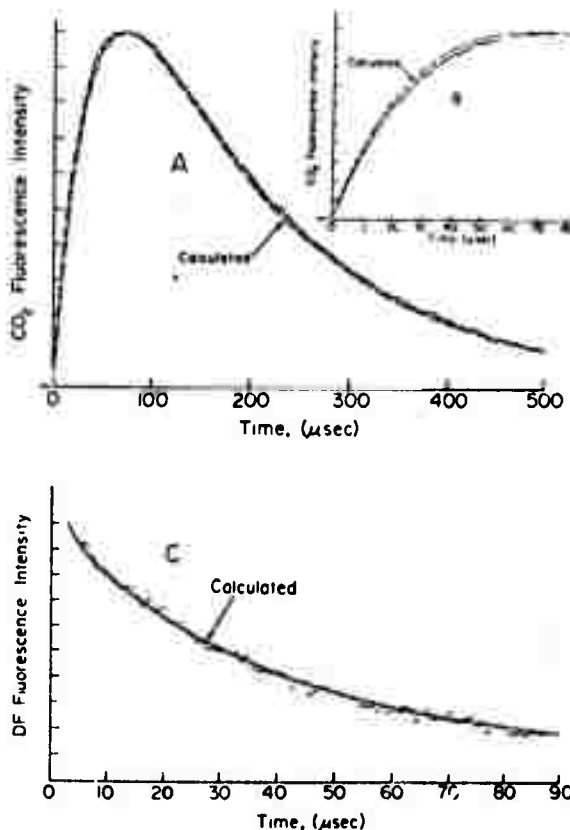


FIG. 11. Observed and calculated DF and CO<sub>2</sub> fluorescence from a DF-CO<sub>2</sub>-argon mixture at 350°K. A: CO<sub>2</sub> fluorescence on a long time scale for the mixture: DF=0.290 torr, CO<sub>2</sub>=0.105 torr, argon=19.7 torr. B: CO<sub>2</sub> fluorescence on a short time scale for the same conditions as in A). C: DF fluorescence for the mixture: DF=0.305 torr, CO<sub>2</sub>=0.105 torr, argon=20.0 torr.

from two DF fluorescence traces which exhibited clearly resolvable double exponential behavior. The two pairs of open data points of Fig. 7 give the  $\lambda_1/p$  and  $\lambda_2/p$  values obtained from these traces in the manner illustrated in Fig. 10 (which was drawn from one of the two DF traces). The upper two data points are in agreement with both the calculated  $\lambda_1/p$  curve and the other DF fluorescence data (solid points); the lower two points show good agreement with the calculated  $\lambda_2/p$  curve and hence also with the CO<sub>2</sub> fluorescence data of Fig. 9 (the solid curve of Fig. 9 is the  $\lambda_2/p$  curve of Fig. 7). We note further that the open data points serve to confirm the  $X_{CO_2}'=0$  intercepts of the calculated dashed curves rather well. That is, in the limit as  $X_{CO_2}'=0$  the values of  $\lambda_1/p$  and  $\lambda_2/p$  are the quantities  $k_{10}'+k_{10}$  and  $k_{20}$ , respectively; here again the data are consistent with the rate constant values.

## 2. Energy Transfer in HF-CO<sub>2</sub> Mixtures

Rate equations for the processes of Eqs. (1)-(8) were solved<sup>26</sup> to provide expressions for the temporal variations in HF( $v=1$ ) and CO<sub>2</sub>(00<sup>0</sup>1) populations. In contrast to the DF-CO<sub>2</sub> case where only the direct coupling model (DCM) was considered, an intermediate state model (ISM) with the alternate coupling scheme of Eqs. (2') and (2'') was considered in addition to the DCM for the HF-CO<sub>2</sub> case. Though the detailed expressions are too lengthy to be usefully included here, one may apprehend that because the Processes (2'') are quite fast (less than 50 collisions)<sup>27</sup> compared to the measured rate of coupling from HF( $v=1$ ) to CO<sub>2</sub>(00<sup>0</sup>1) states (about 200 collisions), the temporal variations of the HF( $v=1$ ) and CO<sub>2</sub>(00<sup>0</sup>1) populations differ little from those predicted by the DCM expressions (11) and (12) of the last section. More precisely, this is true if the inequalities  $k_{20}+k_{20}'' \gg k_{20}$  and  $k_{21}+k_{20}'' \gg k_{12}$  are satisfied, where  $k_{12}$ ,  $k_{20}$ , and  $k_{21}$  have been defined in Eqs. (2') and (2'') and  $k_{20}$  and  $k_{20}''$  are total rate constants for deactivation of the intermediate CO<sub>2</sub>(10<sup>0</sup>1) or CO<sub>2</sub>(02<sup>0</sup>1) states by ground state HF and CO<sub>2</sub>, respectively. The second of these inequalities probably holds, as stated above; however, it is not certain that the first inequality is satisfied since  $k_{20}$  is unknown ( $k_{20}$  cannot be much larger than  $k_{20}''$  since the HF-CO<sub>2</sub> laser is known to be capable of reasonably efficient performance<sup>28</sup>).

Over a very small range of experimental parameters, i.e., when  $X_{CO_2} \ll X_{HF}$ , there are differences in the initial increases of CO<sub>2</sub>(00<sup>0</sup>1) population predicted by the two models, as Fig. 12 illustrates. Two theoretical curves are given in Fig. 12 which are solutions to the rate equations for the DCM and ISM assumptions, respectively; the curves have been calculated with the measured rate constants of this section. A small correction for the finite width of the laser pulse has been accounted for by the introduction of a source

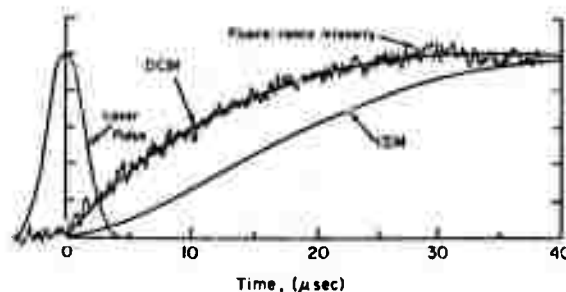


FIG. 12. Calculated initial rise in the CO<sub>2</sub>(00<sup>0</sup>1) population (at low CO<sub>2</sub> concentration) for two different HF-CO<sub>2</sub> coupling mechanisms (see text) compared with observed CO<sub>2</sub> fluorescence at 350°K from the mixture: HF=0.630 torr, CO<sub>2</sub>=0.050 torr, and argon=10.0 torr. Calculated curves have been normalized to the peak fluorescence; the temporal profile of the laser excitation pulse is also shown.

term into the rate equations having a time profile similar to that shown in Fig. 12. In the absence of better information we have assumed  $k_{20}''=k_{10}$  and  $k_{20}''=k_{10}$ . The rate constant for Process (2'') was taken to be  $k_{21}=10^6 \text{ sec}^{-1} \cdot \text{torr}^{-1}$  which corresponds to about 10 collisions. The rise in fluorescence intensity predicted with the ISM exhibits a significant lag with respect to both the variation predicted with the DCM and the experimental fluorescence trace. The fact that the experimental data and the prediction based on the DCM are in excellent agreement does not imply that the ISM is invalid since we must account for the potential existence of fluorescence from the CO<sub>2</sub>(10<sup>0</sup>1) or CO<sub>2</sub>(02<sup>0</sup>1) states superimposed upon that detected from the CO<sub>2</sub>(00<sup>0</sup>1) state. Because the strengths of the "hot" bands at 4.3  $\mu$  [Eq. (8)] are comparable to that of the fundamental CO<sub>2</sub>[(00<sup>0</sup>1)→(00<sup>0</sup>0)] band, no measurable differences in the temporal variations of the aggregate 4.3  $\mu$  fluorescences are predicted by the two models under the present experimental conditions. Thus until an experiment is performed with enough fluorescence intensity to permit the resolution of rotational components of the CO<sub>2</sub>[(00<sup>0</sup>1)→(00<sup>0</sup>0)] band and the identification of the fluorescence (if any) from intermediate states, an unfortunate ambiguity must remain in the  $V \rightarrow V$  coupling mechanism between HF and CO<sub>2</sub>. (See "Second Note Added in Proof" at end of paper.)

The fluorescence data for the HF-CO<sub>2</sub> system are adequately described by the equations:

$$[\text{HF}(v=1)]/[\text{HF}]_0 = \exp(-a_1 t), \quad (11')$$

$$[\text{CO}_2^*]/[\text{HF}]_0 = [a_2/(a_1 - b_2)] [\exp(-b_2 t) - \exp(a_1 t)], \quad (12')$$

where

$$a_2/p = k^* X_{CO_2},$$

$$a_1/p = k_{20} X_{HF} + k^* X_{CO_2} + k_{20}'' X_{A_1} + (p\tau_{11})^{-1},$$

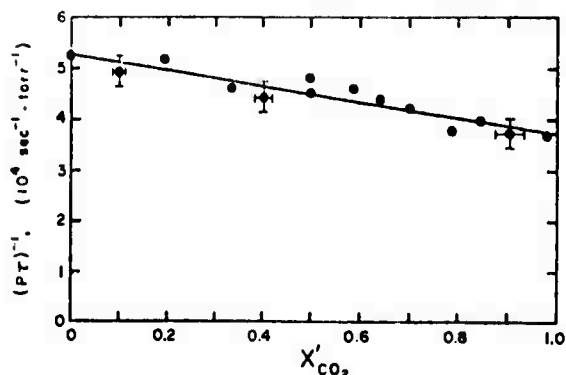


FIG. 13. Observed HF fluorescence decay rates for HF-CO<sub>2</sub>-Ar mixtures at 350°K as a function of the reduced mole fraction of CO<sub>2</sub>;  $X_{CO_2}' = X_{CO_2} / (X_{HF} + X_{CO_2})$ .

and

$$b_2/p = k_{10}X_{HF} + k_{10}^*X_{CO_2} + k_{10}^*X_{Ar} + (p\tau_1)^{-1}. \quad (13')$$

Here  $k^*$  is interpreted as the rate constant  $k_*$  with the DCM, or as the rate constant  $k_{b2}$  with the ISM assumption. These equations are consistent with the neglect of  $k_*$  compared with  $k_*$  for the DCM, and also apply for the ISM as a consequence of the foregoing considerations. CO<sub>2</sub><sup>\*</sup> denotes those states which give rise to fluorescence within the pass band of the CO<sub>2</sub> filters. Since it is expected that  $k_{21} \gg k_{b2}$ , then sufficiently late in the fluorescence decay period CO<sub>2</sub><sup>\*</sup> will represent only the CO<sub>2</sub>(00<sup>0</sup>1) state with either the ISM or DCM assumptions. This circumstance permits the determination of the rate constant  $k_{10}$ .

The procedure for rate constant determination from the fluorescence data for the HF-CO<sub>2</sub> system was similar to that already discussed for the DF-CO<sub>2</sub> case. The HF( $v=1$ ) fluorescence from HF-CO<sub>2</sub> mixtures always exhibited a single exponential decay. Relaxation times for these data are given in Fig. 13 as a function of the quantity  $X_{CO_2}' = (X_{CO_2}) / (X_{HF} + X_{CO_2})$ . Gas compositions consisted of 10 torr argon with selected partial pressures for HF and CO<sub>2</sub> in the respective ranges from 0.04 to 0.41 torr and 0.04 to 1.50 torr. The solid line fit to these data (Fig. 13) gives a value for the  $X_{CO_2}' = 1$  intercept of  $(p\tau)^{-1} = 3.7 \pm 0.3 \times 10^4 \text{ sec}^{-1} \cdot \text{torr}^{-1}$ ; according to Eq. (11') this value is the rate constant  $k_*$ . We note that the left-hand intercept of the solid line of Fig. 13 at  $X_{CO_2}' = 0$  is  $(p\tau)^{-1} = 5.25 \pm 0.4 \times 10^4 \text{ sec}^{-1} \cdot \text{torr}^{-1}$  which is in excellent agreement with the value of  $k_{b2}$  for the self-deactivation rate of HF already discussed. This agreement and the linearity of the solid curve of Fig. 13 is exactly the behavior predicted by Eq. (11').

The rate constant  $k_{10}$  for deactivation of CO<sub>2</sub>(00<sup>0</sup>1) by HF was determined by examination of the late time behavior of the 4.3 $\mu$  fluorescence which exhibited a single exponential decay. Relaxation times for the CO<sub>2</sub> fluorescence data are given in Figs. 14A and 14B for mixtures of HF and CO<sub>2</sub> and HF, CO<sub>2</sub>, and argon,

respectively. Taken together these data cover the entire range of  $X_{HF}' = (X_{HF}) / (X_{HF} + X_{CO_2})$  from zero to unity. The left-hand intercept ( $X_{HF}' = 0$ ) of Fig. 14A gives a value of  $(p\tau)^{-1} = 350 \pm 50 \text{ sec}^{-1} \cdot \text{torr}^{-1}$  in good agreement with the known value<sup>25</sup> for the rate constant  $k_{10}^*$ . The straight solid lines of Figs. 14A and 14B represent a reasonable fit to all of the data, drawn to give less weight to the relatively less reliable  $(p\tau)^{-1}$  values obtained for  $X_{HF}' > 0.8$ . A value of  $(p\tau)^{-1} = 3.6 \pm 0.3 \times 10^4 \text{ sec}^{-1} \cdot \text{torr}^{-1} = k_{10}$  is obtained for  $X_{HF}' = 1$ .

Figures 15A, 15B, and 15C, taken under nearly identical cell conditions, illustrate the close correspondence between the fall of the HF fluorescence and the rise of the CO<sub>2</sub> fluorescence in agreement with the predictions of Eqs. (11') and (12').

The measured rate constants and the corresponding values of  $p\tau$  are summarized in Table I for all of the processes studied here.

#### IV. DISCUSSION

##### A. Vibrational Deactivation of HF and DF

Vibrational relaxation data for HF at high temperatures have recently become available. Bott and Cohen<sup>10</sup> and Solomon *et al.*<sup>9</sup> have performed independent

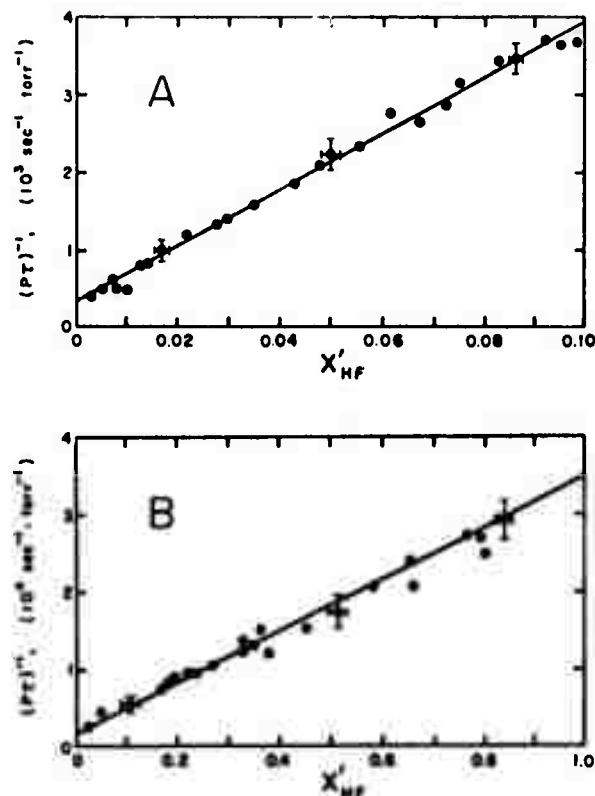


FIG. 14. Observed CO<sub>2</sub> fluorescence relaxation times for the latter stages of relaxation from HF-CO<sub>2</sub> mixtures. A: No argon present; CO<sub>2</sub> at either 10 or 100 torr; and HF pressures from 0.05 to 1.08 torr. B: Argon pressure = 10 torr; CO<sub>2</sub> pressures from 0.05 to 2.0 torr; and HF pressures from 0.05 to 0.90 torr.

TABLE I. Summary of rate measurements at 350°K.

Process	Rate constant 10 <sup>4</sup> sec <sup>-1</sup> ·torr <sup>-1</sup> )	$\rho\tau$ ( $\mu\text{sec}\cdot\text{atm}$ )
DF( $v=1$ ) + DF( $v=0$ ) → 2DF( $v=0$ )	$k=2.0\pm 0.2$	0.066
HF( $v=1$ ) + HF( $v=0$ ) → 2HF( $v=0$ )	$k=5.25\pm 0.30$	0.025
DF( $v=1$ ) + CO <sub>2</sub> (00 <sup>0</sup> ) → DF( $v=0$ ) + CO <sub>2</sub> (00 <sup>1</sup> )	$k=17.25\pm 2.5$	0.0075
HF( $v=1$ ) + CO <sub>2</sub> (00 <sup>0</sup> ) → HF( $v=0$ ) + CO <sub>2</sub> (00 <sup>1</sup> )	$k=3.7\pm 0.3$	0.036
CO <sub>2</sub> (00 <sup>1</sup> ) + DF( $v=0$ ) → CO <sub>2</sub> ( $n\pi n^0$ ) + DF( $v=0$ )	$k=1.9\pm 0.4$	0.069
CO <sub>2</sub> (00 <sup>1</sup> ) + HF( $v=0$ ) → CO <sub>2</sub> ( $n\pi n^0$ ) + HF( $v=0$ )	$k=3.6\pm 0.3$	0.037

studies of the vibrational relaxation of HF behind incident shock waves in the temperature range 1400–4000°K. These data and the value for HF deactivation at 350°K given by Airey and Fried<sup>8</sup> are shown in Fig. 16, along with the HF and DF deactivation rates of the present work, plotted in the customary Landau-Teller fashion with  $\rho\tau$  as a function of  $T^{-1/2}$ . The shock tube data agree closely and both sets give a linear variation in  $\rho\tau$  with  $T^{-1/2}$  for temperatures above 1400°K. The values of  $\rho\tau$  at 350°K are much lower than

the high temperature data, indicative of the effects of a strong attractive HF-HF interaction which has a predominant influence on energy transfer for  $kT \lesssim \Delta E$  where  $\Delta E$  is the attractive potential well depth. The magnitude of the low temperature rates, and the fact that the DF-DF deactivation rate is less than half that for HF-HF deactivation, is conclusive evidence that nearly all of the initial vibrational energy is converted into rotational rather than translational energy of the collision pair in agreement with earlier results for HCl and DCl presented by Chen and Moore.<sup>17</sup>

The qualitative features of the HF and DF relaxation data can be understood in terms of an approximate classical calculation of vibrational deactivation offered by Shin.<sup>13a</sup> In recognition of the importance of energy transfer from vibration to rotation for molecules having small moments of inertia so that rotational velocities can exceed translational velocities,<sup>13</sup> Shin has modeled HX-HX (X = F, Cl, Br, I) collisions in terms of the interaction between a rotation-averaged vibrator molecule (breathing sphere) and a rigid rotator molecule.<sup>13b</sup> The strong hydrogen bonding interaction which is expected to be a predominant feature in the encounters between HF (DF) molecules and to a lesser extent for HCl and HBr collision pairs is accounted for in an approximate manner by considering the attractive interaction between two ideal dipoles. Despite the questionable validity of the model as a representation of the actual interaction at close range, and the several approximations necessary for a mathe-

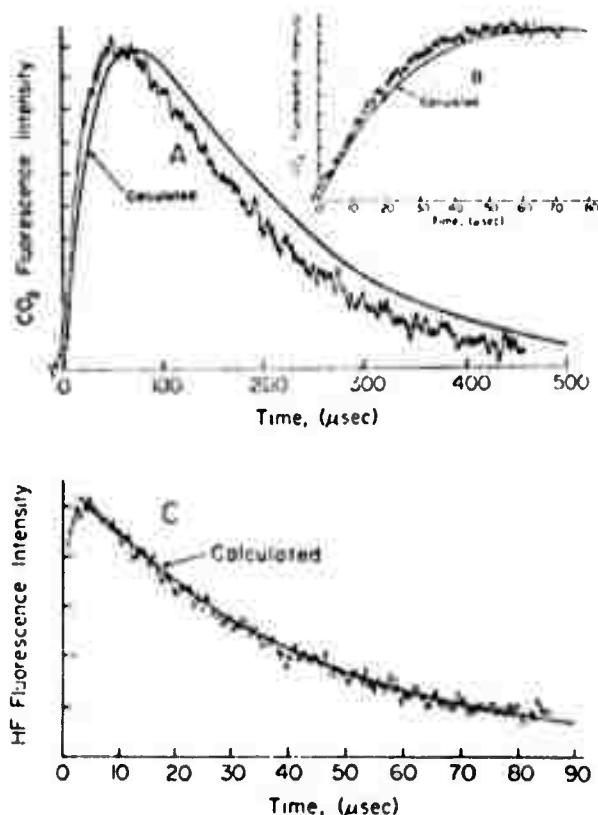


FIG. 15. Observed and calculated HF and CO<sub>2</sub> fluorescence from an HF-CO<sub>2</sub>-argon mixture at 350°K. The calculated curves have been normalized to the fluorescence traces. A: CO<sub>2</sub> fluorescence on a long time scale for the mixture: HF = 0.195 torr, CO<sub>2</sub> = 0.360 torr, argon = 9.90 torr. B: CO<sub>2</sub> fluorescence on a short time scale for the same conditions as in A. C: HF fluorescence for the mixture: HF = 0.200 torr, CO<sub>2</sub> = 0.360 torr, argon = 10.0 torr.

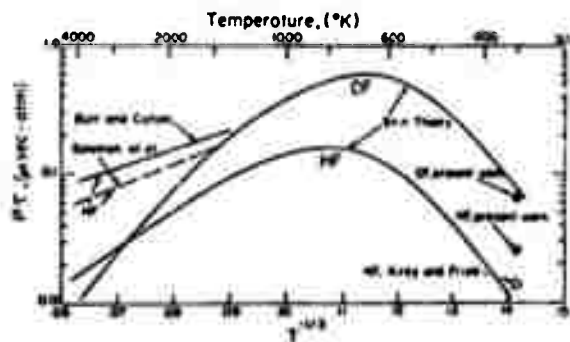


FIG. 16. Landau-Teller plots of the self-deactivation times for HF and DF at 1 atm pressure.

matically tractable analysis, the Shin theory provides results that agree very well with experimental data for the HF, HCl, DCl, HBr, and HI molecules.<sup>13a, 13b</sup> It appears that the major effect of the attractive forces is confined to the acceleration produced by the attractive potential which results in a significantly enhanced repulsion at close range.<sup>13b</sup> For this reason, a rather inexact modeling of the attractive interaction is apparently sufficient to adequately represent existing experimental observations.<sup>10</sup>

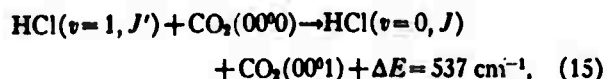
The solid curves shown with the experimental data of Fig. 16 are the calculated results given by Shin in Ref. 13(a). The calculated curves exhibit the correct qualitative variation of  $\rho r$  with temperature, and the predicted values of  $\rho r$  are certainly of the correct magnitude. The quantitative differences between experiment and theory should not be regarded too seriously at present in view of the approximate nature of the theory and the uncertainty in some of the physical parameters that enter the calculation. Bott and Cohen have indicated that a good fit with the high temperature shock tube data can be obtained with a somewhat smaller value of the Lennard-Jones parameter than the value  $\sigma = 3 \text{ \AA}$  used by Shin.<sup>10</sup>

The value for the ratio of relaxation times,  $\tau_{DF}/\tau_{HF}$ , obtained in the present work is 2.6 at 350°K; this is perhaps significantly different from the ratio  $\tau_{DF}/\tau_{HF} = 7.6$  calculated by Shin.<sup>13a</sup> Unfortunately no other data are presently available concerning vibrational relaxation in DF; high temperature shock tube data are needed for a more precise comparison with calculated values.

#### B. Vibration-Vibration Energy Transfer from HF and DF to CO<sub>2</sub>

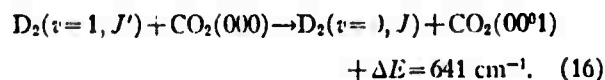
Perhaps the most interesting observation of the present study was the extremely rapid rate of coupling of vibrational energy from DF to CO<sub>2</sub>; the measured rate,  $k = 17.5 \pm 2.5 \times 10^4 \text{ sec}^{-1} \cdot \text{torr}^{-1}$ , corresponds to only about 40 collisions, one of the fastest rates of intermolecular  $V \rightarrow V$  transfer yet measured.<sup>30</sup> The magnitude of this rate is inexplicable in terms of existing theories of  $V \rightarrow V$  transfer because of the large over-all vibrational resonance defect (558  $\text{cm}^{-1}$ ) for Process (2). Because the observed rise in CO<sub>2</sub>(00<sup>0</sup>1) fluorescence exactly matched the decay in DF( $v=1$ ) fluorescence as discussed in the last section, and since coupling by means of an intermediate state in CO<sub>2</sub> is not plausible in this case,<sup>10</sup> there can be little doubt that the direct coupling process of Eq. (2) is correct.

Moore and co-workers<sup>31</sup> have measured both the forward and backward rates for the analogous  $V \rightarrow V$  coupling between HCl and CO<sub>2</sub> and verified that the direct coupling process



is correct and only requires about 80 collisions ( $k = 9.4 \times 10^4 \text{ sec}^{-1} \cdot \text{torr}^{-1}$ ) at 300°K. They also determined that the corresponding process for  $V \rightarrow V$  coupling between HI and CO<sub>2</sub>, with  $\Delta E = -119 \text{ cm}^{-1}$ , requires about 60 collisions;  $k = 12.6 \times 10^4 \text{ sec}^{-1} \cdot \text{torr}^{-1}$ , as determined from the reverse rate at 300°K.

As mentioned in the last section, a clear choice between the alternate mechanisms for  $V \rightarrow V$  coupling between HF and CO<sub>2</sub> [Processes (2) and (2')] could not be made on the basis of the present experimental results. Nevertheless, the rate of  $V \rightarrow V$  transfer from HF to CO<sub>2</sub> was determined to be  $k = 3.7 \times 10^4 \text{ sec}^{-1} \cdot \text{torr}^{-1}$  at 350°K which corresponds to about 200 collisions. No data [Note added in proof: Data on these systems have recently been reported; see H. L. Chen, *J. Chem. Phys.* 55, 5557 (1971).] appear to be available for the rates of coupling to CO<sub>2</sub> from HBr, DBr, DCl, and DI; however, it is of some interest to consider the process



The reported rate for this process,<sup>32</sup>  $k = 10^4 \text{ sec}^{-1} \cdot \text{torr}^{-1}$  at 300°K, corresponds to about 1500 collisions; the relatively slow rate reflects a different mechanism for  $V \rightarrow V$  transfer in this case as will be discussed in the following.

For comparison with experiment, calculations of  $V \rightarrow V$  transfer rates for the HF-CO<sub>2</sub>, DF-CO<sub>2</sub>, HCl-CO<sub>2</sub>, HI-CO<sub>2</sub>, and D<sub>2</sub>-CO<sub>2</sub> systems have been performed<sup>32</sup> within the framework of the theory of  $V \rightarrow V$  transfer by multipole moment interactions discussed by Sharma and Brau.<sup>33</sup> The primary contribution to the over-all rate of transfer comes from the first non-vanishing term in the multipole moment expansion in each case; i.e., dipole-dipole transition moment interactions in all except the D<sub>2</sub>-CO<sub>2</sub> case which has a rate determined by the interaction of quadrupole and dipole transition moments of D<sub>2</sub> and CO<sub>2</sub>, respectively.

A description of these calculations is given in the Appendix. The calculated  $V \rightarrow V$  transfer probabilities are given in Column 8 of Table II for comparison with the experimental probabilities of Column 9. The calculated energy transfer probabilities are several orders of magnitude too small in every instance except for the D<sub>2</sub>-CO<sub>2</sub> case, which is in excellent agreement with experiment.

Considering first the HF-CO<sub>2</sub>, DF-CO<sub>2</sub>, HCl-CO<sub>2</sub>, and HI-CO<sub>2</sub> systems, we note that only certain pairs of vibration-rotation transitions correspond to values of  $\omega$  less than 15  $\text{cm}^{-1}$ , where  $\omega$  is the amount of energy that must go into translational motion. A given pair of allowed vibration-rotation transitions can give a large contribution to the over-all probability of transfer only when  $\omega \lesssim 15 \text{ cm}^{-1}$  for the dipole-dipole case, provided that the initial state populations are not too

TABLE II. Comparison of experimental  $V \rightarrow V$  transfer probabilities with values calculated with multipole moment interaction theory.

Molecular system	Squared vibrational matrix elements <sup>a</sup>		$\Delta E^b$ (cm <sup>-1</sup> )	$\sigma_{LJ}^c$ (Å)	$T$ (°K)	$P_r^d$	$P_{theoret}^e$	$P_{exptl}$
	$ \langle 0   Q_1^{(0)}   1 \rangle ^2$ (10 <sup>-40</sup> esu <sup>2</sup> ·cm <sup>2</sup> )	$ \langle n_2'   Q_1^{(0)}   0 \rangle ^2$ (10 <sup>-40</sup> esu <sup>2</sup> ·cm <sup>2</sup> )						
HF-CO <sub>2</sub> <sup>f</sup>	HF(1→0): 97 <sup>g</sup>	CO [(00 <sup>0</sup> 0)→(10 <sup>0</sup> 1)]: 13 <sup>h</sup>	242	3.45	350	6.7×10 <sup>-3</sup>	1.7×10 <sup>-4</sup>	4.9×10 <sup>-3</sup>
DF-CO <sub>2</sub>	DF(1→0): 70 <sup>i</sup>	CO [(00 <sup>0</sup> 0)→(00 <sup>0</sup> 1)]: 950 <sup>h</sup>	558	3.45	350	0.30	1.0×10 <sup>-3</sup>	2.4×10 <sup>-3</sup>
HCl-CO <sub>2</sub>	HCl(1→0): 45 <sup>j</sup>	CO [(00 <sup>0</sup> 0)→(00 <sup>0</sup> 1)]: 950 <sup>h</sup>	537	3.60	300	0.26	1.1×10 <sup>-3</sup>	1.3×10 <sup>-3</sup>
HI-CO <sub>2</sub>	HI(1→0): 0.16 <sup>k</sup>	CO [(00 <sup>0</sup> 0)→(00 <sup>0</sup> 1)]: 950 <sup>h</sup>	-119	4.01	300	1.23×10 <sup>-3</sup>	2.0×10 <sup>-4</sup>	1.76×10 <sup>-3</sup>
	$ \langle 0   Q_2^{(0)}   1 \rangle ^2$ (10 <sup>-44</sup> esu <sup>2</sup> ·cm <sup>4</sup> )	$ \langle 1   Q_1^{(0)}   0 \rangle ^2$ (10 <sup>-40</sup> esu <sup>2</sup> ·cm <sup>2</sup> )						
D <sub>2</sub> -CO <sub>2</sub>	D <sub>2</sub> ; O <sub>1</sub> (6): 2.76 <sup>l</sup>	CO <sub>2</sub> [(00 <sup>0</sup> 0)→(00 <sup>0</sup> 1)]: 950 <sup>h</sup>	641	3.67	300	...	4.7×10 <sup>-4</sup>	6.7×10 <sup>-4</sup> <sup>m</sup>

<sup>a</sup> The notation of Ref. 33 is adopted here.

<sup>b</sup> Vibrational energy difference between band centers.

<sup>c</sup>  $\sigma_{LJ} = (\sigma_1 + \sigma_2)/2$  is the Lennard-Jones collision diameter, calculated from data in J. O. Herschfelder, C. F. Curtis, and R. B. Bird, *Molecular Theory of Gases and Liquids* (Wiley, New York, 1954), pp. 597, 1200. For HF and DF a value of  $\sigma_1 = 3.0$  Å has been adopted [see Ref. 13(a)].

<sup>d</sup>  $P_r$  denotes the theoretical probability for exact resonance (see Ref. 34).

<sup>e</sup> Calculations of Ref. 32 (see Appendix).

<sup>f</sup> The process HF( $v=1$ ) + CO<sub>2</sub>(00<sup>0</sup>0) → HF( $v=0$ ) + CO<sub>2</sub>(02<sup>0</sup>1) +  $\Delta E = 342$  cm<sup>-1</sup> can be neglected by comparison owing to the larger resonance defect and the smaller CO<sub>2</sub> matrix element for this process.

<sup>g</sup> R. J. Lovell and W. F. Herget, *J. Opt. Soc. Am.* **52**, 1374 (1962).

<sup>h</sup> H. Statz, C. L. Tang, and G. F. Koster, *J. Appl. Phys.* **37**, 4278 (1966).

<sup>i</sup> See Ref. 18.

<sup>j</sup> W. S. Benedict, R. Herman, and G. E. Moore, *J. Chem. Phys.* **26**, 1671 (1957); R. A. Toth, R. H. Hunt, and E. K. Plyler, *J. Mol. Spectry.* **35**, 110 (1970).

<sup>k</sup> W. Benesch, *J. Chem. Phys.* **39**, 1048 (1963).

<sup>l</sup> Calculation is based on matrix elements for the O<sub>1</sub>(5), O<sub>1</sub>(6), and O<sub>1</sub>(7) transitions in deuterium obtained by extrapolation from the results for hydrogen given by G. Karl and J. D. Poll, *J. Chem. Phys.* **46**, 2944 (1967) and T. C. James, *J. Mol. Spectry.* **32**, 512 (1969); the value given is for the O<sub>1</sub>(6) transition.

<sup>m</sup> Reference 12.

small. In the HF-CO<sub>2</sub> calculation, for example, the  $P(6)$  transition in HF combines with a large fraction of the allowed CO<sub>2</sub>(00<sup>0</sup>0)→CO<sub>2</sub>(10<sup>0</sup>1) vibration-rotation transitions to give values of  $\omega < 15$  cm<sup>-1</sup>. However, the population of the  $J'=5$  rotational state is only about 1/13 of the total HF( $v=1$ ) population at 350°K; unfortunately because of the large rotational spacing of HF, other possible  $P$  and  $R$  branch transitions correspond to larger values of  $\omega$  and thus the total calculated probability of transfer is small. The large effect attributable to the fact that  $\omega$  values greatly exceed 15 cm<sup>-1</sup> for the DF-CO<sub>2</sub> and HCl-CO<sub>2</sub> systems can be ascertained by comparison of Column 8 with the probabilities of Column 7 which have been calculated with the totally unrealistic assumption of exact resonance<sup>34</sup>; i.e.  $\omega = 0$  for all possible transitions.

It is clear from the results of Table II that the long range multipole interaction theory cannot explain  $V \rightarrow V$  transfer in the HF-CO<sub>2</sub>, DF-CO<sub>2</sub>, HCl-CO<sub>2</sub>, and HI-CO<sub>2</sub> systems. There are other examples of  $V \rightarrow V$  transfer processes that do not agree with existing theory, as discussed by Stephenson and Moore.<sup>23</sup> Just as in the cases cited by these authors, conventional

theories of  $V \rightarrow V$  transfer of the "SSH type"<sup>35</sup> based upon transitions caused primarily by short range repulsive forces are also quite inadequate in the present case. As is well known, these theories predict transfer probabilities many orders of magnitude too low at the present temperatures for processes with resonance defects as large as are considered here.

One source of the difficulty in reconciling the present experimental data with theoretical analysis seems clear. A successful theory must necessarily allow the major portion of the vibrational energy defect between initial and final states to be taken up as rotational motion of the collision partners. The rotational selection rules which are a feature of the long range multipole interaction calculation do not permit this in general when the rotational energy level spacings are large. Even though consideration of interactions between higher moments and extension of the calculations to higher orders of perturbation theory should provide some increase in the theoretical values, it is unreasonable to expect them to even remotely approach the large experimental rates. We are thus led to abandon the long range interaction small-perturbation approach as an ex-

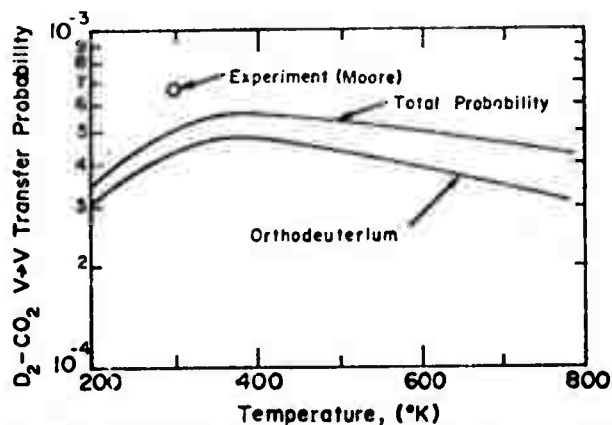
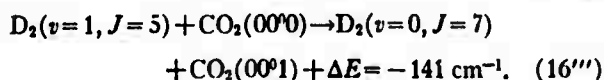
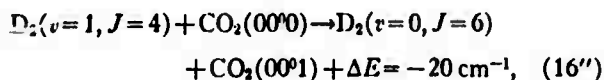
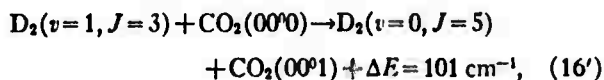


FIG. 17. Comparison of the calculated probability for  $V \rightarrow V$  transfer between  $D_2$  and  $CO_2$  (Ref. 32) with experiment (Ref. 12).

planation for the  $HF-CO_2$ ,  $DF-CO_2$ ,  $HCl-CO_2$ , and  $HI-CO_2$  data. Happily, however, the  $D_2-CO_2$  case is another story.

Sharma has explained deactivation of  $CO_2(01^0)$  by  $H_2$  and  $D_2$  in terms of a dipole-quadrupole interaction.<sup>36</sup> Kolker<sup>37</sup> has offered a similar calculation for the deactivation of  $CO_2(00^1)$  by  $H_2$ . Calculations<sup>32</sup> summarized in the Appendix indicate that the observed probability for Process (16) (see Table II) can be also satisfactorily explained in terms of an interaction between the dipole transition moment for the asymmetric stretch of  $CO_2$  and a quadrupole transition moment of  $D_2$  which permits energy transfer by means of the following processes:



The temperature dependence of the calculated  $D_2-CO_2$   $V \rightarrow V$  transfer probability is given in Fig. 17. The lower curve indicates the contribution to the total probability of transfer made by Process (16''). The probability for transfer decreases markedly for temperatures below 300°K because of the reduced population in the  $J=4$  rotational level of  $D_2$ . At higher temperatures the probability decreases with increasing temperature as is characteristic of weak attractive interactions. The good agreement with experiment at 300°K is encouraging since there are no "adjustable parameters" in the theory.

It should be noted that the mechanism proposed by Moore *et al.*<sup>28</sup> for the  $D_2$  to  $CO_2$   $V \rightarrow V$  process, i.e.,  $D_2(v=1) + CO_2(00^0) \rightarrow D_2(v=0) + CO_2(01^1)$  followed by  $CO_2(01^1) + CO_2(00^0) \rightarrow CO_2(01^0) + CO_2(00^1)$  is

unlikely within the framework of the multipole moment interaction theory because of the strongly forbidden nature of the  $CO_2(00^0) \rightarrow CO_2(01^1)$  transition.<sup>39</sup>

An important conclusion to be drawn from the foregoing discussion can be best illustrated by comparison of the  $DF-CO_2$  and  $D_2-CO_2$  cases. The differences in the rotational velocities and energy level spacings are not large enough to account for the significantly greater  $V \rightarrow V$  transfer rate for the  $DF-CO_2$  system with simply the recognition that most of the vibrational energy defect must be converted to rotational motion; this conversion is clearly accomplished by different mechanisms in the two cases. The apparent success of the weak long range interaction hypothesis for the  $D_2-CO_2$  system and the inapplicability of this assumption for the  $DF-CO_2$  system suggests that in the latter case a strong attractive interaction is involved. This interaction causes a strongly enhanced repulsion at short range which results in a violation of the rotational selection rules.

A search of the literature reveals several references to possible complex formation in  $HF-CO_2$  and  $HCl-CO_2$  gas mixtures.<sup>40-43</sup> Measurements of microwave absorption near the far infrared rotational lines of  $HCl$  and  $HBr$  give evidence of sufficiently strong attractive interactions between  $HCl-CO_2$  and  $HBr-CO_2$  collision pairs to cause a violation of the rotational selection rules.<sup>40</sup> Similar data exist for  $HF-CO_2$  mixtures.<sup>41</sup> Mixtures of  $HCl$  and  $HBr$  with nonpolar gases such as  $He$  or  $H_2$  do not show similar effects.<sup>40</sup> Values for the apparent binding energies of  $HF-CO_2$  and  $HCl-CO_2$  complexes have been given as 3.5 and 2.5 kcal/mole, respectively.<sup>43</sup>

In view of the above, and since it is known that the  $CO_2$  molecule possesses an electron charge distribution strongly localized in the vicinity of the oxygen atoms,<sup>44</sup> it is probable that the hydrogen bonded configurations



are influential in vibrational energy transfer processes. It is doubtful, however, that the hydrogen bonding energies exceed 2-4 kcal/mole in contrast with the

TABLE III. Probability for deactivation of  $CO_2(00^1)$ .

Molecular system	T (°K)	$P_{\text{expt}}$
$CO_2-HF$	350	$4.75 \times 10^{-3}$
$CO_2-DF$	350	$2.55 \times 10^{-3}$
$CO_2-H_2$	300	$2.41 \times 10^{-4}$ <sup>a</sup>
$CO_2-D_2$	300	$2.88 \times 10^{-4}$ <sup>a</sup>
$CO_2-HCl$	300	$5.6 \times 10^{-4}$ <sup>b</sup>

<sup>a</sup> Reference 38.

<sup>b</sup> Reference 31.

relatively large (6.8 kcal/mole) bonding in HF pairs. Since the dipole moments become progressively smaller in the sequence 1.83, 1.08, 0.80, and 0.42 D for DF, HCl, HBr, and HI, respectively, the case for the existence of a hydrogen bonded HI-CO<sub>2</sub> configuration is not quite as convincing in the absence of experimental data. Notice, however, that since the vibrational resonance defects for energy transfer from each of these molecules to CO<sub>2</sub> decrease in the sequence 558, 537, 210, and -119 cm<sup>-1</sup>, a compensating effect exists to explain the large rate of *V*→*V* transfer from HI to CO<sub>2</sub>.

### C. Deactivation of CO<sub>2</sub>(00<sup>0</sup>1) by HF and DF

Here again because of the possibility of relatively strong attractive interactions we expect relatively large probabilities for deactivation in comparison with H<sub>2</sub> and D<sub>2</sub>, as Table III illustrates. Because the rates for deactivation for HF and DF are both large and since the probability for deactivation by HF exceeds that for DF, vibration-rotation transfer is indicated; however, conclusions are difficult to draw when the CO<sub>2</sub>(*nm*'0) states are not defined.

Preliminary results indicate an inverse temperature dependence for the deactivation probability of CO<sub>2</sub>(00<sup>0</sup>1) by HF<sup>46</sup>; if this result is confirmed with more careful measurements, it would tend to support the hypothesis that attractive influences are important in the deactivation of CO<sub>2</sub> by HF and DF. The deactivation rate of CO<sub>2</sub>(00<sup>0</sup>1) in collisions with H<sub>2</sub>, D<sub>2</sub>, and HD increases with increasing temperatures<sup>28</sup>; therefore a strong attractive interaction is not a feature of the intermolecular potentials in these cases.

Until more data concerning deactivation of the CO<sub>2</sub>(00<sup>0</sup>1) level by other hydrogen and deuterium halides become available, it is difficult to generalize. However, the relatively small value of the probability for deactivation by HCl compared with that by DF (see Table III) is quite likely the effect of the weaker intermolecular attractive potential for the HCl-CO<sub>2</sub> case since the similarity of the energy levels in HCl and DF would argue against a change in mechanism between the two cases.

## V. CONCLUSIONS

(1) All three types of vibrational energy transfer processes studied here have large rates near room temperature which can be attributed to energy transfer to rotation under the influence of a sizable attractive intermolecular potential well and enhanced repulsion at close range.

(2) The approximations inherent in the first order perturbation theory of multipole moment interactions are invalid for treatment of the energy transfers to CO<sub>2</sub>(00<sup>0</sup>1) from HX(*v*=1) and DX(*v*=1) molecules.

(3) The vibrational energy transfer from D<sub>2</sub>(*v*=1)

to CO<sub>2</sub>(00<sup>0</sup>1) can be explained in terms of a quadrupole-dipole interaction at long range which causes a significant transfer to rotation of orthodeuterium at room temperature.

(4) A hydrogen bonding interaction between HF or DF and CO<sub>2</sub> is suggested here to account for the rapid transfer rates for the HF-CO<sub>2</sub> and DF-CO<sub>2</sub> systems. A similar mechanism is believed to occur in HX-HX deactivation.<sup>47</sup> Since CO<sub>2</sub> has no permanent dipole moment, the approximation made by Shin<sup>48</sup> in treating the HX-HX interaction as one between ideal dipoles will not account for the HX-CO<sub>2</sub> results and may be questionable in the HX-HX case as well. Nevertheless, Shin's results agree well with experiment for HX and DX deactivation.

*Second Note Added in Proof:* W. H. Green and J. K. Hancock have recently employed a filter cell to determine that the contribution of the hot bands to the total fluorescence is negligible for the conditions of Fig. 12. We may therefore conclude from the data of Fig. 12 that the coupling of vibrational energy from HF to CO<sub>2</sub> occurs by the direct process of Eq. (2). We thank them for their timely interest in the resolution of this important question.

## ACKNOWLEDGMENTS

We wish to thank John C. Kershenstein for setting up the computer programs and Garry L. Schott for a useful suggestion.

## APPENDIX

The probability for vibrational energy transfer from a molecule 1 to a molecule 2 under the interaction of the respective multipoles *l*<sub>1</sub> and *l*<sub>2</sub> can be written

$$P(\sigma_{1,2}, T) = \sum_{j_1, j_2; j_1', j_2'} f(j_1) f(j_2) \left[ \langle P_{l_1 l_2}(\sigma_{1,2}, \omega, T) \rangle_{\omega} + \frac{2}{\sigma_{1,2}^2} \int_{\sigma_{1,2}}^{\infty} \langle P_{l_1 l_2}(b, \omega, T) \rangle_{\omega} b db \right], \quad (A1)$$

where *f*(*j*<sub>1</sub>) and *f*(*j*<sub>2</sub>) are the rotational distribution functions for molecules 1 and 2 with initial rotational quantum numbers *j*<sub>1</sub> and *j*<sub>2</sub>. The summation includes all of the respective allowed choices of initial and final rotational quantum numbers *j*<sub>1</sub>→*j*<sub>1</sub>' and *j*<sub>2</sub>→*j*<sub>2</sub>' for molecules 1 and 2. The velocity averaged probability  $\langle P_{l_1 l_2}(b, \omega, T) \rangle_{\omega}$  is defined in Eq. (13) of Ref. 33.

The integration over impact parameter *b* of Eq. (A1) follows the approximation of J. Fiutak and J. Van Kranendonk [Can. J. Phys. 41, 21 (1963)] which those authors have referred to as "Case II." This approximation is necessary because the constant velocity trajectory assumption becomes invalid for close collisions, (*b* < σ<sub>L1</sub>); Expression (A1) leads to a somewhat overestimated value for the over-all probability of transfer.<sup>35,48</sup>

The parameters which enter the computer calculation of  $\langle P_{i10}(b, \omega, T) \rangle_n$  are given in Table II; the notation used here is the same as that of Ref. 33.

\* Supported by the Advanced Research Projects Agency under ONR contract N00014-67-A-0077-0006, by the U.S. Air Force Office of Scientific Research under Grant AFOSR-70-1952, and by the National Aeronautics and Space Administration under Grant NGL 33-010-064.

† NSF Trainee, present address: Hughes Research Laboratories, Malibu, Calif.

<sup>1</sup> D. J. Spencer, H. Mirels, T. A. Jacobs, and R. W. F. Gross, *Appl. Phys. Letters* **16**, 235 (1970).

<sup>2</sup> T. A. Cool, R. R. Stephens, and J. A. Shirley, *J. Appl. Phys.* **41**, 4038 (1970).

<sup>3</sup> C. Wittig, J. C. Hassler, and P. D. Coleman, *Nature* **226**, 645 (1970).

<sup>4</sup> J. A. Glaze, J. Finzi, and W. F. Krupke, *Appl. Phys. Letters* **18**, 173 (1971).

<sup>5</sup> R. A. Meinzer, *Intern. J. Chem. Kinetics* **2**, 335 (1970).

<sup>6</sup> The term "chemical laser" refers to the fact that the laser pumping requires conversion of the energy release of chemical reactions into the specific (nonthermal) vibrational excitation of reaction products [K. E. Shuler, *Appl. Opt. Suppl.* **2**, 1 (1965)]. The term "transfer chemical laser" distinguishes those systems for which a vibrational energy transfer process from a product molecule to another molecule (e.g., CO<sub>2</sub>) is requisite to laser operation.

<sup>7</sup> T. A. Cool, T. J. Falk, and R. R. Stephens, *Appl. Phys. Letters* **15**, 318 (1969).

<sup>8</sup> J. R. Airey and S. F. Fried, *Chem. Phys. Letters* **8**, 23 (1971).

<sup>9</sup> W. C. Solomon, J. A. Blauer, F. C. Jaye, and J. G. Hnat, *Intern. J. Chem. Kinetics* **3**, 215 (1971).

<sup>10</sup> J. F. Bott and N. Cohen, *J. Chem. Phys.* **55**, 5124 (1971).

<sup>11</sup> R. S. Chang, R. A. McFarlane, and G. J. Wolga, *J. Chem. Phys.* **6**, 667 (1972).

<sup>12</sup> C. B. Moore, *Fluorescence*, edited by C. G. Guilbault (Dekker, New York, 1967), pp. 133-198.

<sup>13</sup> (a) H. K. Shin, *Chem. Phys. Letters* **10**, 81 (1971); (b) H. K. Shin, *J. Phys. Chem.* **75**, 1079 (1971).

<sup>14</sup> R. R. Stephens and T. A. Cool, *Rev. Sci. Instr.* **42**, 1489 (1971).

<sup>15</sup> An rf discharge was used for partial dissociation of F<sub>2</sub> (instead of SF<sub>6</sub> as described in Ref. 14); further details are given in Ref. 26.

<sup>16</sup> G. T. Armstrong and R. S. Jessup, *J. Res. Natl. Bur. Std.* **64A**, 49 (1960).

<sup>17</sup> H. L. Chen and C. B. Moore, *J. Chem. Phys.* **54**, 4072 (1971).

<sup>18</sup> The radiative lifetime of the CO<sub>2</sub>(00<sup>0</sup>1) state is approximately 2.4 msec [D. Weber, R. J. Holm, and S. S. Penner, *J. Chem. Phys.* **20**, 1820 (1952)]; R. J. Lovell and W. F. Herget [*J. Opt. Soc. Am.* **52**, 1374 (1962)] have given a value for the dipole derivative of HF of  $M_1 = 1.5 \times 10^{-20}$  esu and a value for the square of the transition dipole moment of  $|R_0|^2 = 0.97 \times 10^{-20}$  esu<sup>2</sup>·cm<sup>2</sup> for HF. The square of the transition dipole moment for DF may be estimated from the relationship  $|R_0|^2 = (M_1/r_e)^2 B_e/\omega_e$ , if we assume that  $M_1$  is the same for both HF and DF; this leads to the estimate  $|R_0|^2 = 7 \times 10^{-20}$  esu<sup>2</sup>·cm<sup>2</sup> for DF. The radiative lifetimes corresponding to the above matrix elements are about 5.5 and 19 msec, respectively.

<sup>19</sup> The measured rate of V→V transfer from DF to CO<sub>2</sub> cor-

responds to only about 40 collisions; the creation of an intermediate state, e.g., DF(v=1) + CO<sub>2</sub>(00<sup>0</sup>0) → DF(v=0) + CO<sub>2</sub>(01<sup>1</sup>1) + ΔE = -73 cm<sup>-1</sup>, followed by the process CO<sub>2</sub>(01<sup>1</sup>1) + CO<sub>2</sub>(00<sup>0</sup>0) → CO<sub>2</sub>(01<sup>1</sup>0) + CO<sub>2</sub>(00<sup>0</sup>1) seems unlikely because of the smallness of the matrix element associated with the CO<sub>2</sub>(00<sup>0</sup>0) → CO<sub>2</sub>(01<sup>1</sup>1) transition.

<sup>20</sup> R. Oberley, K. N. Rao, Y. H. Hahn, and T. K. McCubbin, *J. Mol. Spectry.* **25**, 138 (1968).

<sup>21</sup> An estimate of the highest possible intercept of the ordinate of Fig. 4 for X<sub>DF</sub>→0 consistent with 5% error estimates on the 100 torr argon data points leads to the bound:  $k_{21} < 100 \text{ sec}^{-1} \text{ torr}^{-1}$ . The same bound on the HF-argon deactivation rate,  $k_{21} < 100 \text{ sec}^{-1} \text{ torr}^{-1}$ , was obtained from the HF data of Fig. 6.

<sup>22</sup> C. T. Bowman and D. J. Seery, *J. Chem. Phys.* **50**, 1604 (1969).

<sup>23</sup> J. T. Yardley and C. B. Moore, *J. Chem. Phys.* **46**, 4491 (1967).

<sup>24</sup> If the observed relaxation times  $\tau$  exceeded 50 μsec, then corrections were made to the decay times for the effect of the 2.4 msec spontaneous emission lifetime.

<sup>25</sup> J. C. Stephenson and C. B. Moore, *J. Chem. Phys.* **52**, 2333 (1970).

<sup>26</sup> R. R. Stephens, Ph.D. thesis, Cornell University.

<sup>27</sup> Near resonant processes of this type in CO<sub>2</sub> are known to be fast. Examples are the processes CO<sub>2</sub>(10<sup>0</sup>0) + CO<sub>2</sub>(00<sup>0</sup>0) → 2CO<sub>2</sub>(01<sup>1</sup>0) + ΔE = -51 cm<sup>-1</sup>, and CO<sub>2</sub>(02<sup>0</sup>0) + CO<sub>2</sub>(00<sup>0</sup>0) → 2CO<sub>2</sub>(01<sup>1</sup>0) + ΔE = -49 cm<sup>-1</sup> which require about 50 collisions [C. K. Rhodes, M. J. Kelly, and A. Javan, *J. Chem. Phys.* **48**, 5730 (1968)].

<sup>28</sup> J. A. Shirley, R. N. Sileo, R. R. Stephens, and T. A. Cool, "Purely chemical laser operation in the HF, DF, HF-CO<sub>2</sub>, and DF-CO<sub>2</sub> systems," AIAA Paper No. 71-27, AIAA 9th Aerospace Sciences Meeting, New York, 25-27 January 1971.

<sup>29</sup> C. B. Moore, *J. Chem. Phys.* **43**, 2979 (1965).

<sup>30</sup> Note that the measured rate is over 4 times faster than the value estimated indirectly by N. G. Basov *et al.*, *Appl. Opt.* **10**, 814 (1971).

<sup>31</sup> H. L. Chen, J. C. Stephenson, and C. B. Moore, *Chem. Phys. Letters* **2**, 593 (1968).

<sup>32</sup> T. A. Cool and J. C. Kershenstein, "Vibrational Energy Transfer between D<sub>2</sub> and CO<sub>2</sub>" (unpublished).

<sup>33</sup> R. D. Sharma and C. A. Brau, *J. Chem. Phys.* **50**, 924 (1969).

<sup>34</sup> J. C. Stephenson, R. E. Wood, and C. B. Moore, *J. Chem. Phys.* **48**, 4760 (1968).

<sup>35</sup> K. F. Herzfeld and T. A. Litovitz, *Absorption and Dispersion of Ultrasonic Waves* (Academic, New York, 1959), Chap. 7.

<sup>36</sup> R. D. Sharma, *J. Chem. Phys.* **50**, 919 (1969).

<sup>37</sup> H. J. Kolker, *Chem. Phys. Letters* **10**, 498 (1967).

<sup>38</sup> J. Stephenson, R. E. Wood, and C. B. Moore, *J. Chem. Phys.* **54**, 3097 (1971).

<sup>39</sup> S. S. Penner, *Quantitative Molecular Spectroscopy and Gas Emissivities* (Addison-Wesley, Reading, Mass., 1959), p. 152.

<sup>40</sup> A. A. Maryott and G. Birnbaum, *J. Chem. Phys.* **47**, 3200 (1967).

<sup>41</sup> M. R. Atwood, H. Vu, and B. Vodar, *Spectrochim. Acta* **A23**, 553 (1967).

<sup>42</sup> S. Bratoz and M. L. Martin, *J. Chem. Phys.* **42**, 1051 (1965).

<sup>43</sup> T. G. Burke and D. F. Smith, *J. Mol. Spectry.* **3**, 381 (1967).

<sup>44</sup> J. E. Lennard-Jones, *J. Chem. Phys.* **20**, 1024 (1952).

<sup>45</sup> Unpublished data (this laboratory).

<sup>46</sup> C. J. Gray and J. Van Kranendonk, *Can. J. Phys.* **44**, 2411 (1966).

## II. Rapid Gas Mixing Studies (D. Turcotte)

In most chemical lasers the reactants are mixed and then react spontaneously. The mixing process introduces a mixing time which may or may not be shorter than the characteristic time for the chemical reaction. In order to get the expected performance from a chemical laser the mixing time should be of the same order as the chemical reaction time. The failure of several chemical lasers to perform up to the expected power levels has been blamed in part on inadequate mixing.

Rapid mixing may be achieved by decreasing the mixing scale. However the design of very small injectors is expensive and may in fact be impossible for large devices. For small injectors mixing is expected to be laminar and the laminar theory of mixing is well developed. One method of providing more rapid mixing is to introduce turbulence. It is known that turbulent mixing may be orders of magnitude more rapid than laminar mixing. Turbulence may be produced simply by using injectors which are sufficiently large to produce turbulent eddies or the turbulence may be introduced artificially by using grids upstream of the mixing region. No adequate theory exists for turbulent mixing and very few experiments have been carried out on turbulent mixing at low pressures.

In order to study mixing at low pressures a mixing wind tunnel has been designed and built. The mixing tunnel is illustrated in Figure 1. The plenum chamber of the wind tunnel is divided into two parts by a splitter plate. The two gases that are to be mixed are metered into the two plenum chambers. All experiments used helium and argon. The splitter plate ends

with a sharp edge at the beginning of the constant area mixing section. The mixing section has a 3/8" by 3/4" cross section and is 4" long. The mixing section exhausts into a plenum which is maintained at a low pressure by a vacuum pump. Just upstream of the mixing region grids of various size wires could be placed to induce turbulence.

Flow velocities were obtained using a pitot probe. The pitot probe was also used to obtain the variation in static pressure across the mixing zone. Concentration profiles were obtained using a sampling probe. Gas samples extracted from the mixing region were analyzed using a thermal conductivity cell. This cell is illustrated in Figure 2. The cell contains four heated, thin resistance wires. The sampled gas passes over two of the wires while a reference gas (in this case argon) passes over the two remaining wires. The four wires comprise a bridge circuit which measures the difference in the voltage drop between a wire in the reference gas and a wire in the sampled gas. This voltage difference  $\Delta V$  is related to the thermal conductivities  $k$  of the two gases by

$$\Delta V = C \left( \frac{1}{k_{\text{ref}}} - \frac{1}{k_{\text{sample}}} \right) \quad (1)$$

where  $C$  is a constant that is evaluated by calibration. With the probe sampling pure helium the two thermal conductivities are known,  $\Delta V$  is measured, and  $C$  is determined. Using this value of  $C$ ,  $\Delta V$  is measured across the mixing zone and the thermal conductivity profile is determined. The dependence of thermal conductivity on the relative ratios of helium and argon is known<sup>1</sup> so that the concentration profile is then determined. A complete schematic diagram is shown in Figure 3.

---

<sup>1</sup>S. Chapman and T. G. Cowling. The Mathematical Theory of Non-Uniform Gases (Cambridge, 1960).

### Laminar Measurements

For the constant velocity ( $u$ ), laminar mixing of helium and argon it is expected that the molal concentration of helium,  $c_{\text{He}}$ , will satisfy the equation

$$u \frac{\partial c_{\text{He}}}{\partial x} = D_{\text{HeA}} \frac{\partial^2 c_{\text{He}}}{\partial y^2} \quad (2)$$

where  $x$  is measured along the channel and  $y$  is measured across it with  $D_{\text{HeA}}$  the binary diffusion coefficient for the mixing of helium and argon. Since mixing occurs only in the central part of the channel it is appropriate to apply the boundary conditions  $c_{\text{He}} \rightarrow 0$  as  $y \rightarrow -\infty$  and  $c_{\text{He}} \rightarrow 1$  as  $y \rightarrow +\infty$ . The solution of eq. (1) that satisfies these boundary conditions is

$$c_{\text{He}} = \frac{1}{2} \left[ 1 + \operatorname{erf} \left( \frac{y}{2} \left\{ \frac{u}{D_{\text{HeA}} x} \right\}^{\frac{1}{2}} \right) \right] \quad (3)$$

Three measured concentration profiles are given in Figure 4. These were obtained at  $x = 5.2$  cm. Velocities of 100 and 200 m/sec and pressures of 20 and 30 torr were considered. The measurements are compared with the profile given in eq. (2) using the accepted value<sup>1</sup> for  $D_{\text{HeA}}$ ,  $D_{\text{HeA}} = 17.8 \text{ cm}^2/\text{sec}$  for  $p = 30$  torr. The agreement between theory and experiment is reasonably good.

The most significant result of the laminar measurements is not illustrated in the above analysis. The observed center line for mixing is given in Table 1 for the three cases considered. With equal velocities of helium and argon about 60% of the channel is filled with argon. If equal amounts of argon and helium were metered into the channel, it was found that the velocity of the helium would be nearly

Table 1

pressure torr	velocity m/s	fraction of channel filled with argon	$\frac{P_A - P_{He}}{\frac{1}{2} \rho_{He} u^2}$
30	100	0.605	1.35
30	200	0.575	1.27
20	200	0.622	1.22

twice as large as the velocity of argon and that about two-thirds of the channel would be filled with argon. The thickness of the mixing region in this situation would be about one-half that observed for constant velocity mixing.

In order to investigate this peculiar behavior the static pressure was measured across the mixing zone. If the variation in static pressure across the zone is a significant fraction of  $\frac{1}{2} \rho_{He} u^2$  then an influence of mixing on flow is to be expected. In Table 1 the measured values of  $(P_A - P_{He}) / \frac{1}{2} \rho_{He} u^2$  are given for the three cases. It is seen that this ratio is in fact of order unity so that it is not surprising that the mixing induced pressure gradient has a significant effect on the flow.

This lateral pressure gradient is clearly a deviation from ideal mixing. In ideal mixing the interaction forces between the two gases are equal and opposite as they mix so that a symmetric mixing profile is obtained as shown in Figure 4. However the argon being heavier than helium has a greater inertia. In the rapid mixing studies considered here this inertia is significant and the slowness of the argon to move into the helium results in the higher pressure in the argon which is measured here. To date a quantitative theory has not been developed.

### Turbulent Measurements

In order to study the influence of turbulence on mixing, screens were placed across the flow at the entrance to the mixing section. The results for two screens are shown in Figure 5. These measurements were carried out with  $p = 30$  torr,  $u = 100$  m/s, and  $x = 5.2$  sec. The screens had wire diameters of 0.012 in. and 0.018 in. For the finer screen the concentration in helium-rich mixtures was unaffected but a turbulent enhancement of mixing is noted for the argon-rich mixtures. This difference can be explained by the different densities for argon and helium and the resultant differences in Reynolds number based on screen wire diameter. The Reynolds number for the screen in argon is a factor of ten larger than the Reynolds number for the screen in helium. For the coarser screen no additional mixing is observed in the argon but the mixing in the helium is now as effective as in the argon. Apparently the transition Reynolds number for the screen in helium has now been exceeded and turbulence is being produced.

It should be noted that the pressure drop across the screen in the argon is much greater than the pressure drop in the helium. This is because the pressure drop is proportional to  $\rho u^2$ . Because of this effect the helium may be accelerated through the screen relative to the argon and a "jet" effect obtained, thereby inhibiting mixing. It is necessary that turbulence be introduced before mixing takes place to prevent this effect.

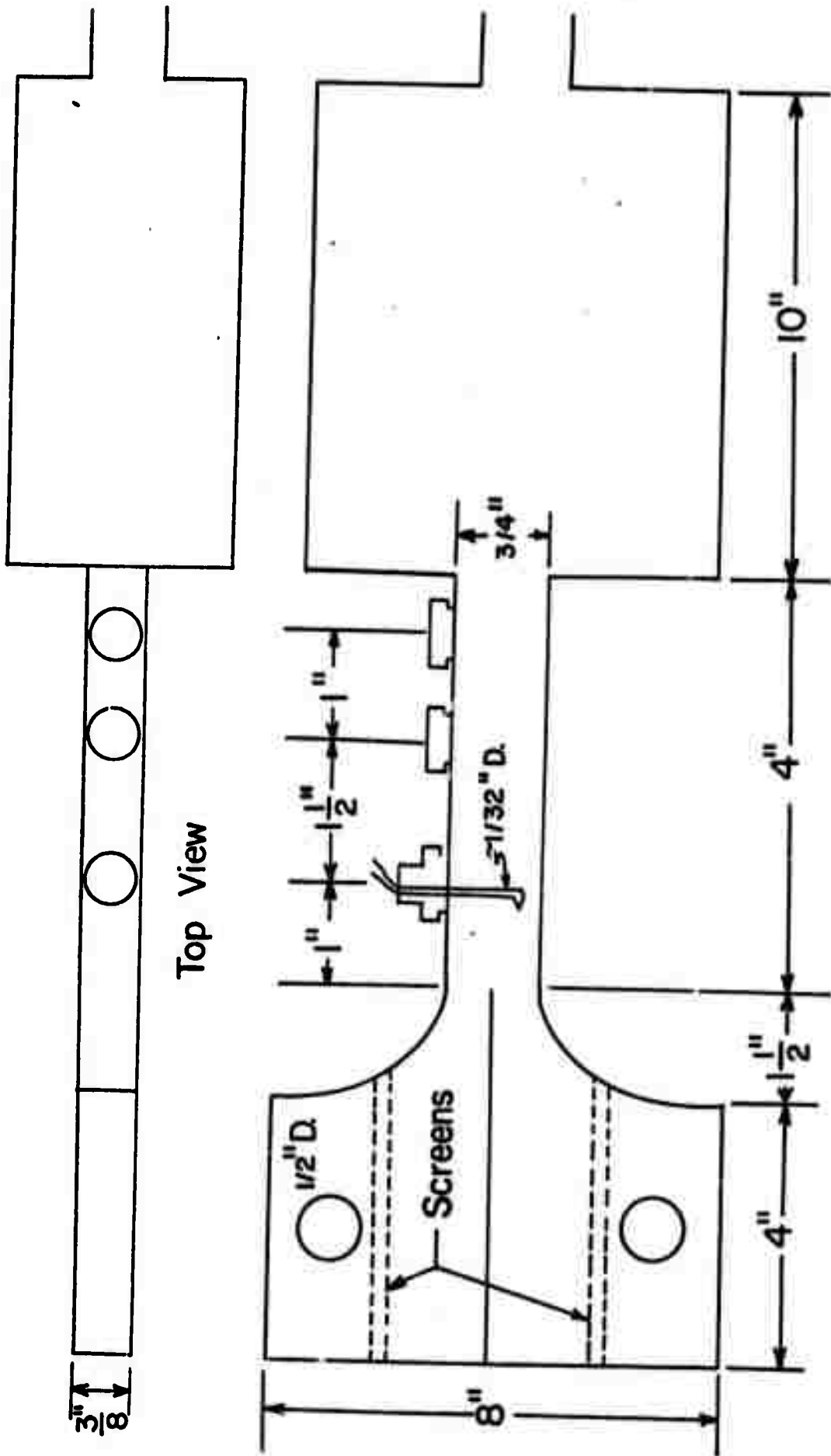
In Figure 6 the development of the turbulent mixing is shown. Mixing profiles at the three measuring stations are compared with the laminar measurement at  $x = 5.2$  cm and the laminar theory. These

results are for the 0.012 in. screen. It should be noted that the increase in mixing observed in this figure is in addition to the spread of the laminar mixing profile.

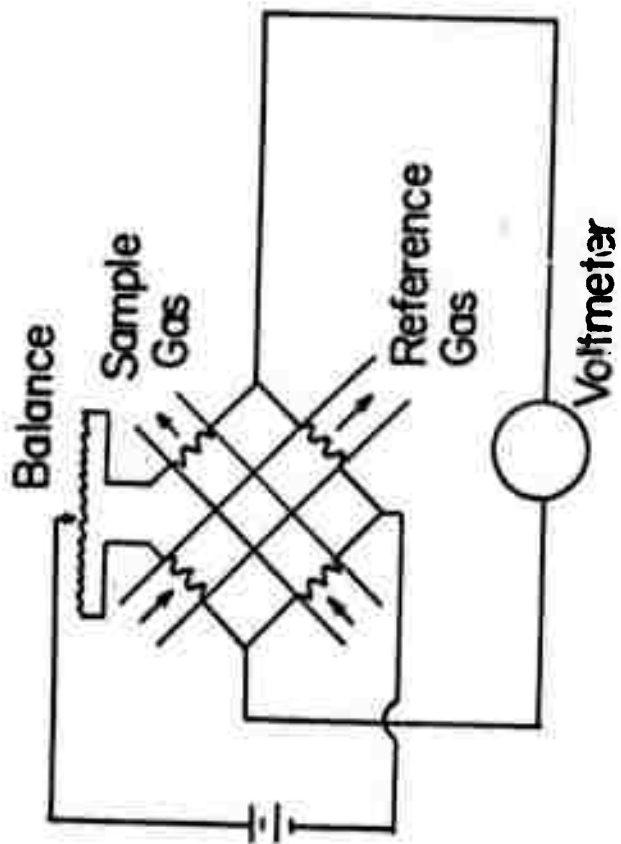
In conclusion two important results have been obtained:

- (1) Turbulence can be introduced to enhance mixing at low pressures.
- (2) Transverse pressure gradients heretofore neglected can strongly influence relative velocities of the mixing gas streams and thereby inhibit mixing. Care must be taken to prevent this effect. If a simple jet of a low molecular weight gas is introduced into a high molecular weight gas the transverse pressure effect will accelerate the low molecular weight jet thereby reducing the mixing predicted by the usual laminar theory by a factor of two to three.

# Test Chamber



Side View  
Figure 1



Thermoconductivity Cell Circuit

Figure 2

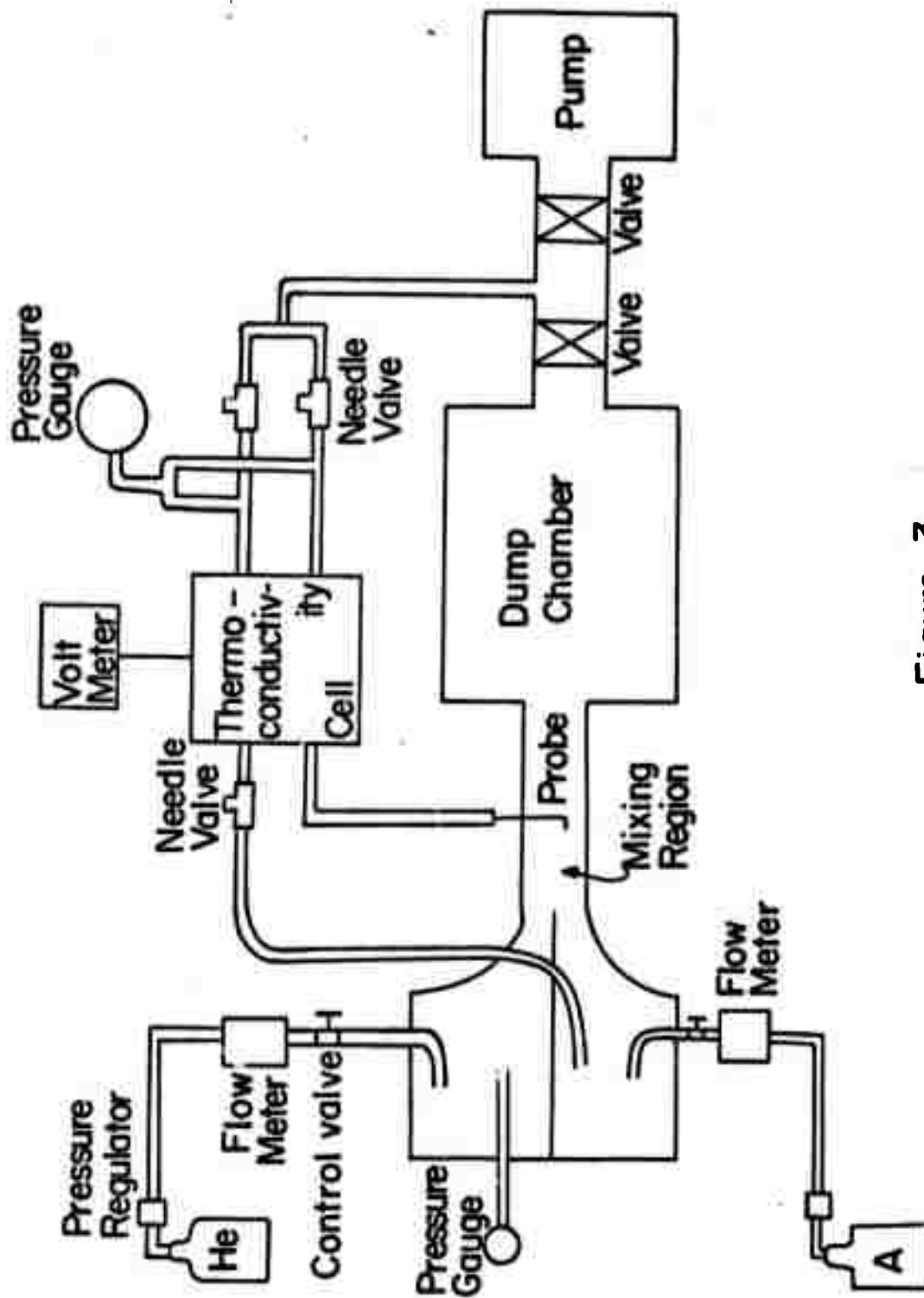


Figure 3

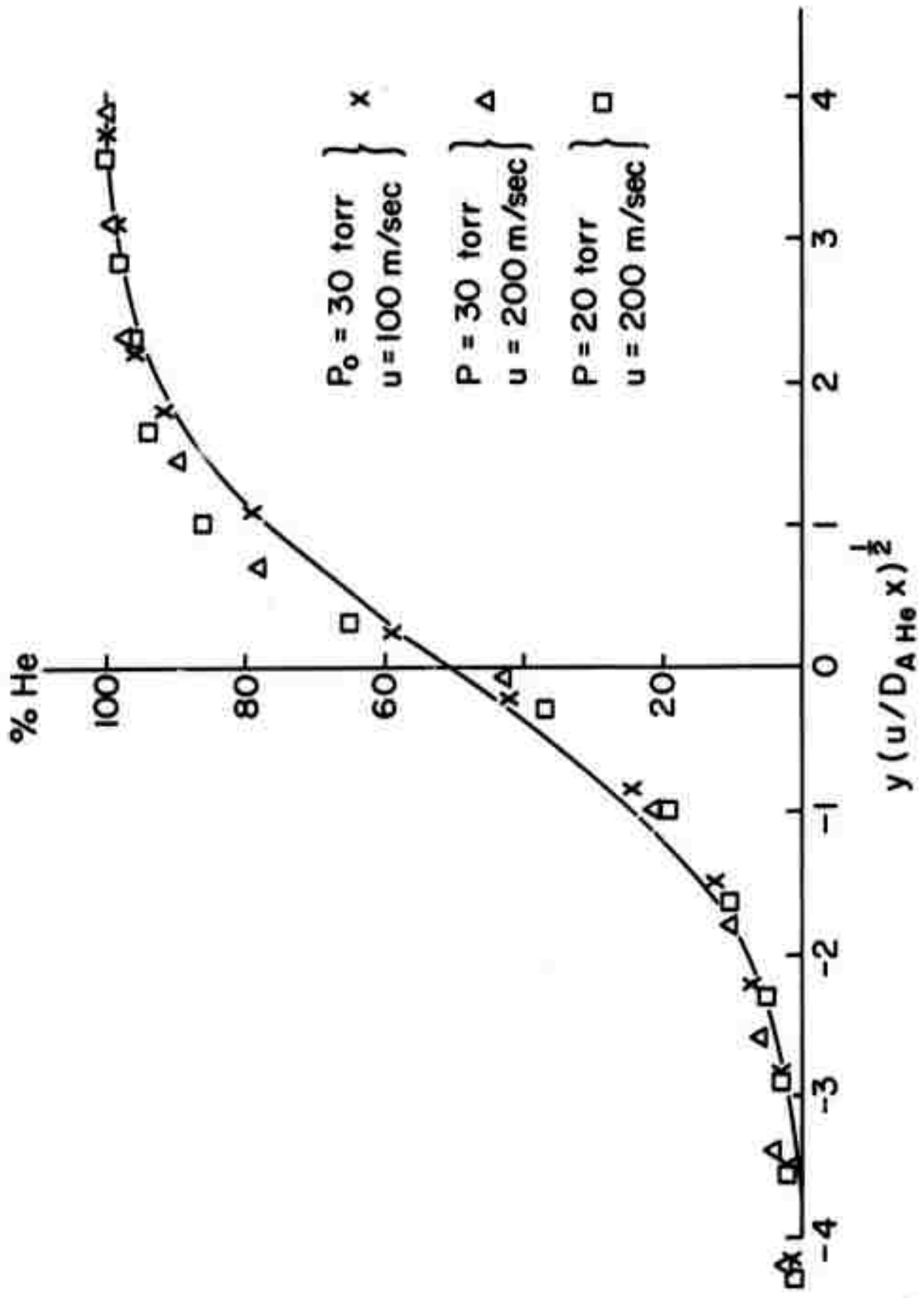


Figure 4

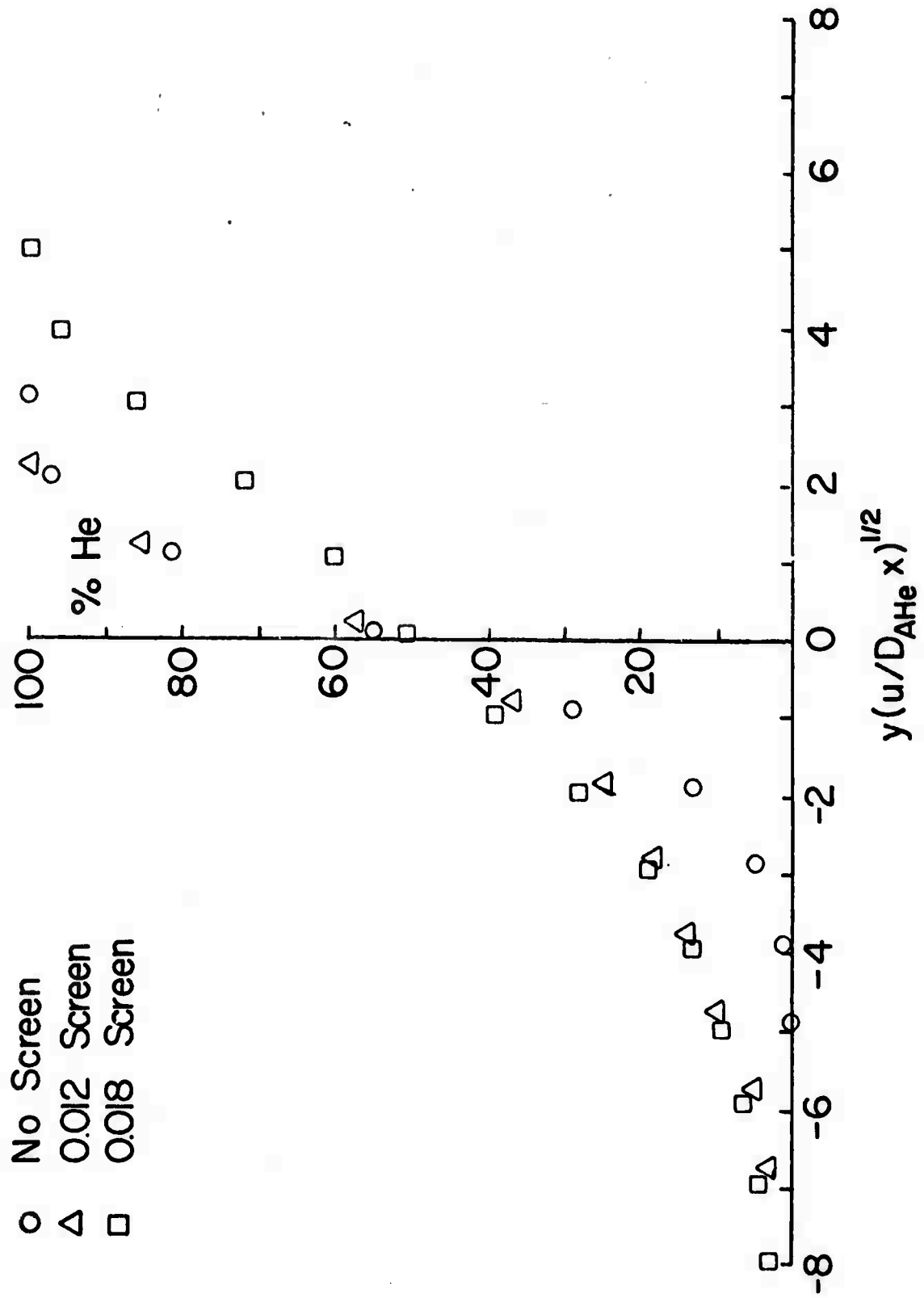


Figure 5

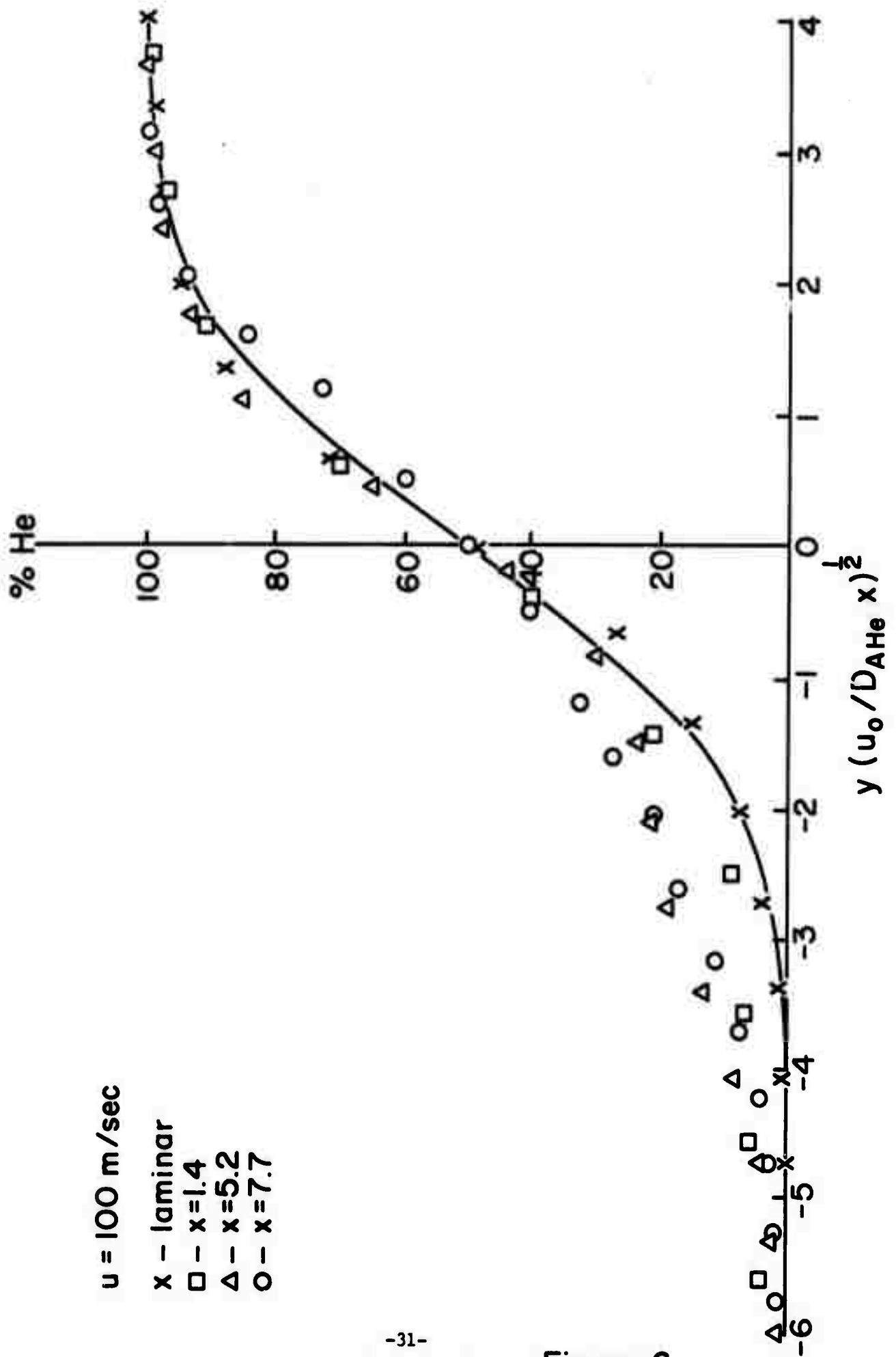


Figure 6

### III. Vibrational Relaxation

#### A. High Pressure Relaxation in CO<sub>2</sub>(00<sup>1</sup>) (Wolga)

##### 1. HBr Chemical Laser Studies

The object of this program is to determine the relaxation time of CO<sub>2</sub>(00<sup>1</sup>) due to collisions with CO<sub>2</sub>, N<sub>2</sub>, He, etc., in the pressure range 1-100 atm. and at temperatures up to 600°K. The experimental plan is to use laser induced fluorescence from the CO<sub>2</sub>(00<sup>1</sup>) state with laser pumping by  $v = 2 \rightarrow 1$  transitions in the HBr chemical laser. In the process of developing an HBr laser with adequate performance as a pump source for this experiment extensive studies were carried out to study beneficial additives if any, and possibly improved H atom sources. The latter study was motivated by the fact that the chain propagating step in the  $H_2 + Br_2$  chemical reaction,  $Br + H_2 \rightarrow HBr + H$ , is endothermic by 16.7 K cal/mole, is very slow, and does not therefore contribute to the reaction within the short time of the chemical laser pulse. A detailed discussion of our studies of H atom sources for pulsed, electrical discharge initiated hydrogen halide chemical lasers, and of our design and construction of a powerful HBr chemical laser with substantial emission at 4.2  $\mu$  was included in our Semi Annual Report for 1972 and will not be repeated here.

2. The remainder of the past contract year was devoted to completing preparations for the measurement of the high pressure V-T relaxation of CO<sub>2</sub>(00<sup>1</sup>). The HBr laser yields pulses of several microsecond duration. Since the CO<sub>2</sub> fluorescence will be monitored in this experiment it is necessary that the exciting laser pulse be short compared to the V-T relaxation time of CO<sub>2</sub>. We plan to employ an electrooptic shutter to select a portion of the HBr laser

pulse, external to the laser cavity thereby achieving the required short, variable pumping pulse. An electrooptic shutter has been designed and constructed. It uses an  $(\bar{1}\bar{1}0)$  oriented, 40 mm long single crystal slab of GaAs that is electroded transverse to the optical path through the crystal on  $1\bar{1}0$  faces. An appropriate triggerable, high voltage source was purchased to drive the GaAs crystal. The GaAs crystal operates in conjunction with a Ge slab analyzer to divert a selected portion of the output laser pulse.

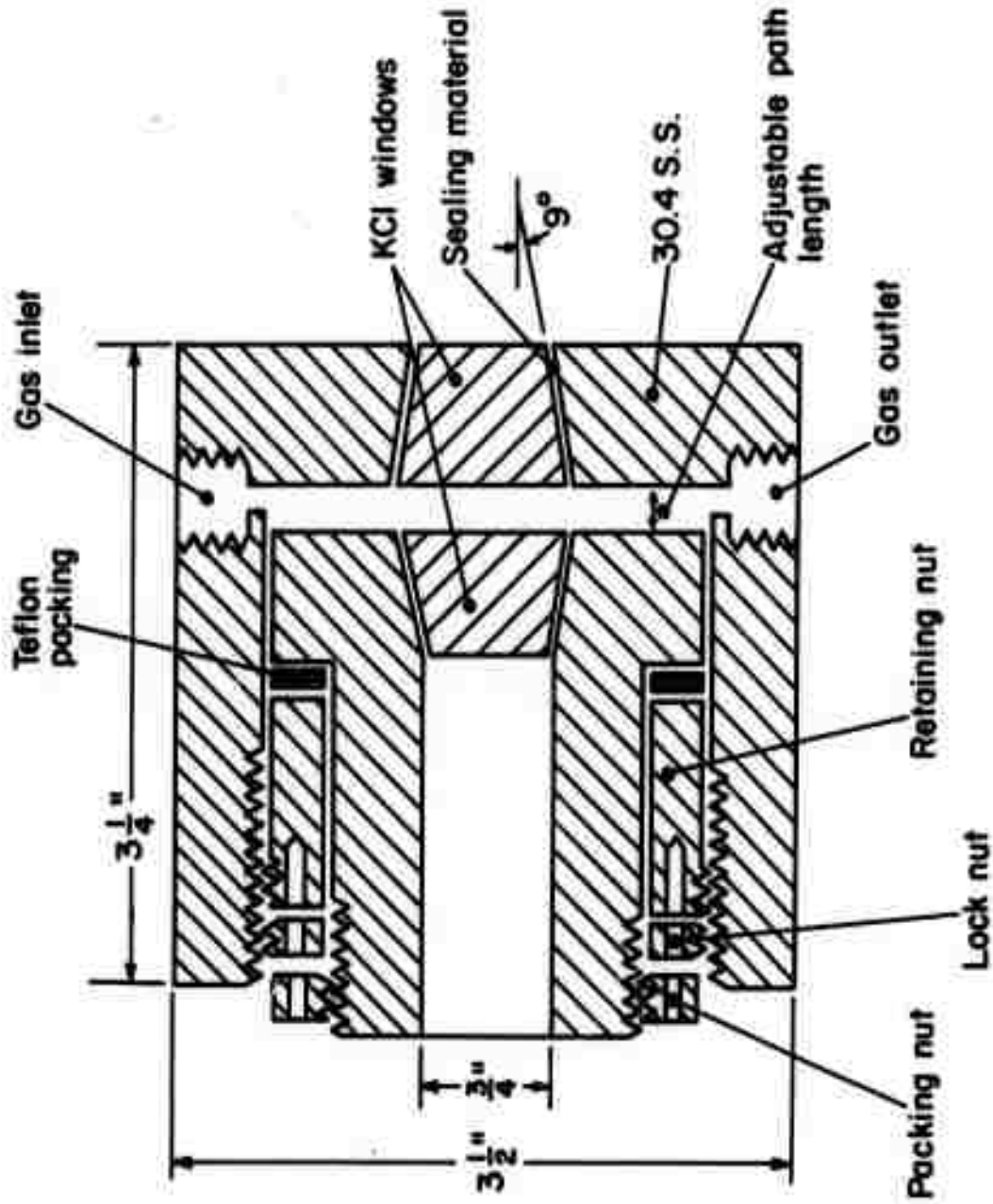
An optical cell was designed and constructed for carrying out the laser induced fluorescence measurement. The cell is capable of operating from good vacuum conditions to an overpressure of 100 atmospheres. Its design is compatible with installation in a dewar for experiments at low temperatures and it can be externally heated as well. The path length within the cell is made variable to accommodate the very short absorption lengths to be expected at high pressures. A schematic drawing of the cell is shown in the figure.

At the time this report was in preparation experiments were in progress.

B. Vibrational Relaxation and Chemical Reactions (Bauer)

During the past summer we undertook a concerted effort to assemble and test several computer programs for modeling chemically reacting systems which V-T and V-V processes are specifically included. While such programs are available in many other laboratories we have not been able to obtain sufficiently detailed statements to permit their direct use on our IBM 360-65 computer. Another drawback (besides the problem of adaptation) is the length and consequent excessive cost of running these computer programs in

# HIGH PRESSURE IR CELL



in our installation. During July-September a modified Runge-Kutta integration scheme for multiple, concurrent, first order non-linear differential equations was set up and tested on two reactions:  $[F_2 + NO]$  and  $[CS_2 + O_2 (10\% \text{ dissociated})]$ . This program incorporates (a) the Treanor modifications for rapid convergence (b) reverse steps for all reactions, (c) V-T relaxation processes, and (d) the option of running the system either isothermally or adiabatically, at constant pressure, to simulate rapid flow or shock conditions. In addition, a program developed by Professor E. R. Fisher (Wayne State University) has been adopted for our computer. This includes subroutines for calculating V-V transition probabilities, and their incorporation into the kinetic scheme. More important, to permit integration of "stiff" equations (when fast rates of destruction approach fast rates of production, such that the system enters a steady state condition) the program switches from integration of differential equations to the solution of algebraic equations (Keneshea technique). This program is currently being tested on an artificial model, the dissociation of hydrogen at room temperature initiated by exciting 1% of the molecules to the  $v = 1$  state.

#### IV. Chemical Laser Studies and Rate Determination

##### A. EPR Study of the NO + F<sub>2</sub> Reaction (G. J. Wolga)

The chemical decomposition of F<sub>2</sub> by reaction with NO has been extensively employed in the purely chemical, DF/HF - CO<sub>2</sub>, transfer studies by Cool, Falk and others. Until now, the rates for the primary reaction  $\text{NO} \xrightarrow{k_1} \text{NOF} + \text{F}$  and the secondary reaction  $\text{F} + \text{NO} \xrightarrow{k_2} \text{NOF}$  have been taken from the work of Rapp & Johnson<sup>(1)</sup> who used visible emission studies of light emitted from a dilute diffusion flame together with extensive analysis to deduce these rates. These authors stated that the interpretation of their results was somewhat ambiguous. Since both NO and F are paramagnetic, their concentrations may be followed quantitatively in a flow system using EPR absorption measurements. We have done this by fitting a fast-flow mixing system to an x-band EPR spectrometer and thereby measuring the growth of F concentration and the decay of NO concentration as a function of reaction time. The analysis of our results is entirely straightforward since the experiment is a simple one. A calibrated flow of NO is established upstream of the microwave cavity. A calibrated flow of F<sub>2</sub> is injected into the NO stream and the F and NO concentrations are monitored as a function of position downstream of the injection position. With a constant flow speed a conversion of downstream position to time of reaction is easily made.

The rates we have determined in this study are:

---

(1) Donald Rapp and Harold S. Johnson, J. Chem. Phys. 33, No. 3, 695 (Sept., 1960).

$$k_1 = 2.6 \times 10^9 \text{ cm}^3/\text{mole sec}$$

$$k_2 = 1.1 \times 10^{17} \text{ cm}^6/\text{mole}^2 \text{ sec}$$

The details concerning the experiment and the rate determinations are discussed more fully in the accompanying manuscript. It is clear from our work that mathematical modeling studies of the DF - CO<sub>2</sub> laser utilizing the NO + F<sub>2</sub> → NOF + F reaction as a source of F atoms must use the rates determined in this work rather than those of Rapp & Johnson.

REACTION KINETICS OF  $\text{NO} + \text{F}_2 \rightarrow \text{FNO} + \text{F}$  AND  
 $\text{F} + \text{NO} + \text{M} \rightarrow \text{FNO} + \text{M}$  USING EPR DETECTION

by

E. S. Mooberry and G. J. Wolga

Laboratory of Plasma Studies

and

School of Electrical Engineering

July 1972

Cornell University

Ithaca, New York 14850

This research was supported by the Advanced Research Projects Agency of the Department of Defense and was monitored by ONR under Contract No. N00014-67-A-0077-0006. Use of the central facilities of the Cornell Materials Science is acknowledged.

ABSTRACT

The reactions of nitric oxide with fluorine molecules and fluorine atoms were studied using EPR detection. The two rate constants determined are: the reaction  $\text{NO} + \text{F}_2 \xrightarrow{k_1} \text{FNO} + \text{F}$ ,  $k_1 = 2.6 \times 10^9 \text{ cm}^3/\text{mole sec}$ ; and for the reaction  $\text{NO} + \text{F} + \text{M} \xrightarrow{k_2} \text{FNO} + \text{M}$ ,  $k_2 = 1.1 \times 10^{17} \text{ cm}^6/\text{mole}^2 \text{ sec}$ .

REACTION KINETICS OF  $\text{NO} + \text{F}_2 \rightarrow \text{FNO} + \text{F}$  AND  
 $\text{F} + \text{NO} + \text{M} \rightarrow \text{FNO} + \text{M}$  USING EPR DETECTION

by

E. S. Mooberry and G. J. Wolga

Laboratory of Plasma Studies

and

School of Electrical Engineering

Cornell University, Ithaca, New York

Because of the interest in the reaction



as a fluorine atom source for chemical lasers<sup>1</sup> the rate constants for reaction (1) and also the succeeding step



were measured. The reactions above have been studied previously by Rapp and Johnston<sup>2</sup> using the dilute diffusion flame method. At 298°K the rate constant for reaction (1) was determined to be  $4.9 \times 10^{10}$  cm<sup>3</sup>/mole sec. In an effort to check this value a study by EPR detection was undertaken.

The experimental setup was similar in design to that of Westenberg and DeHaas<sup>3</sup> utilizing a fixed EPR cavity and movable injector. Reaction (1) was studied by measuring the decay of [NO] with time under the condition  $[\text{NO}] < [\text{F}_2] < [\text{He}]$ . Good logarithmic decay plots of [NO] were found. See Fig. 1. Table I gives the data for several determinations of  $k_1$ . The fluorine atom concentration was also monitored by EPR detection and found to increase linearly with time for reaction distances up to ~40 cm. The [F] was found to correspond to the loss of [NO] down the reaction tube so that

for small distances the effect of reaction (2) was small, see Fig. 2. Reaction (2) was studied by discharging  $[F_2]$  in a sidearm and measuring the F atom decay as a function of distance down the reaction tube under the flow conditions:  $[F_2], [F] < [NO] < [He]$ . Table II gives the operating conditions and the values for  $k_2$  that were calculated from the logarithmic decay of F atoms as plotted in Fig. 3.

As reaction (2) is 55.4 kcal. exothermic it is assumed to be a three body reaction. The rate constant for the three body reaction of Cl atoms with NO has a similar rate in Helium of  $3 \times 10^{16} \text{ cm}^6/\text{mole}^2 \text{ sec.}^4$  The reactions of O and H atoms with NO are three body and have rates of the order of  $10^{16}$  also<sup>5,6</sup>.

A third reaction must be considered and that is the three body recombination of fluorine atoms:



where M is He or the wall. This reaction was found to be negligible under the present experimental conditions. The microwave discharge cavity was placed at several positions along the reaction tube while flowing a mixture of  $F_2$  with excess helium at a pressure of ca. 1 torr. No measureable difference in the EPR fluorine atom signal height was found at different distances from the cavity. This contrasts with the fast recombination found for chlorine atoms with uncoated quartz tubing.

The rate constants for the reaction of fluorine with nitric oxide have been measured in the present work. The value of  $k_1$  was found to be  $2.6 \times 10^9$  cc/mole sec which is more than an order of magnitude lower than the previous result. The present value of  $k_1$  was determined by loss of NO in the

reaction and by the production of F atoms and therefore should be a reliable indication of the reaction rate. On the other hand the present determination of  $k_2$  is somewhat more uncertain. The measured value determined from the direct reaction of F with NO when used in the computer analysis of the  $F_2 + NO$  reaction data leads to a prediction of about half the fluorine atom production actually observed. The value of  $8 \times 10^9$  cc/mole sec seems reasonable on comparison with the other NO reactions mentioned previously. Using these considerations the value of  $8 \times 10^9$  cc/mole sec should probably be considered only as an upper limit. Further study will be undertaken to clarify the second reaction rate.

REFERENCES

1. T. A. Cool and R. P. Stephens, J. Chem. Phys. 51, 5175 (1969).
2. D. Rapp and H. S. Johnston, J. Chem. Phys. 33, 695 (1960).
3. A. A. Westenberg and N. DeHaas, J. Chem. Phys. 46, 490 (1967).
4. T. R. Clark, M. A. A. Clyne and D. H. Stedman, Trans. Faraday Soc. 62, 3354 (1966).
5. F. S. Klein and J. T. Herron, J. Chem. Phys. 41, 1285 (1964).
6. M. A. A. Clyne and B. A. Thrush, Proc. Roy. Soc. (London), A275, 559 (1963).
7. S. W. Rabideau, H. G. Hecht and W. B. Lewis, 4th International Symposium on Magnetic Resonance, Rehovot and Jerusalem, Israel Aug. 23-31 (1971).

TABLE I

Summary of Measurements of the Rate Coefficient

 $k_1$  for  $F_2 + NO \rightarrow FNO + F$  298K

Pressure mm	Velocity cm/sec	$[F_2]$ moles/cm <sup>3</sup>	$3k_1$ cm <sup>3</sup> /mole sec
0.60	1190	$5.9 \times 10^{-9}$	$3.0 \times 10^9$
1.00	1770	6.5	2.6
1.00	1840	8.2	3.0
0.83	1460	10.6	2.0
			ave = $2.6 \pm 0.5 \times 10^9$

TABLE II

Summary of Measurements of the Rate Coefficient

for  $F + NO + M \xrightarrow{k_2} FNO + M$  298K

Pressure mm	Velocity cm/sec	[NO] moles/cm <sup>3</sup>	cm <sup>3</sup> k <sub>2</sub> [M] /mole sec	[M] moles/cm <sup>3</sup>	cm <sup>6</sup> k <sub>2</sub> /mole <sup>2</sup> sec
1.0	1950	4.4 x 10 <sup>-9</sup>	8.1 x 10 <sup>9</sup>	5.9 x 10 <sup>-8</sup>	1.4 x 10 <sup>17</sup>
1.3	2520	5.9	8.4	7.6 x 10 <sup>-8</sup>	1.1 x 10 <sup>17</sup>
1.3	2600	8.2	7.9	7.6 x 10 <sup>-8</sup>	1.0 x 10 <sup>17</sup>
					ave = 1.1 x 10 <sup>17</sup>

FIGURE CAPTIONS

Figure 1. Plots of  $\ln[\text{NO}]/[\text{NO}]_0$  vs. time. (1) Velocity = 1770 cm/sec,  $P = 1.0$  torr,  $[\text{NO}]_0 = 3.2 \times 10^{-9}$  mole/cm<sup>3</sup>,  $[\text{F}_2] = 6.5 \times 10^{-9}$  mole/cm<sup>3</sup>. (2) Velocity = 1840 cm/sec,  $P = 1.0$  torr,  $[\text{NO}]_0 = 3.2 \times 10^{-9}$  mole/cm<sup>3</sup>,  $[\text{F}_2] = 8.2 \times 10^{-9}$  mole/cm<sup>3</sup>.

Figure 2. Plot of  $[\text{F}]$  vs. time. Velocity = 1930 cm/sec,  $P = .92$  torr,  $[\text{F}_2] = 5.9 \times 10^{-9}$  mole/cm<sup>3</sup>,  $[\text{NO}]_0 = 3.0 \times 10^{-9}$  mole/cm<sup>3</sup>. Absolute F atom concentration determined by comparison of line "d" of atomic fluorine with line "E" of molecular oxygen<sup>7</sup>.

Figure 3. Plot of  $[\text{F}]$  vs. time for the reaction  $\text{F} + \text{NO} \rightarrow \text{FNO}$ . Velocity = 1950 cm/sec,  $P = 1.0$  torr,  $[\text{NO}] = 4.4 \times 10^{-9}$  mole/cm<sup>3</sup>,  $[\text{F}] = 1.35 \times 10^{-9}$  mole/cm<sup>3</sup> assuming complete dissociation of  $\text{F}_2$  by microwave discharge.

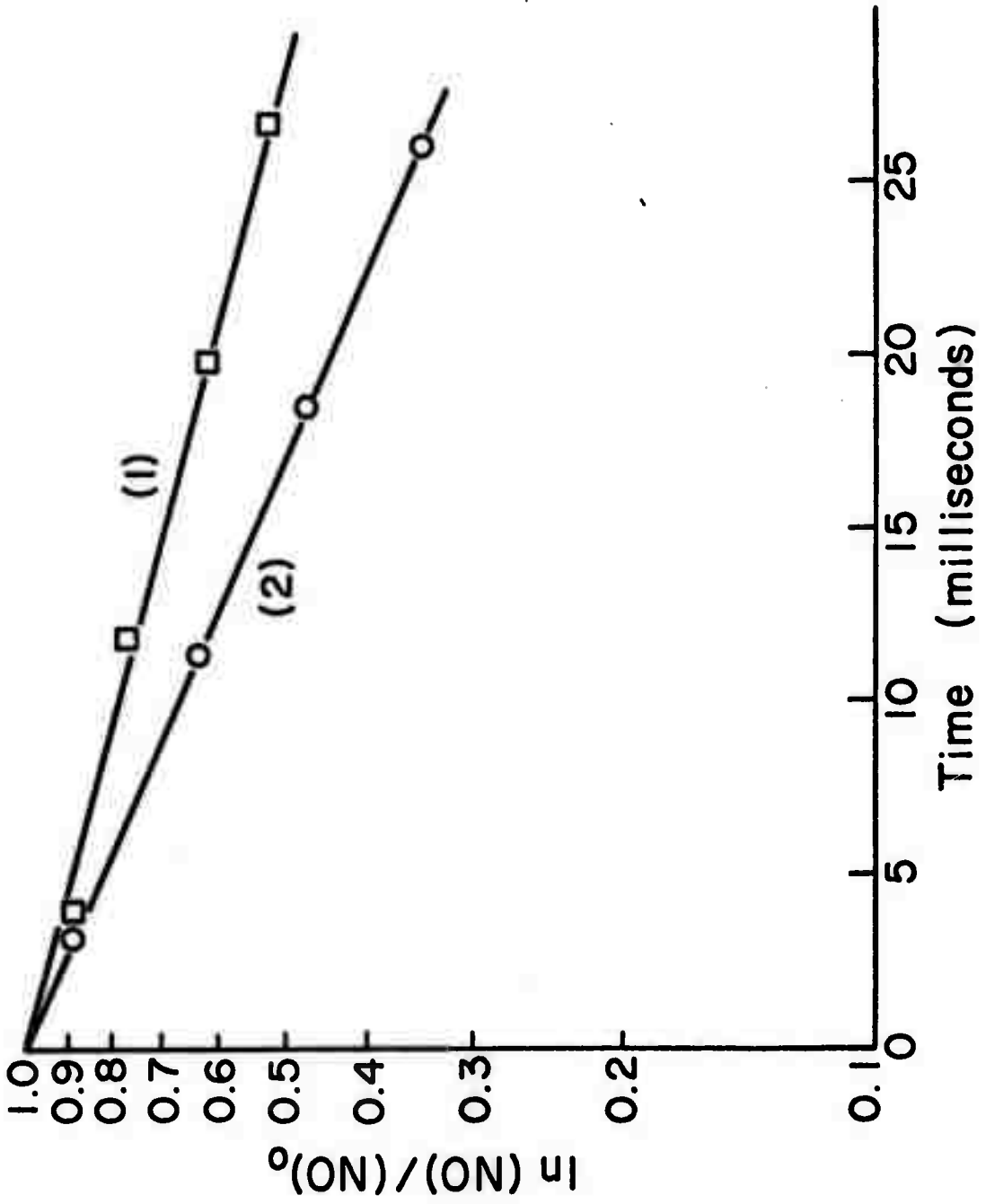


Figure 1.

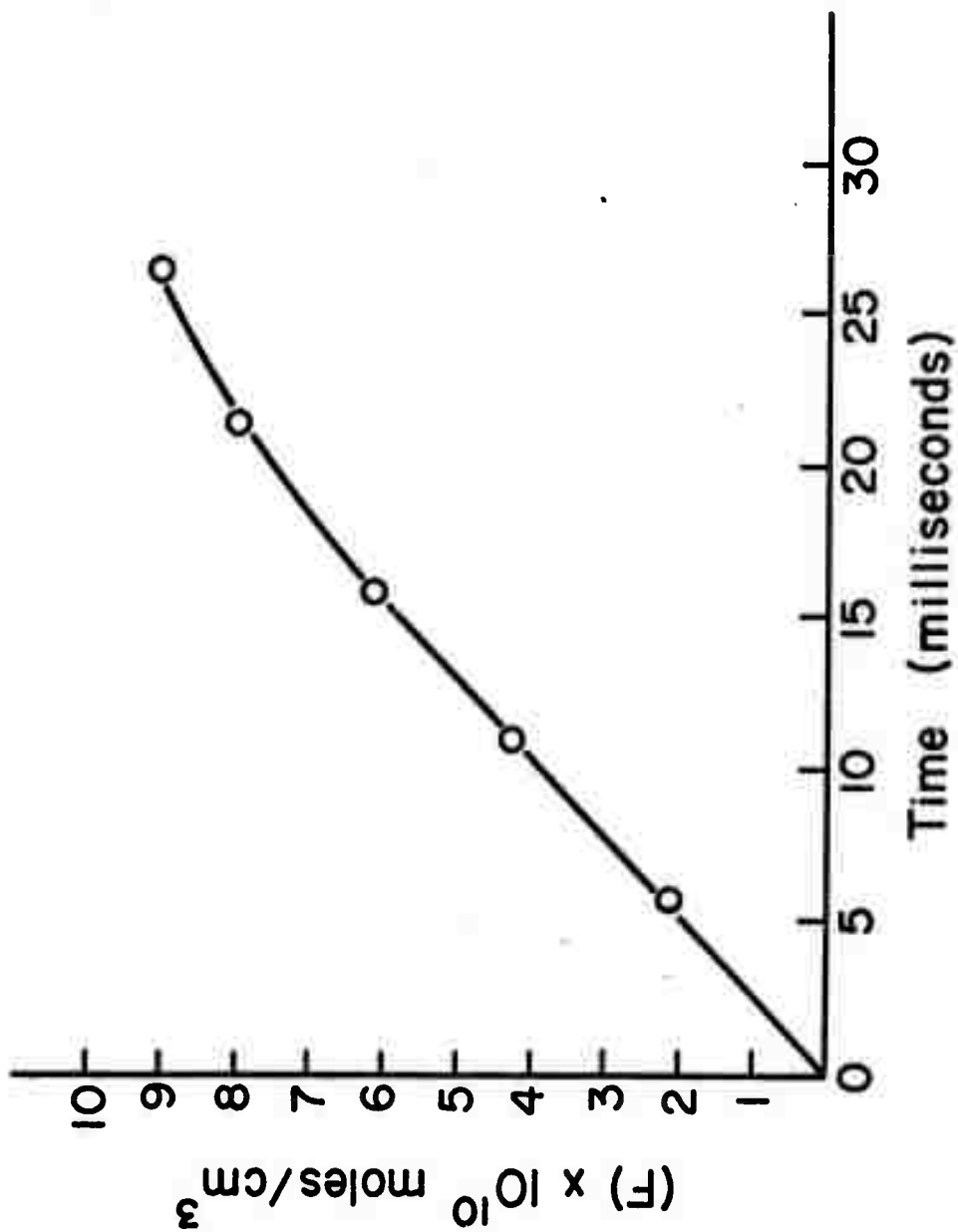


Figure 2.

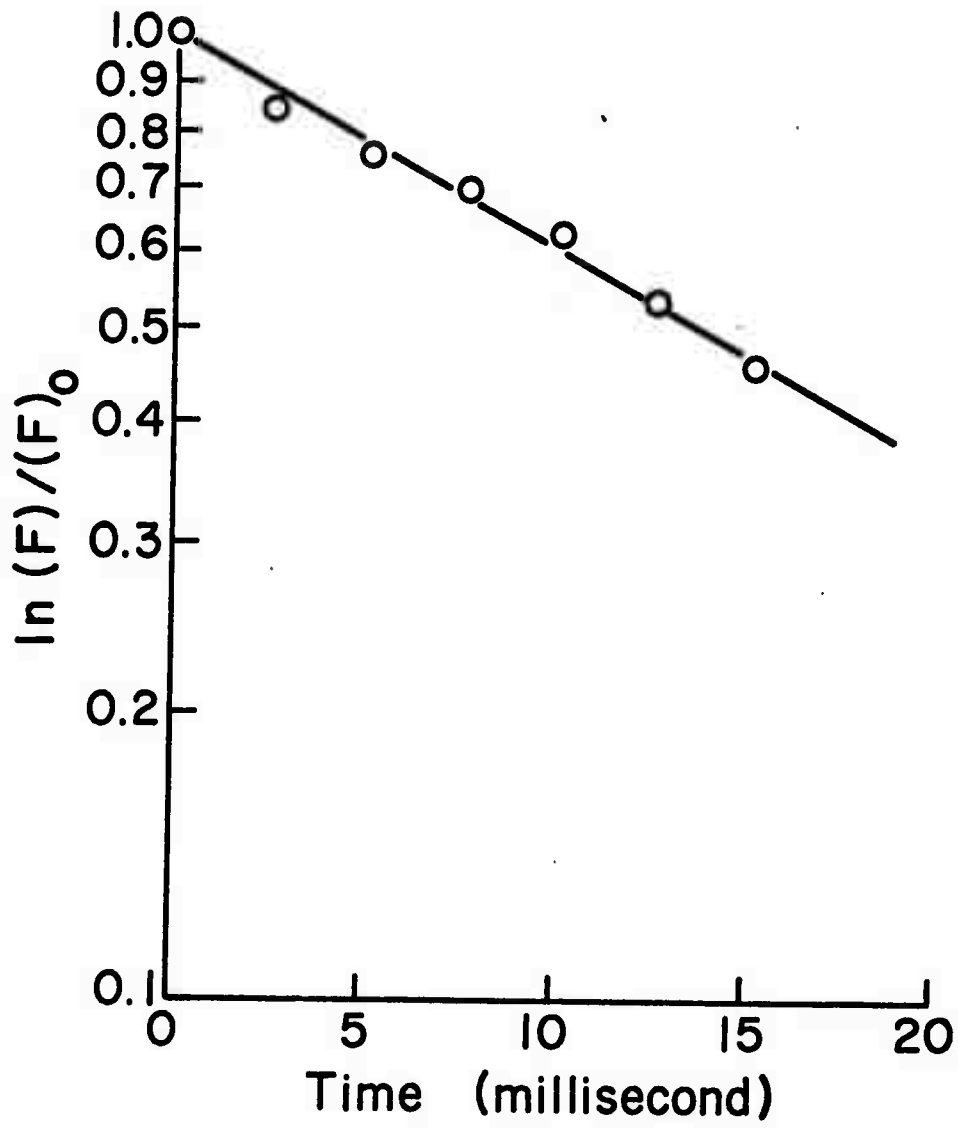


Figure 3.

B. Vibrational Excitation in the CS<sub>2</sub>-O<sub>2</sub> Laser Reaction (S. H. Bauer)

The major portion of our study of a pulse initiated chemical CO<sup>(v)</sup> laser, based on the CS<sub>2</sub> + O<sub>2</sub> reaction, has been completed and the results summarized in the appended manuscript. This has been somewhat revised and submitted for publication in the Journal of Physical Chemistry. The two salient features derived in this investigation are: (a) Deduced the nascent CO<sup>(v)</sup> vibrational distribution, as described below, and concluded that in a pulse initiated system, such as developed here, there appear to be two mechanisms which generate CO<sup>(v)</sup>, one identified with the reaction CS + O → CO<sup>(v)</sup> + S, and another as yet undetermined process; (b) Established the fact that the initiating electrical discharge produces vibrationally excited CS<sup>(w)</sup> [w = 0,1,2,3,4], which are long lived species.

In our investigations lasing was initiated by a fractional μs pulse discharge in flowing CS<sub>2</sub> + O<sub>2</sub> + He mixtures, maintained at about 3 torr. Two types of cavities were used; one with two spherical mirrors and the other with a grating for wavelength selection. In the first configuration we determined the optimum discharge voltage to maximize laser power. When the impressed voltage was higher than the optimum, CS and O

were directly involved in the lasing reaction. When the discharge voltage was lower, a chain reaction was the principal mechanism for lasing. In the tuned cavity, the measured  $\tau_d$ 's (intervals between termination of the discharge and initiation of lasing) followed a characteristic sequence; the minimum delay ( $\approx 10 \mu\text{s}$ ) occurred for the  $12 \rightarrow 11$  transition, with longer times for higher and low vibrational states. The recorded delay sequence was explained on the basis of the initially generated distribution of vibrationally excited CO. The relative populations were also estimated from chemiluminescence intensities recorded under conditions identical to laser operation but in the absence of mirrors; these are:  $e_{17}/\dots/e_1 = 0.13/0.30/0.49/0.72/1.00/1.03/0.90/0.80/0.71/0.62/0.65/0.61/0.57/0.60/0.91/1.20/2.10$ , in general agreement with the laser delay measurements. While this distribution is close to that reported from other laboratories for  $v > 8$ , there is a significant difference for the  $v \leq 7$  range, in that our data show that substantial fractions are also generated in the low  $v$  states.

To date we have demonstrated that the rates of production of total CO and that of destruction of total CS are approximately exponential and have about the same rate constant (Fig. a). Our current efforts are directed at obtaining more data on the  $\text{CS}_2 + \text{O}_2$  system via time dependent UV emission and UV absorption spectra, to ascertain the fate of  $\text{CS}^{(w)}$  species, and to exploit the computer modeling programs, described in IIIB, for checking the proposed mechanisms.

In a preliminary communication from this laboratory [M. C. Lin and S. H. Bauer, Chemical Physics Letters, 7, 223 (1970)] we stated that mixtures of  $\text{C}_3\text{O}_2 + \text{O}_2$  produce inverted  $\text{CO}^{(v)}$  populations, and do lase when subjected to a pulse discharge. We have now initiated a detailed study of this system,

analogous to that concluded for the  $CS_2 + O_2$  pair. In the first stage of the program shall to develop a synthetic procedure for generating abundant quantities of  $C_3O_2$  in pure form and at acceptable yields. Concurrently we shall test for lasing under cw conditions by utilizing Professor McFarlane's 1 Kw microwave generator for producing copious levels of dissociated oxygen. Our primary objective is to measure the nascent distribution of  $CO^{(v)}$  produced in  $C_3O_2 + O_2 + He$  mixtures when subjected to a pulse discharge.

LASING ACTION AND THE  
RELATIVE POPULATIONS OF VIBRATIONALLY EXCITED CO PRODUCED  
IN PULSE-DISCHARGED CS<sub>2</sub> + O<sub>2</sub> + He MIXTURES

S. Tsuchiya<sup>‡</sup>, N. Nielsen and S. H. Bauer

Department of Chemistry, Cornell University, Ithaca, New York 14850

ABSTRACT

Lasing was initiated by a fractional  $\mu$ s pulse discharge ( $\approx 15$  Kv) in flowing CS<sub>2</sub> + O<sub>2</sub> + He mixtures, maintained at about 3 torr. Two types of cavities were tested; one with two spherical mirrors and the other with a grating for wavelength selection. In the first configuration we determined the optimum discharge voltage to maximize laser power. When the impressed voltage was higher than the optimum, CS and O generated by fragmentation of the CS<sub>2</sub> and O<sub>2</sub> were directly involved in the lasing reaction. When the discharge voltage was lower, a chain reaction was the principal mechanism for lasing. In the tuned cavity, the measured  $\tau_d$ 's (intervals between termination of the discharge and initiation of lasing) followed a characteristic sequence; the minimum delay ( $\approx 10 \mu$ s) occurred for the 12  $\rightarrow$  11 transition, with longer times for higher and lower vibrational states. The recorded delay sequence was explained on the basis of the initially generated distribution of vibrationally excited CO. The relative populations were also estimated from chemiluminescence intensities recorded under conditions identical to laser operation but in the absence of mirrors; these are:

$\varphi_{17}/\dots/\varphi_1 = 0.13/0.30/0.49/0.72/1.00/1.03/0.90/0.80/0.71/0.62/0.65/0.61/0.57/0.60/0.91/1.20/2.10$ , in general agreement with the laser delay measurements. While

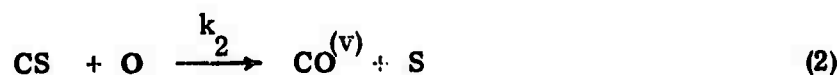
---

<sup>‡</sup> Permanent Address: Department of Pure and Applied Science, University of Tokyo

this distribution is close to that reported from other laboratories for  $v > 8$ , there is a significant difference for the  $v \leq 7$  range, in that our data show that substantial fractions are also generated in the low  $v$  states.

## INTRODUCTION

The reaction between carbon disulfide and oxygen which, under suitable conditions, generates inverted populations of vibrationally excited CO, has many intriguing aspects. While this process has been investigated assiduously during the past five years, and a consensus has been reached regarding the two principal reactions:



as yet there has been no complete identification of all the steps which do occur, nor has any detailed study been made of the lifetimes and concentrations of intermediates in the chain which must be present in the flame laser<sup>(1)</sup>. Only a few quantitative measurements of the reaction rates have been published<sup>(2-5)</sup>. For computer modeling of CS<sub>2</sub>-O<sub>2</sub> lasers it is essential to establish the partition of vibrational energy among the wide range of states as initially produced in reaction (2). We have no knowledge of any proposed 3-center potential energy surface for the S/C/O system nor of trajectory calculations on such a surface which would provide from a theoretical analysis some inkling of how the exothermicity is distributed in the product species.

In this manuscript we report on the deduction of the vibrational population distribution for the nascent species from measurements of delay times for lasing ( $\tau$ ), at specified frequencies, subsequent to initiation of the reaction by a pulsed electrical discharge. We have also measured relative chemiluminescence intensities under conditions identical to the above but in the absence of cavity mirrors. In the meantime the reports by Hancock and Smith<sup>(5,6)</sup> provided complimentary data on this distribution, based on

their measured chemiluminescence intensities in a rapid flow apparatus, in which oxygen atoms produced by<sup>a</sup> microwave discharge were mixed with carbon disulfide. Dawson and Tam<sup>(26)</sup> suggested corrections to Hancock and Smith's initial distribution. The results of these investigations are compared with ours. Also, we made preliminary measurements on CS level populations via UV absorption spectra. While these data are as yet qualitative, their implication regarding the mechanism are unexpected and significant.

### APPARATUS

#### I. R.

The configuration used for the investigations is shown schematically in Fig. 1. The laser tube is 1 m long, 2.54 cm in diameter. Two aluminum ring electrodes are placed at each end, and between them the charge from a capacitor (0.01  $\mu$ F) is released through an ignitron (WL-7703), which is triggered at a rate of 6 Hz. The current pulse width depends on the pressure and composition of<sup>the</sup> gas, as well as the voltage; shorter pulse-widths and larger peak currents result from higher discharge voltages. A typical combination has a half-width of 0.3  $\mu$ sec, a peak current of 550A in a mixture consisting of 0.05 torr CS<sub>2</sub>, 0.35 torr O<sub>2</sub>, and 1.8 torr He, for a discharge voltage of 15 kV.

Fine needle valves (vernier settings) were used to control the flow of each gas. The flow rates were calibrated by measuring the rate of decline of pressure in a vessel of known volume. Most of the experiments were done with mixtures of CS<sub>2</sub> 0.015 ~ 0.05 torr, O<sub>2</sub> 0.01 ~ 0.8 torr, and He 2 ~ 3 torr, and a linear flow velocity of 8 m/sec.

Two types of cavities were tested. In the<sup>first,</sup> two gold coated spherical Ge mirrors with a radius of 4 m were used. The mirrors were placed 1.5 m apart, and one had an uncoated hole in the center of 0.75 mm diameter, for coupling out the laser emission. The

total power generated in the laser was monitored by a Au doped Ge detector through a tilted NaCl plate with rough surfaces used for attenuation, and an I.R. filter having a flat response between  $4.1 \sim 5.6 \mu$ . The output from the detector passed through an FET impedance reducer, and was displayed on an oscilloscope (Tektronix 535). For dispersed wavelength studies, an I.R. grating monochromator, Perkin-Elmer 88G, with a Bausch-Lomb, 150  $\ell/\text{mm}$  blazed at  $6\mu$ , and a Au doped Ge detector (Santa Barbara Research Lab, 70R) were used. The monochromator was calibrated by measuring several lines of a low pressure mercury lamp in high orders. The wavelength response of the monochromator and detector system was calibrated by recording the emission of a Nernst glower lamp whose temperature was measured with an optical pyrometer, assuming the emissivity was constant over the  $0.65\mu - 5\mu$  region. In order to measure integrated power the vertical signal output from the oscilloscope was passed through a pulse stretcher in which the signal was integrated by a  $0.47\mu\text{F}$  capacitor through a Ge diode, and lead to the input of a lock-in amplifier (PAR Model 120); the reference signal was synchronized with the trigger pulse that initiated the discharge. The accuracy of response of the lock-in amplifier output was compared with the total power obtained by integration of the laser pulse as displayed on the oscilloscope. The proportionality between the two measured outputs was good except for very weak laser signals.

In the second arrangement a wavelength controlled cavity was used. A grating (Bausch and Lomb, 300  $\ell/\text{mm}$ , blazed at  $3.5 \mu$ ) was set at one end, replacing the totally reflecting spherical mirror. The measuring system remained the same as for the conventional cavity. Since the laser transitions of CO are close to each other, it was difficult to isolate a single transition by tuning the grating. Most of the tuned laser lines were accompanied by 2 or 3 weak satellite lines. Usually, an effort was made to reduce the

intensity of these satellite lines to less than 10% of the main oscillating lines. Thus, cascading due to stimulated transitions had little effect on the measured delay times of the laser pulses.

The fundamental CO emission was measured from one end of the laser tube. The Brewster angle window was replaced with a NaCl window set perpendicular to the axis of the tube. The arrangement of the discharge pulse was the same as in the former case. The signal from the monochromator was sampled with a Boxcar integrator, PAR 160, for a duration of 2.5  $\mu$ sec, using a constant preset delay time after the discharge. The monochromator was scanned very slowly over the wavelength region that covers the CO fundamental region, 4.5 to 5.8  $\mu$ . Thus the emission spectrum of CO at a given delay time could be obtained. The method used to estimate the vibrational population from the recorded spectrum will be described later.

## EXPERIMENTAL RESULTS

### Laser with a Conventional Cavity

Figures 2a and 2b are oscilloscope records of the laser pulses. These clearly show definite delays after initiation by the discharge. In the O<sub>2</sub>-rich case, the laser power peaks very rapidly and then decreases in an oscillatory manner. In contrast, for low O<sub>2</sub> content, the laser pulse delays are longer, and the pulses attain their maximum more gradually. Low discharge voltages and excess O<sub>2</sub> show pulse shapes very similar to the case of low O<sub>2</sub> content. Thus, two types of pulse shapes were found: one for high discharge voltage and O<sub>2</sub>-rich mixtures, and the other for low discharge voltages and either

low or high  $O_2$  content. This suggests that two lasing mechanisms are operative, possibly differing in detail; this is supported by experiments on the dependence of the laser power on the discharge voltage, the measured delay for lasing onset, and the laser spectrum.

The oscillations of the laser pulse may be related to radially propagating acoustic waves. The oscillating period does not depend on the discharge voltage. However, the addition of He to the system, while maintaining constant  $CS_2$  and  $O_2$  content, results in a reduction of the period of oscillation as well as its amplitude. The latter fact can be explained by the higher sound velocity and the more homogeneous discharge when additional He was present in the system. Figure 3 shows changes in the shape of the laser output pulse with increasing He pressures.

The dependence of the integrated laser power on the discharge voltage and  $O_2$  concentration is shown in Figure 4. There is an optimum in the discharge voltage for maximizing the laser power. This voltage depends on the  $O_2$  content of the system; the lesser  $O_2$  the higher the optimum voltage. If it is assumed that there is an optimum discharge voltage for the formation of CS from  $CS_2$  and that the concentration of O atoms increases with the discharge voltage, the above result is understandable.

For high discharge voltages the laser power increases monotonically with  $CS_2$ , as does the optimum discharge voltage. This is reasonable, because a larger amount of energy is required to decompose the  $CS_2$  to CS. The overall effect of added He is small.

With increasing He pressure, the optimum discharge voltage for laser power shifts slightly to the high side, but the power does not change. Apparently, the He atoms act as decelerators for the electrons. The shift of the optimum discharge voltage was also observed when the size of the discharge capacitor was changed. With  $0.01 \mu F$ ,

a mixture of 0.016 torr  $\text{CS}_2$  + 0.68 torr  $\text{O}_2$  + 1.7 torr He produces peak power at 9.5 kV; with a 0.0036  $\mu\text{F}$  capacitor, the peak power for the same gas mixture was observed at 14.5 kV. Both cases have almost the same electrical energy: 0.45 and 0.38 J, respectively.

The delay times for the initiation of laser pulses are determined by the discharge voltage as well as the  $\text{CS}_2$  and  $\text{O}_2$  concentrations. As shown in Figure 5, the dependence is complex. This is not unexpected since the nature of the discharge depends on the amount of  $\text{CS}_2$  and  $\text{O}_2$  present. The composition factor is apparent in the case of low voltage discharges (6 ~ 9 kV); a small increase of  $\text{O}_2$  or  $\text{CS}_2$  reduces the laser delay times but a large increase reverses the trend. While on one hand higher pressures decelerate the electrons, on the other, they provide more abundant sources for CS or O. In the high voltage discharges the plasma electrons retain sufficient energy to dissociate  $\text{O}_2$  and  $\text{CS}_2$  so that small changes in  $\text{O}_2$  or  $\text{CS}_2$  content do not produce significant changes in the plasma state. In this respect, some information can be obtained from measurement of the current pulses. For voltages higher than 10 kV, the half-width is generally constant, at about 0.3  $\mu\text{sec}$ , and is not affected by small changes in  $\text{CS}_2$  or  $\text{O}_2$  content. However, for discharge voltages below 10 kV the half-width is larger, and an increase in  $\text{CS}_2$  or  $\text{O}_2$  produces an increase in the half-width. This implies that the addition of  $\text{CS}_2$  or  $\text{O}_2$  to the system reduces the discharge peak current, i. e., the resistance of the discharge gas is larger. Therefore, when the system has sufficient discharge energy, the extent of dissociation is proportional to the  $\text{CS}_2$  and  $\text{O}_2$  content, and the lasing process is accelerated. From Figure 5, it appears that the inverse of the delay time ( $\tau$ ) is proportional to the  $\text{O}_2$  and  $\text{CS}_2$  concentrations when the discharge voltage is 13 ~ 15 kV:

$$1/\tau \propto [\text{CS}_2] [\text{O}_2]$$

Ninety vibration-rotation transitions were found; these were assigned to various transitions from  $v = 14 \rightarrow 13$  to  $v = 2 \rightarrow 1$ . These spectra were taken for a gas mixture consisting of 0.017 torr  $\text{CS}_2$  + 0.65 torr  $\text{O}_2$  + 1.7 torr He; the discharge voltages were 7, 9, and 12 kV. In the 7 kV discharges, the recorded laser transitions were mostly  $P(16) \sim P(11)$  of  $v = 14 \rightarrow 13$  to  $v = 4 \rightarrow 3$  vibrational transitions. The spectrum initiated by 12 kV discharges shows  $P(19) \sim P(14)$  of  $v = 13 \rightarrow 12$  to  $v = 6 \rightarrow 5$  transitions. The spectrum produced with a 9 kV discharge exhibits characteristics of both the low and high voltage discharges. Possibly the higher J transitions are favored for the higher voltage discharges because the corresponding rotational temperatures of the system are higher. In Figure 6, the sums of intensities of the various rotational transitions for each vibrational transition are plotted vs.  $(v \rightarrow v-1)$ . Maxima appear at  $v = 11 \rightarrow 10$  and  $v = 9 \rightarrow 8$  for the high and low voltage discharges, respectively. This suggests that for the higher voltage discharges there is a larger contribution to the emitted intensity from chemical pumping in contrast to secondary effects, such as collisional or stimulated transitions.

The lasing mechanism in this system is complex because three factors strongly interact to generate the observed population distribution among the lasing levels: the many chemical reactions (with some rates dependent on the states of vibrational excitation of the reactants), collisional relaxation, and stimulated optical transitions. Below, we shall describe the result of  $\text{CO}^{(v)}$  spontaneous emission measurements, from which it is evident that collisional relaxation is a dominant factor in determining the intensities of lasing at the low vibrational transitions. The pulse shape for a specified vibration/rotation transition is essentially

the same as the one for the total power, and a distinct cascading phenomenon, such as reported by Patel<sup>(7)</sup> is not seen. The sequence of delay times for each vibration-rotation laser pulse were also measured (see below) using the tuned cavity. These are significantly different from observations made with a conventional cavity.

In summary, two types of voltage dependent lasing behavior were found. In high voltage discharges the laser pulses are short, high vibrational and high J transitions are favored, and the laser power decreases with increasing discharge voltage. In low voltage discharges the delay times for the laser pulse are long, as is the duration of lasing, and the power increases with increasing discharge voltage. The optimum laser power can be obtained at an intermediate discharge voltage that depends on the CS<sub>2</sub> and O<sub>2</sub> content. The discharge voltage for optimum lasing is higher with increasing CS<sub>2</sub> and decreasing O<sub>2</sub>. However, the dependence on CS<sub>2</sub> is more sensitive than on O<sub>2</sub>. When the O<sub>2</sub> content is fairly high the optimum laser power is almost directly proportional to the CS<sub>2</sub> content.

#### Laser with Tuned Cavity

In order to eliminate the effect of stimulated transitions, oscillations for specific rotation-vibration transitions were selected in the cavity with the aid of a grating. These measurements were carried out mostly with 15 kV discharges because the former experiments suggested that under high voltage conditions the species produced by the discharge contributed directly to lasing.

Typical oscilloscope traces that show a sequence of delay times for lasing, as these depend on the vibrational transition, for the selected rotational transition P(10), are reproduced in Fig. 7. Each transition starts with a sharp rise in laser output at a distinct delay time  $\tau_{v,v-1}(J)$ . The graphs in Fig. 8 show the dependence of  $\tau_{v,v-1}(J)$

on  $v \rightarrow (v-1)$ , and indicate the effect of added CO to the mixture. Also shown are the estimated termination times for the corresponding laser pulses. It is evident that the addition of a small amount of CO has little effect on  $\tau_{v,v-1}^{(J)}$  for the initiation of lasing for  $v \geq 9$ , but produces progressively increasing delays, up to about a factor of two, for the lower  $v$ 's, down to  $v = 5$ . Depending on the CO content the intensities for the lower transitions diminish. At a partial pressure of CO half of that of the initial  $\text{CS}_2$  (0.04 torr) the effect is marked. Added CO also reduces the duration of lasing for transition from levels lower than  $v = 9$  (Fig. 8) thus accounting for the decrease in measured total integrated intensities at P(9) for each vibrational transition; the effect is marked for transitions from  $v \leq 9$ , as shown in Fig. 9. The decrement is monotonic with the amount of gas added. This effect will be discussed further below.

At our operating pressures translation and rotation should be in equilibrium. To estimate the rotational temperature, a small amount of HCl was introduced to serve as a tracer radiator. Then the relative emitted intensities of rotational lines R(0) ~ R(6) of the fundamental vibrational band for HCl were observed. The HCl was at a partial pressure of 0.14 torr, for a total operating pressure of 3.8 torr. The deduced temperatures were  $440^\circ$  and  $450^\circ$  K at 11.5 and 26.5  $\mu\text{sec}$ , respectively, after a discharge pulse with 15 kV. Correction for self-absorption was made by the method of Ladenburg and Levy<sup>(5)</sup>. These values are lower limits, because the added HCl extracted some part of the discharge energy. However, this temperature was used for the analysis of the delay data and the CO fluorescence results. Considering the accuracy of data and the approximations made, a temperature change of  $50^\circ$  K does not lead to significantly different conclusions.

### Measurement of Spontaneous Emission

The emission spectra at the CO fundamental were recorded at selected delay times after the discharge pulse to establish the time dependence of the population distribution for each vibrational level. The emission was too weak to permit measurement of individual rotation-vibration lines, and the higher vibrational transitions overlap appreciably. The monochromator slits were set so that the equivalent triangular slit function had a width of  $2.9 \text{ cm}^{-1}$  at half-height. With this low resolution the chemiluminescent spectrum appears as a smooth function (except for noise). The spectrum was scanned slowly ( $\approx 1 \mu\text{m/hr.}$ ).

### DATA REDUCTION

A computer program was written to calculate the expected spectra for various assumed distributions for comparison with the spectra recorded at the specified delay times. The intensity of a vibration-rotation line ( $v', J' \rightarrow v'', J''$ ) for a diatomic molecule is given by

$$I(v', J' \rightarrow v'', J'') = \frac{hc \omega_{v'J', v''J''}^4}{\omega_{v'v''}^3} \frac{F_J S_J A_{v'v''}}{Q_{\text{rot}}} \frac{\exp[-B'J'(J'+1)hc/kT]}{N_{v'}} \quad (3)$$

where  $\omega_{v'J', v''J''}$  is the wave number of the line;  $\omega_{v'v''}$  is the wave number of the band origin;  $S_J$  is the rotational transition matrix [ $S_J = (J'+1)$  for a P-branch and  $S_J = J'$  for an R-branch line];  $F_J$  is the vibration-rotation interaction factor;  $A_{v'v''}$  is the spontaneous emission coefficient for the vibrational transition ( $v' \rightarrow v''$ );  $N_{v'}$  is the population in the upper vibrational level, and  $Q_{\text{rot}}$  is the rotational partition function.

A rotational temperature of  $450^\circ$  was assumed. The wave numbers for the lines were calculated from the molecular constants given by Mantz, et. al. <sup>(9)</sup>; values for

$A_{v'v''}$  and  $F_J$  were given by Fisher<sup>(10)</sup> and by Toth, et. al.<sup>(11)</sup>, respectively. First, the contribution from each vibrational transition to the observed intensity was calculated when the monochromator was set at the wave number  $\omega_1$ , using a triangular slit function  $f(\omega, \omega_1)$ :

$$U(v', \omega_1) = \sum_{J'} I(v'J' \rightarrow v''J'') f(\omega, \omega_1), \quad (4)$$

where  $N_{v'} = 1$  and  $v'' = (v'-1)$ . Since the slit width is much wider than the Doppler line width, the spectrometer transmission factor is the magnitude of the normalized slit function at the line frequency. The summation was taken over the 90 P- and R-branch lines.

The observed intensity record was then represented by

$$I(\omega_1) = \sum_{v'} U(v', \omega_1) N_{v'} . \quad (5)$$

The best set of relative  $N_{v'}$ 's that reproduces the observed  $I(\omega_1)$ 's [which were measured at  $4 \text{ cm}^{-1}$  intervals over the range  $2219\text{-}1691 \text{ cm}^{-1}$ ] was sought by a least square procedure for  $v' = 1 \sim 17$ . The deduced sets of  $N_{v'}$ 's were graphically smoothed. Figure 10 shows three examples of the observed and calculated spectra.

The principal sources of inaccuracy in the above procedure are lack of a precise rotational temperature, absorption by water vapor in the region of the higher vibrational transitions, and overlap of the CO emission by that of OCS. The first was readily checked by recalculation, using  $400$  and  $500^\circ\text{K}$  as trial temperatures. The changes in the resulting distributions were less than 10%. Regarding interference by water, the monochromator was flushed with dry  $\text{N}_2$ , while the light path of about 30 cm from the laser tube to the spectrometer slit was left open to the air. Absorption by water was clearly indicated. Therefore, our deduced distribution at the high vibrational states  $v = 12 \sim 17$  may be somewhat underestimated. With respect to OCS absorption, Hancock and Smith<sup>(5)</sup> in their study of the  $\text{O} + \text{CS}_2$  system found that emission by OCS did overlap the CO fundamentals

However, we found that when a cell 10 cm in length filled with OCS at 1 torr was placed in front of the entrance slit of the monochromator, no change in the spectrum was observed. Hancock and Smith suggested that at most 1.5% of the  $\text{CS}_2$  is converted to OCS in  $\text{O}_2$  rich mixtures. If the excitation of OCS is due to collisions with CO, 10 collisions require about 40  $\mu\text{sec}$ . Since the pressure of CO cannot exceed the initial pressure of  $\text{CS}_2$ , which in these experiments is less than 0.05 torr, CO starts at zero and increases exponentially following the initiation discharge pulse, at a rate of order  $10^4 \text{sec}^{-1}$ . Hancock and Smith<sup>(12)</sup> showed that the V-V collision probability between CO in levels of  $v = 7 \sim 4$  and OCS was of the order of  $10^{-1}$ , but the above estimate of the collision number includes collisions with CO in any state. Therefore, the contribution of OCS emission to the spectrum cannot be large during the first 100  $\mu\text{sec}$  after the discharge. Were excited OCS generated directly, an overestimate of CO population at  $v = 5 \sim 3$  may occur depending on the rate of  $\text{OCS}^\ddagger$  formation.

In Fig. 11 the deduced relative population distributions (normalized to unity at  $v = 13$ ) are shown as a function of the delay time after the discharge pulse. At a delay of 23  $\mu\text{sec}$  a peak in the population appears at  $v = 11$  or 12 and a minimum population occurs at  $v = 4$ . As the delay time increases, the peak shifts to lower  $v$  values and the distribution becomes more Boltzmann-like. Figure 11 also shows the initial distribution estimated by graphical linear extrapolation to  $t = 0$ , together with the recent results of Hancock, Morley and Smith.<sup>(6)</sup>

To obtain the rate of formation of CO, the observed relative populations in levels  $v = 1$  to  $v = 17$  were summed; this is shown in Fig. 12. However, the population in the  $v = 0$  level cannot be observed by any emission measurement, and the relaxation process

produces a significant amount of CO in the ground state during the latter stages.

Therefore, we were forced to estimate  $\text{CO}(v=0)$  by a linear extrapolation from the higher levels; this is subject to considerable uncertainty. The estimated total CO was also plotted in Fig. 12. The carbon monoxide accumulates exponentially as a function of time,

$$[\text{CO}] \sim (1 - e^{-kt}) \quad (6)$$

where  $k = 2.3 \times 10^4 \text{ sec}^{-1}$ , when the initial pressures of He,  $\text{O}_2$ , and  $\text{CS}_2$  are 3.1, 0.75, and 0.046 torr, respectively and the discharge voltage is 15 kV. It is interesting to note that the rate of decrease of  $[\text{CS}]$ , as measured via absorption in the UV, follows a decay rate that closely parallels the growth of CO. <sup>(13)</sup> Two types of the relaxation processes deactivate the excited CO, V-V and V-T energy transfers. The former is a near-resonant exchange with a small amount of energy (equal to the anharmonicity defect) transferred to the translational motion. This process very efficiently modifies the initial distribution of  $\text{CO}^{(v)}$  generated in the reaction. However, the V-V process does not change the total number of vibrational quanta produced by the reaction. In contrast, when V-T energy transfers occur, the total number of quanta are reduced. The average number of vibrational quanta for CO is estimated to be 6.0, which corresponds to 42% of the exothermicity of the pumping reaction:  $\text{CS} + \text{O} \rightarrow \text{CO}^{(v)} + \text{S}$ . This average number of quanta is retained during the first 60  $\mu\text{sec}$  after the discharge, and then gradually decreases. Thus, prior to 60  $\mu\text{sec}$ , V-T relaxation is not as important as V-V relaxation, which dominates. The decrement rate for the number of vibrational quanta after 60  $\mu\text{sec}$  is about  $4 \times 10^3 \text{ sec}^{-1}$ , which is much larger than the spontaneous emission rate for  $v = 6 \rightarrow 5$  ( $1.61 \times 10^2 \text{ sec}^{-1}$ ). V-T relaxation of CO in collisions with He or  $\text{O}_2$  is very slow at room temperature, and therefore, the CO is efficiently deactivated either at the walls of the tube or by collision with the active species such as O, S or CS.

### Interpretation of $\tau_v$ 's

As shown above, the total CO concentration increases exponentially to an equilibrium value. Before relaxation processes become dominant the population of level  $v$  may be expressed by

$$N_v = \phi_v N(1 - e^{-kt}), \quad (7)$$

where  $N$  is the final concentration of CO, and  $\phi_v = k_v / \sum_v k_v$ , the fraction of production channeled to that level. The distribution of CO changes rapidly due to V-V relaxation as shown in Fig. 11. For these experiments the partial pressure of  $\text{CS}_2$  was 0.05 torr, and this limits the amount of CO that can be produced. An upper bound for the collision frequency between CO molecules is  $4 \times 10^5 \text{ sec}^{-1}$ ; this is an overestimate since CO increases gradually during the initial period of the reaction and reaches its maximum value only when all the  $\text{CS}_2$  is converted. We recorded delay times of less than  $20 \mu\text{sec}$ , except for the lower vibrational transitions. The latter are involved in V-V relaxation, because the addition of a small amount of CO affects significantly their delay times. Hence laser pulses from  $14 \rightarrow 13$  to  $7 \rightarrow 6$  can be interpreted in terms of the initially generated vibrational distribution. For these, collisional or radiative deactivation processes other than the V-V relaxation cannot make an appreciable contribution since the average vibration quanta of CO are conserved in the system during the first  $60 \mu\text{sec}$  after the discharge.

To deduce population ratios for adjacent levels from laser delay data an additional assumption was made, that the loss in the laser cavity is independent of a small change in the grating angle, which in the range of  $7^\circ$ . The theoretical gain for a P-branch transition,  $(v, J-1) \rightarrow (v-1, J)$  is:

$$\alpha_{v,v-1}(J) = \frac{8\pi^3 c^4 A_{v,v-1}}{3kT(2\pi kT/m)^{\frac{1}{2}}} \times J [N_v B_v \exp\{-F_v(J-1) \frac{hc}{kT}\} - N_{v-1} B_{v-1} \exp\{-F_{v-1}(J) \frac{hc}{kT}\}] \quad (8)$$

where  $A_{v,v-1}$  = transition matrix element for  $v \rightarrow (v-1)$

$N_v$  = molecule density of CO in level  $v$

$m$  = mass of CO

$T$  = translational = rotational temperature

$F_v(J)$  = rotational term value for vibrational level  $v = B_v J(J+1) - D_v J^2(J+1)^2$ .

For a sequence of transitions  $(v, J-1) \rightarrow (v-1, J)$ , with  $J$  fixed, the time dependent relative gain after the discharge pulse, may be written in terms Eq. (7),

$$\alpha_{v,v-1}(J) = \text{const} \cdot A_{v,v-1} (1 - e^{-kt}) \cdot [\phi_v B_v \exp\{-F_v(J-1) \frac{hc}{kT}\} - \phi_{v-1} B_{v-1} \exp\{-F_{v-1}(J) \frac{hc}{kT}\}]. \quad (9)$$

In the limiting case, as  $t \rightarrow \infty$ ,

$$\alpha_{v,v-1}^{\infty}(J) = \text{const} \cdot A_{v,v-1} [\phi_v B_v \exp\{-F_v(J-1) \frac{hc}{kT}\} - \phi_{v-1} B_{v-1} \exp\{-F_{v-1}(J) \frac{hc}{kT}\}], \quad (10)$$

This is the maximum gain were the chemically produced excited species not to make transitions to lower levels. Equation (9) simplifies to

$$\alpha_{v,v-1}(J) = \alpha_{v,v-1}^{\infty}(J) (1 - e^{-kt}). \quad (9')$$

Laser oscillations start when the gain exceeds the cavity loss. Therefore, the delay time  $\tau_{v,v-1}(J)$  may be defined by

$$\tau_{v,v-1}(J) = -(1/k) \ln [1 - (L/\alpha_{v,v-1}^{\infty}(J))] \quad (11)$$

where  $L$  is the loss in the cavity (equal to  $\alpha$  at threshold). When a value for  $k$  is available it is more convenient to work with the equation.

$$T_{v,v-1}(J) = L/\alpha_{v,v-1}^{\infty}(J) \quad (12)$$

where  $T_{v,v-1}(J) \equiv 1 - \exp[-k\tau_{v,v-1}(J)]$ . When relative values for adjacent  $\phi_v$ 's are available one may compare  $T_{v,v-1}(J)$  with that of  $T_{v-1,v-2}(J)$ :

$$\frac{T_{v-1,v-2}(J)}{T_{v,v-1}(J)} = \frac{A_{v,v-1}}{A_{v-1,v-2}} \frac{(\phi_v/\phi_{v-1})B_v \exp\{-F_v(J-1)\frac{hc}{kT}\} - B_{v-1} \exp\{-F_{v-1}(J)\frac{hc}{kT}\}}{B_{v-1} \exp\{-F_{v-1}(J-1)\frac{hc}{kT}\} - (\phi_{v-2}/\phi_{v-1})B_{v-2} \exp\{-F_{v-2}(J)\frac{hc}{kT}\}} \quad (13)$$

Thus, once a population ratio for one pair of adjacent vibrational levels is specified, the population ratios for other pairs may be derived.

Additional information on population ratios may be derived from the dependence of  $\tau_{v,v-1}(J)$  on  $J$ . From Eqs. (10) and (12), the following relation is obtained for a fixed vibrational transition at different  $J$ 's;

$$1/T_{v,v-1}(J) \propto J \left[ 1 - \frac{\phi_{v-1}}{\phi_v} \frac{B_{v-1}}{B_v} \exp\{-[F_{v-1}(J) - F_v(J-1)]\frac{hc}{kT}\} \right] \quad (14)$$

Relative values of  $1/T_{v,v-1}(J)$  for P(3) to P(22) of the 12→11 transition for a range of population ratios  $\phi_{11}/\phi_{12}$  at  $T = 450^\circ\text{K}$  are plotted vs  $J$  in Fig. 13. Superposed on these are  $1/T_{v,v-1}$  from observed  $\tau$ 's for  $k = 2.86 \times 10^4 \text{ sec}^{-1}$ . Although there is considerable scatter, on comparing the experimental points with the calculated curves best agreement is indicated for  $(\phi_{11}/\phi_{12})$  in the range of 0.8 ~ 0.9. This range is consistent with the value of 0.88 derived from the CO spontaneous emission measurements.

To estimate population ratios for this range of  $(\phi_{11}/\phi_{12})$ 's, Eq. (13) was applied, assuming 0.80, 0.85, and 0.90. The results are shown in Table I. They are compared with the relative population distributions deduced from the spontaneous emission measurements obtained in this laboratory and those reported by Hancock,

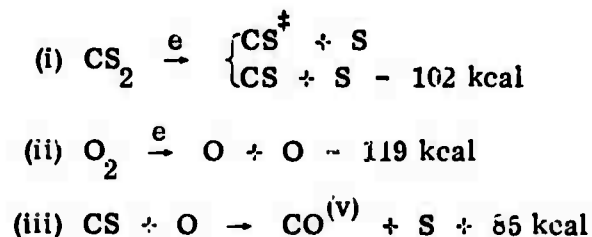
Morley, and Smith<sup>(6)</sup>. The assumption  $\varphi_{11}/\varphi_{12} = 0.8$  gives a population ratio for  $(\varphi_7/\varphi_6)$  which is negative; this is physically unacceptable. However, for  $(\varphi_{11}/\varphi_{12}) = 0.85 \sim 0.9$  the relative populations derived from the  $\tau$  values are in general agreement with those from the spontaneous emission measurements, except for the low  $v$ 's,  $7 \sim 5$ . As shown in Fig. 8, for transitions lower than  $8 \rightarrow 7$  the relatively long delay is significantly affected by added CO. Hence it is not valid to assume that the population of levels lower than  $v = 8$  are predominantly determined by the chemical production step at a time when the laser begins to oscillate at these transitions.

We may now compare the gain calculated from the distribution based on the spontaneous emission measurements with the laser delay data shown in Fig. 8. Though fluorescence distributions have been recorded for only 5 different times after the discharge, and these are not sufficient to permit unravelling of the entire history of the gain for each rotation-vibration transition, reasonable estimates of the gain-time relation can be made using eq. 8, since  $N_v$  is now a known function of time. The results are plotted in Fig. 14a, b. The P(9) transitions of  $13 \rightarrow 12$  to  $5 \rightarrow 4$  have positive gains which initially increase with time, attain maxima and then decrease to negative values. The gain for the  $8 \rightarrow 7$  transition remains positive for the longest time, while that for  $9 \rightarrow 8$  is largest. The gains for the  $4 \rightarrow 3$  and  $3 \rightarrow 2$  transitions are negative initially; these increase to a positive value before decreasing again to become negative. From Figs. 8 and 9, the maximum power appears at  $10 \rightarrow 9$  and the laser duration is longest for  $8 \rightarrow 7$ . Also, a short lasing duration was found for the higher transitions along with short delay times, while the  $4 \rightarrow 3$  and  $3 \rightarrow 2$  transitions have long delay times.

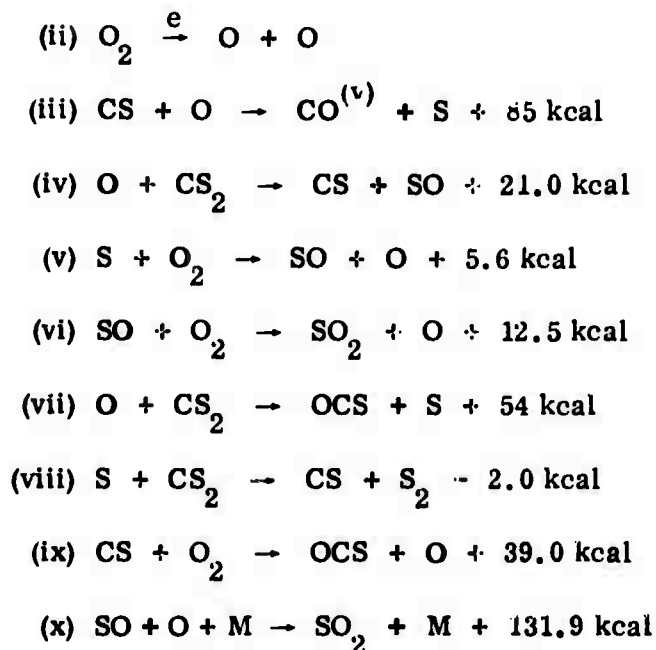
## DISCUSSION

Reaction Mechanism

The data summarized in the preceding section suggest that the mechanisms for the high and low voltage discharges differ to some extent. When the discharge voltage is high the electrical energy is sufficient to dissociate most of the  $\text{CS}_2$  and the  $\text{O}_2$ , so that an inverted CO population and hence lasing occur directly, i.e.,



The recently redetermined value for the heat of dissociation of  $\text{CS}_2$ , as measured by Okabe<sup>(14)</sup>, was used. In contrast, during low voltage discharges an inverted CO population occurs subsequent to the initiation of a chain reaction. The principal steps in the sequence are:



of these (vi), (viii), (ix) and (x) are of lesser importance; the chain is propagated via (v).

The argument for two types of initiation processes is supported by our observations of CS absorption in the ultraviolet. Subsequent to a high voltage discharge the concentration of CS decays exponentially approaching a constant value, while after a low voltage discharge the concentration of CS remains almost constant for more than one msec.<sup>(13)</sup> The latter indicates that CS is a reaction intermediate which attains a stationary state concentration, whereas in the former case, the decay rate of CS agrees with the observed increasing rate of production of CO. Also, an optimum discharge voltage to generate CS in [CS<sub>2</sub> + He] mixtures was found, and this corresponds to the observed optimum discharge voltage for laser power production. Apparently, when discharge voltages greater than the optimum are used CS<sub>2</sub> decomposes to give species other than CS. The experimental results on CS monitoring in the UV and computer calculations of the reaction kinetics will be presented in a later report.

Recently, Rosenwaks and Yatsiv<sup>(15)</sup> suggested that the reaction



contributes substantially to population inversion. Our observations of CS indicate that a rapid reaction between CS and O<sub>2</sub> does not occur since the concentration of CS (v=0...4) remains constant long after the end of the CO formation period, even with O<sub>2</sub> present in excess. That the life-time of CS produced by the flash photolysis was not affected by the presence of O<sub>2</sub> was also reported by Callear<sup>(16)</sup>. The low probability for reaction (xi) was also discussed by Hancock and Smith<sup>(5)</sup>.

#### Comparison with Other Experiments

The only published data on the delay sequence for CO lasing are those of Gregg and Thomas<sup>(17)</sup>. They observed laser pulses in flash photolyzed CS<sub>2</sub>-O<sub>2</sub> mixtures using a cavity with a grating and a rotating mirror and found two minima in delay times, those associated with 13→12 and 10→9 transitions. This led them to the conclusion that the

$\text{CO}^{(v)}$  was produced chemically as well as by collisions with electronically excited  $\text{SO}_2$ . The latter part of their conclusion is in question. Hancock and Smith<sup>(18)</sup> found only a weak CO emission associated with the slow recombination reaction:  $\text{SO} + \text{O} \rightarrow \text{SO}_2^*$ . Also, our observation of the correlation between the CS and CO concentrations shows that the main source of CO is the reaction between CS and O. However, Gregg and Thomas'  $\tau$ 's are roughly in agreement with our results, except for our finding one minimum in the delay time sequence at 12  $\rightarrow$  11.

Literature reports on the effect of added CO on laser power suggest that the manner of excitation may be an important factor. Pollack,<sup>(19)</sup> who initiated lasing in  $[\text{CS}_2 + \text{O}_2 + \text{He}]$  mixtures by flash photolysis, and Arnold and Kimbell,<sup>(20)</sup> who used an axial spark discharge, found that the addition of CO to the mixture decreased the output power. On the other hand, Suart, Arnold and Kimbell<sup>(21)</sup> observed enhanced lasing when they added cold CO to a  $\text{CS}_2/\text{He}$  flow, and mixed it with discharged oxygen; the same result was reported by Foster<sup>(21a)</sup>. They attributed this effect to an increase in the population inversion density through selective depopulation by V-V exchange of the lower vibrational states produced via chemical excitation, by the ground state carbon monoxide. Similarly, Jeffers<sup>(22)</sup> reported a factor of two increase in power in a transverse flow configuration when he added CO to the  $\text{CS}_2$  flow and subsequently mixed these with discharged  $[\text{O}_2 + \text{He}]$ . A positive effect due to carbon monoxide was also reported by Searles and Djeu<sup>(23)</sup> in a  $\text{CS}_2/\text{O}_2$  flame laser. Our experimental configuration is similar to that used by Arnold and Kimbell and we found that the addition of CO to the mixture resulted in a decrease of laser power both in grating tuned and in conventional cavities. Figures 9 and 15 show the results for the former and the latter cases, respectively. In these experiments the added CO might be excited by the pulsed discharge, but the population in the higher levels would be smaller than in the ground state by several orders of magnitude. This is suggested by experiment and by theoretical predictions<sup>(24,25)</sup>

Our observations on the effect of added CO may be qualitatively correlated to the substantial production of  $\text{CO}^{(v \leq 7)}$  via reaction (iii). For an initial distribution such as shown in Figure 11 the chemically unexcited diluent merely raises the relative population in the low  $v$  states to produce a distribution with a shallow minimum, one that resembles a somewhat relaxed system. This accelerates relaxation to an equilibrium state and accounts for the observed shortening of laser duration for each transition, as shown in Figure 8.

Recent measurements of relative rates for (iii) by Hancock, Morley and Smith<sup>(6)</sup> and by Foster<sup>(21a)</sup> provide no information for vibrational levels  $v < 6$ ; where their data overlap ours the agreement is good, particularly with the latter, in view of the assigned error limits. H. M. & S. made two types of measurements. In one they estimated the stationary distribution of  $\text{CO}^{(v)}$  in a flowing  $[\text{CS}_2 + \text{O}]$  mixture. The recorded light intensities were interpreted in terms of specific chemical excitation rates, using the relative spontaneous emission intensities and collisional relaxation rates. They indicated the possible presence of large errors in the rates for  $v < 7$ , because the latter were given by the difference between deactivating rates of CO from  $v$  to lower levels, and from higher levels to  $v$ . In their second method they directly monitored the population of excited  $\text{CO}^{(v)}$  in flash-photolyzed  $[\text{CS}_2 + \text{O}_2 + \text{Ar}]$  mixtures, using the CO cw laser lines  $20 \rightarrow 19$  to  $5 \rightarrow 4$  transitions as a light source. Though the concentration of CO is of the order of  $10^{-3}$  torr, the observed distribution at  $50 \mu\text{sec}$  after the flash is determined by both the chemical production rate and V-V relaxation. Extrapolation to zero time shows  $\phi_4$  and  $\phi_5 \approx 0$ . In our measurements of CO emission the scanning time of the monochromator, which required 2 hrs. to cover the CO fundamental region, limits the integration time of the signal, and the signal-to-noise ratio is not as good as desired for the weak bands. The lower transitions, with small radiative transition

probabilities, do not overlap each other as much as do the higher transitions. In any case the observed spectrum is quite different from the one calculated using the distribution given by Hancock, et. al., as seen from Fig. 10(c). In this respect, an interesting analysis was presented by Dawson and Tam<sup>(26)</sup> who calculated the stationary vibrational state distribution of CO, including chemical formation of CO in each level, V-V and V-T energy transfers, spontaneous radiation loss, and removal of CO by pumping. They could explain the two sets of experimental CO distributions reported by Hancock and Smith<sup>(12)</sup> by using the initial formation rates proposed by Hancock, Morley and Smith<sup>(6)</sup>. However, the results of Arnold, et. al. which required a distribution with a large rate of CO formation was difficult to simulate without assuming CO formation in the low levels. Since the distribution with a high formation rate of CO should be more sensitive to the form of the initial distribution of CO, this conclusion supports the initial formation rates of CO<sup>(v)</sup> given by our experiments. Note that the analysis by Dawson and Tam was made on the basis of calculated V-V rates according to the modified SSH theory, which leads to rates for the low v levels that are smaller by a factor of about 6, than those of Hancock and Smith, or the ones estimated from the Sharma-Brau theory. Therefore, the conclusion derived by Dawson and Tam requires further analysis.

When the chemical reaction is initiated by a discharge the initial conditions may differ significantly from those in (O + CS<sub>2</sub>) flow systems. We assumed that the plasma state disappeared within about 1 μsec, since the half-width of the current pulse was about 0.3 μsec. However, ionic or electronically excited species with lifetimes longer than 0.3 μsec might contribute to the formation of CO by reactions, such as

$$CS^+ + O \rightarrow CO + S^+; CS^+ + O \rightarrow CO^+ + S, \text{ or } CS^{\ddagger} + O_2 \rightarrow CO + SO, \text{ etc.}$$

Vibrational states of CO in up to v = 17 were seen in the present system. The relative populations at v = 13 ~ 17 agree well with those based on the flash-photolyzed

(CS<sub>2</sub> + O<sub>2</sub>) mixtures as reported by Hancock, et. al.<sup>(6)</sup> Using the new value for the heat of formation of CS<sup>(14)</sup>, the exothermicity for (iii) is 84.6 kcal/mole; this permits excitation to  $v = 15$ . However, as suggested by Hancock, et. al., CS is also vibrationally excited since CS in levels  $v = 0 \sim 4$  were detected in our U. V. absorption experiments with a vibrational temperature of about 12000°K<sup>(13)</sup>. If the vibrational energy of the CS can be converted to that of CO, CS( $v=4$ ) can supply 14.6 kcal extra and the  $v=16$  level for CO can be reached.

#### SUMMARY

(1) In the pulse initiated [CS<sub>2</sub> + O<sub>2</sub> + He] laser system there is an optimum discharge voltage for maximizing laser power. The optimum voltage is higher for mixtures lean in O<sub>2</sub> and rich in CS<sub>2</sub>. The maximum power of the laser is proportional to the CS<sub>2</sub> content in O<sub>2</sub>-rich mixtures.

(2) When the discharge voltage is higher than the optimum, CS and O are generated by dissociation of the reactants in the discharge, and these are directly involved in the lasing reaction [O + CS → CO<sup>(v)</sup> + S]. When the discharge voltage is low, a chain reaction is initiated.

(3) The delay sequence of laser pulses for each vibrational transition was recorded using a grating cavity. The minimum delay occurs for the 12 → 11 transition, with longer delays for both the higher and lower states.

(4) The time-resolved emission spectra of CO[ $v \rightarrow v-1$ ] fundamentals were observed in order to deduce the vibrational distribution of chemically generated CO<sup>(v)</sup>. The distribution at 23 μsec subsequent to the discharge pulse shows a maximum at  $v = 12$ , a minimum at  $v = 4$ , and a population that increases toward lower  $v$ .

(5) The relative population for each vibrational level in  $v = 14 \sim 5$  was calculated from the laser delay data; the results were found to be consistent with those obtained

from the CO spontaneous emission measurements. Also, from the time-history of the vibrational distribution one can predict qualitatively the power and the duration of the lasing pulse for each vibrational transition. These agree with observations.

(6) The shape of the normalized nascent  $\text{CO}^{(v)}$  population distribution [Fig. 11] suggests the presence of two mechanisms for the generation of vibrationally excited CO, but it is not known which reactions other than  $[\text{O} + \text{CS} \rightarrow \text{CO}^{(v)} + \text{S}]$  contribute to the populations in these lower levels for pulse-discharged  $[\text{CS}_2 + \text{O}_2 + \text{He}]$  mixtures.

#### ACKNOWLEDGEMENTS

This work was supported by the Advanced Research Projects Agency of the Department of Defense and monitored by the Office of Naval Research under Contract No. N00014-67-A-0077-0006.

REFERENCES

1. H. S. Pilloff, S. K. Searles and N. Djeu, *Appl. Phys. Letters*, 19, 9 (1971).
2. A. B. Callear and I.W.M. Smith, *Nature*, 213, 382 (1967).
3. A. A. Westenberg and N. deHaas, *J. Chem. Phys.* 50, 707 (1969).
4. I.W.M. Smith, *Trans. Faraday Soc.*, 64, 378 (1968).
5. G. Hancock and I.W.M. Smith, *Trans. Faraday Soc.*, 67, 2586 (1971).
6. G. Hancock, C. Morley and I.W.M. Smith, *Chem. Phys. Letters*, 12, 193 (1971).
7. C.K.N. Patel, *Phys. Rev.*, 141, 71 (1966).
8. R. Ladenburg and S. Levy, *Z. Physik*, 65, 185 (1930).
9. A. W. Mantz, E.R. Nichols, B. D. Alpert and K. N. Rao, *J. Mol. Spectros.*, 35, 325 (1970).
10. G. Abraham and E. R. Fisher, Report from Wayne State University, RIES 71-39, October 1971.
11. R. A. Toth, R. H. Hunt, and E. K. Plyler, *J. Mol. Spectros.*, 32, 85 (1969).
12. G. Hancock and I.W.M. Smith, *Appl. Optics*, 10, 1827 (1971).
13. Our unpublished work.
14. H. Okabe, *J. Chem. Phys.*, 56, 4381 (1972).
15. S. Rosenwaks and S. Yatsiv, *Chem. Phys. Letters*, 9, 266 (1971).
16. A. B. Callear, *Proc. Roy. Soc.*, A276, 401 (1963).
17. D. W. Gregg and S. J. Thomas, *J. Appl. Phys.*, 39, 4399 (1968).
18. G. Hancock and I.W.M. Smith, *Chem. Phys. Letters*, 3, 573 (1969).
19. M. A. Pollack, *Appl. Phys. Letters*, 8, 237 (1966).
20. S. J. Arnold and G. H. Kimbell, *Appl. Phys. Letters*, 15, 351 (1969).
21. R.D. Suart, S.J. Arnold and G.H. Kimbell, *Chem. Phys. Letters*, 7, 337 (1970).
- 21a. K. D. Foster, *J. Chem. Phys.* 57, 2451 (1972).

22. W. Q. Jeffers, Appl. Phys. Letters, 17, 67 (1970).
23. S. K. Searles and N. Djcu, Chem. Phys. Letters, 12, 53 (1971).
24. J. W. Rich and H. M. Thompson, Appl. Phys. Letters, 19, 3 (1971).
25. W. Q. Jeffers and C. E. Wiswall, IEEE J. QE, QE-7, 407 (1971).
26. P. H. Dawson and W. G. Tamm, Can. J. Phys., 50, 889 (1972).
27. R. D. Suart, P. H. Dawson and G. H. Kimbell, J. App. Phys., 43, 1022 (1972).

TABLE I  
Relative Populations of CO Vibrational Levels

Laser Delay Measurements							IR Emission Measurements		
Assumed $\phi_{11}/\phi_{12}$	0.9		0.85		0.8		this work	Hancock, et. al.	
$v$	$\phi_{v-1}/\phi_v$	$\phi_v$	$\phi_{v-1}/\phi_v$	$\phi_v$	$\phi_{v-1}/\phi_v$	$\phi_v$		$\phi_v^{(a)}$	$\phi_v^{(b)}$
17							0.13	0	0.18
16							0.30	0	0.32
15							0.49	~0.2	0.58
14	1.07	0.93	1.06	0.94	1.02	0.98	0.72	0.64	0.90
13	0.93	<u>1.00</u>	0.90	<u>1.00</u>	0.87	<u>1.00</u>	<u>1.00</u>	<u>1.00</u>	<u>1.00</u>
12	0.90	0.93	0.85	0.90	0.80	0.87	1.03	0.87	0.85
11	0.88	0.84	0.83	0.77	0.75	0.70	0.90	0.80	0.65
10	0.89	0.75	0.81	0.64	0.69	0.52	0.80	0.66	0.55
9	0.88	0.66	0.78	0.51	0.55	0.36	0.71	0.61	0.41
8	0.87	0.58	0.73	0.40	0.18	0.20	0.62	0.27	0.32
7	0.90	0.50	0.72	0.29	-2.9	0.036	0.65	~0.06	0.17
6	0.89	0.45	0.60	0.17			0.61		0.05
5	0.87	0.39	0.29	0.05			0.57		
4		0.35		0.015			0.60		
3							0.91		
2							1.20		
1							2.10		

(a) Derived from O + CS<sub>2</sub> system

(b) Derived from flash-photolyzed CS<sub>2</sub> + O<sub>2</sub>

LEGENDS FOR FIGURES

- Figure 1. Schematic for tuned laser intensity measurements.
- Figure 2. Signal profiles as a function of discharge voltage and O<sub>2</sub> content.  
Time progresses from left to right.  
(a) Abscissa 200 μsec/cm; ordinate 0.2 V/cm.  
(b) Abscissa 100 μsec/cm; ordinate 0.2 V/cm.
- Figure 3. Signal profiles as a function of He content.
- Figure 4. Integrated power dependence on O<sub>2</sub> partial pressure.
- Figure 5. Dependence of delay times on operating conditions.
- Figure 6. Integrated laser power output, as a function of vibrational level, normalized to peak value; CS<sub>2</sub> 0.017 torr + O<sub>2</sub> 0.68 torr + He 1.7 torr.
- Figure 7. Change of time delay for initiation of P(19) laser pulse, as a function of vibrational level (abscissa: 20 μsec/div; ordinate for v = 13 → 12 through v = 6 → 5 transitions: 0.01, 0.05, 0.05, 0.02 V/div.)
- Figure 8. Time history of P(9) lasing line, for no added CO (a); 0.016 torr CO added (b); 0.032 torr CO added (c).
- Figure 9. Dependence of integrated power for P(9) on vibrational transition and the amount of added CO. [Conditions same as in Figure 8.]
- Figure 10. Observed (O) vs calculated (T) [via eq. 5] superposed spectral intensities of CO spontaneous emissions: 0.045 torr CS<sub>2</sub> + 0.76 torr O<sub>2</sub> + 3.0 torr He; 15 kV discharge; (a) 23 μsec, (b) 148 μsec after the discharge pulse, (c) calculated spectrum on the basis of Hancock, Morley and Smith distribution.
- Figure 11. Normalized vibrational population at selected delay times.

Figure 12. Total population, total excited state population, total vibrational quanta and average quanta per  $\text{CO}^{(v)}$ , as a function of time. The experimental data are from Figure 11.

Figure 13. Dependence of  $1/T_{12 \rightarrow 11}^{(J)}$  on  $\phi$  ratio. The observed (O) were normalized to the calculated curves at P(11).

Figure 14. Relative gain vs time after initiation, measured at P(9) for various  $v \rightarrow (v-1)$ . Derived from experimental data, Fig. 11.

Figure 15. Dependence of total integrated power on the amount of CO added, for various discharge voltages.

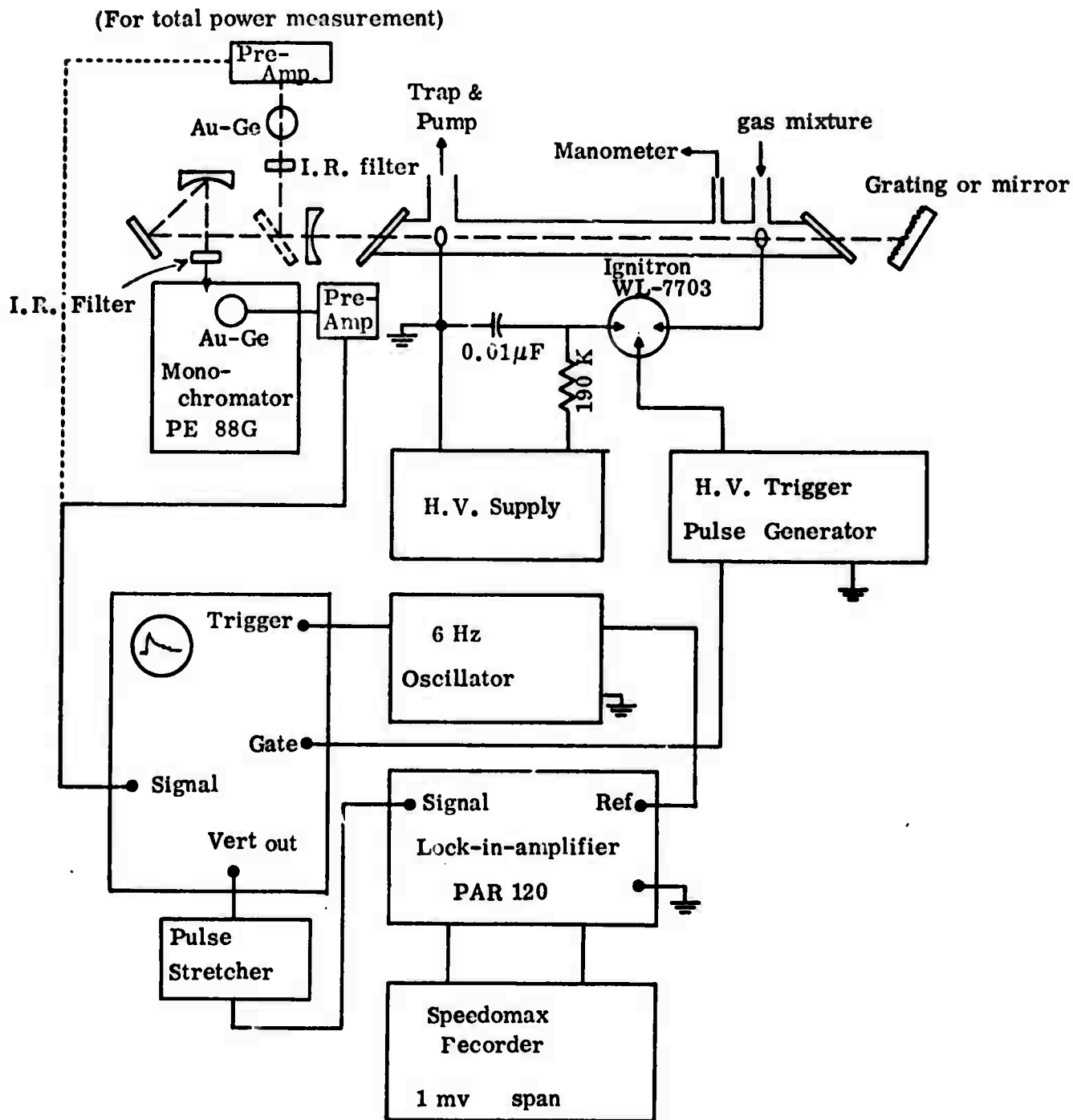
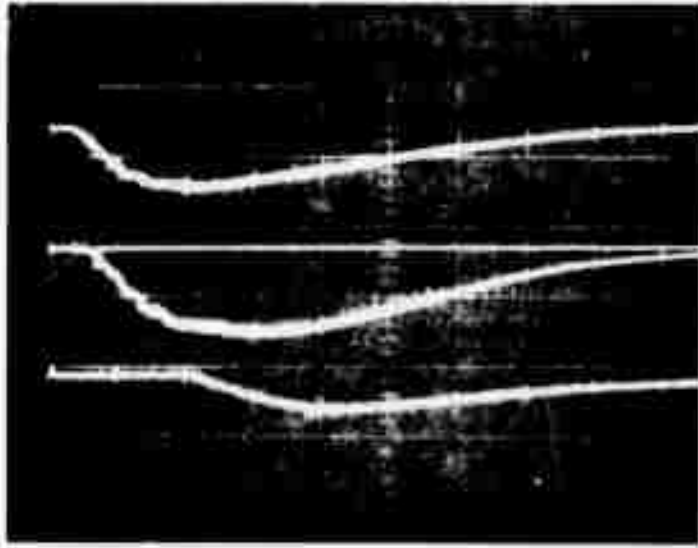


FIGURE 1. Schematic for Tuned Laser Intensity Measurements



Discharge  
Voltage

7 Kv

10

13

FIGURE 2a

CS<sub>2</sub> 0.018 torr

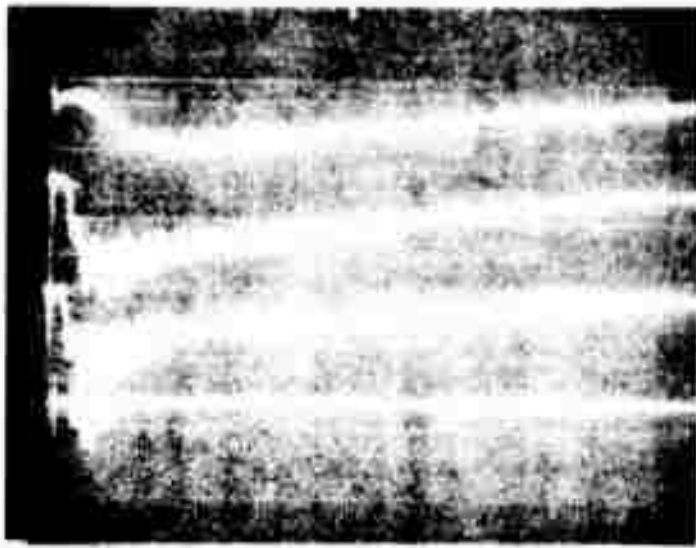
O<sub>2</sub> 0.037 torr

He 1.86 torr

---

Total 1.91 torr

Reproduced from  
best available copy. 



Discharge  
Voltage

7 Kv

9

10

12

FIGURE 2b

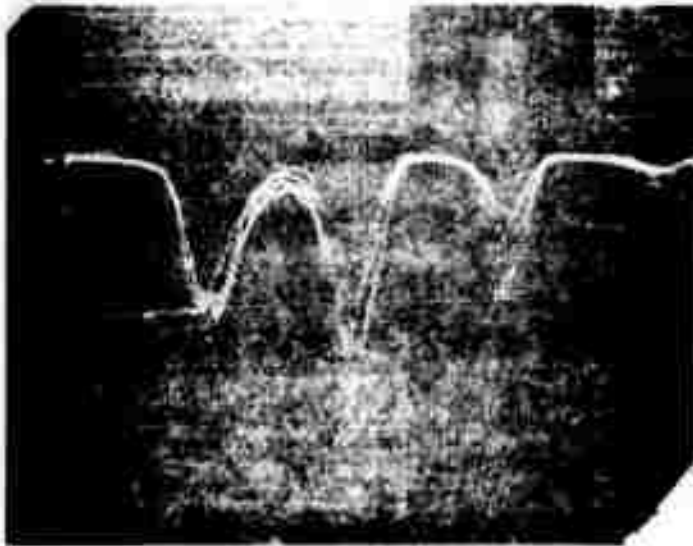
CS<sub>2</sub> 0.018 torr

O<sub>2</sub> 0.36 torr

He 1.73 torr

---

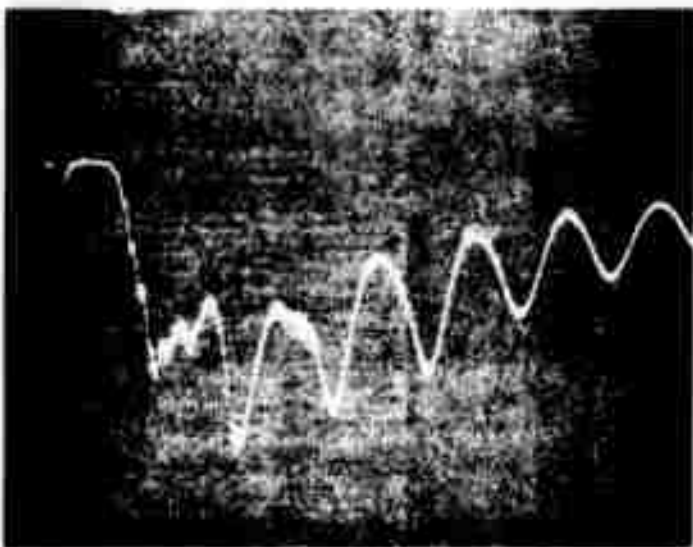
Total 2.16 torr



(a)  $\left\{ \begin{array}{l} \text{CS}_2 \\ \text{O}_2 \\ \text{He} \end{array} \right. \begin{array}{l} 0.02 \text{ torr} \\ 0.85 \text{ torr} \\ 0 \text{ torr} \end{array}$

20 $\mu$ s/div

10 Kv

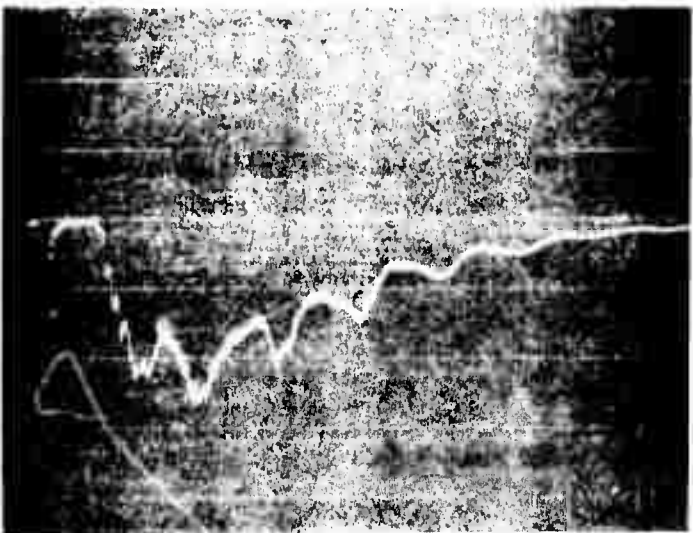


(b)  $\left\{ \begin{array}{l} \text{CS}_2 \\ \text{O}_2 \\ \text{He} \end{array} \right. \begin{array}{l} 0.02 \text{ torr} \\ 0.6 \text{ torr} \\ 3.1 \text{ torr} \end{array}$

20 $\mu$ s/div

10 Kv

Reproduced from  
best available copy. 



(c)  $\left\{ \begin{array}{l} \text{CS}_2 \\ \text{O}_2 \\ \text{He} \end{array} \right. \begin{array}{l} 0.02 \text{ torr} \\ 0.6 \text{ torr} \\ 6.6 \text{ torr} \end{array}$

20 $\mu$ s/div

12 Kv

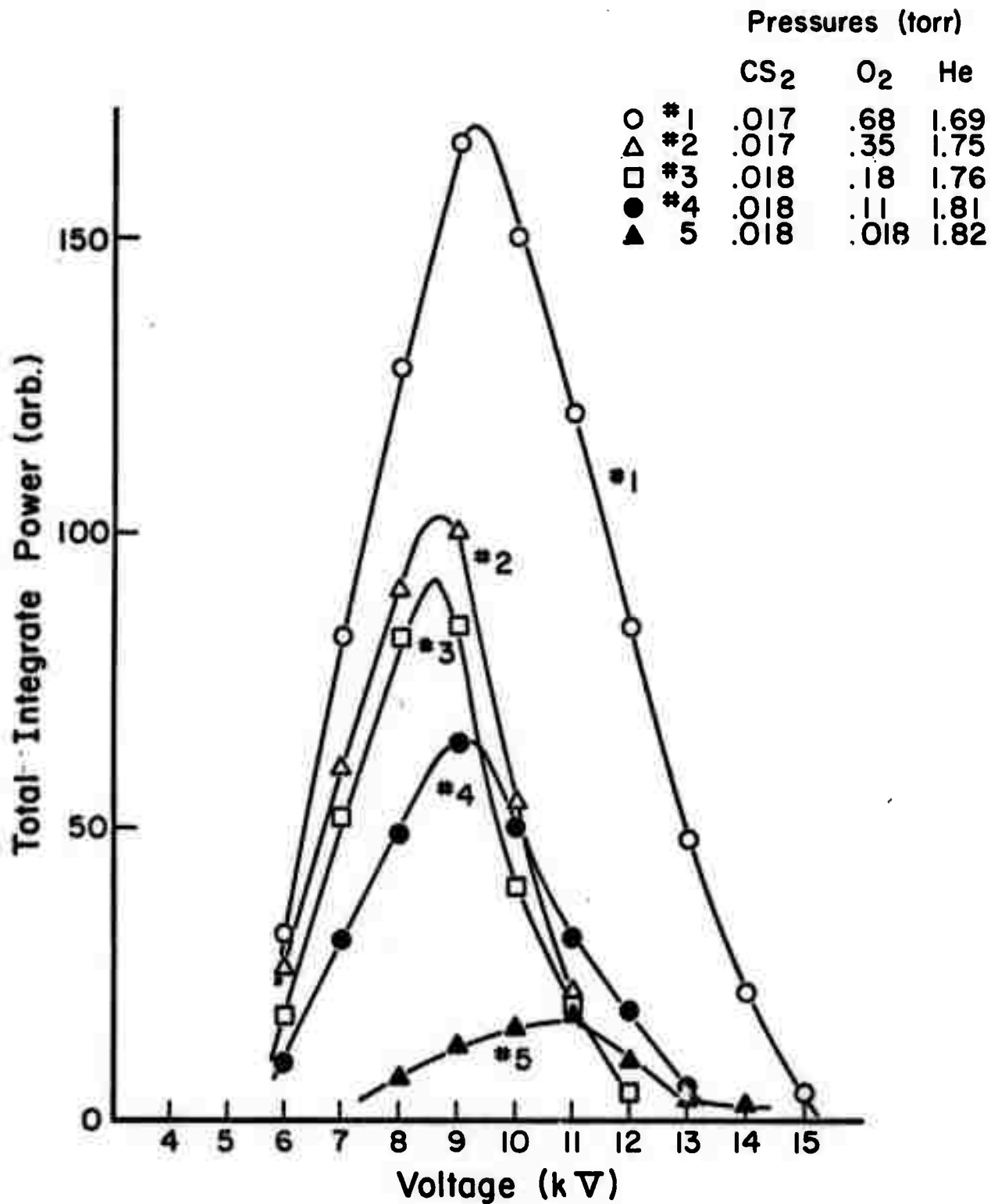


Fig. 4 Integrated power dependence on O<sub>2</sub> partial pressure.

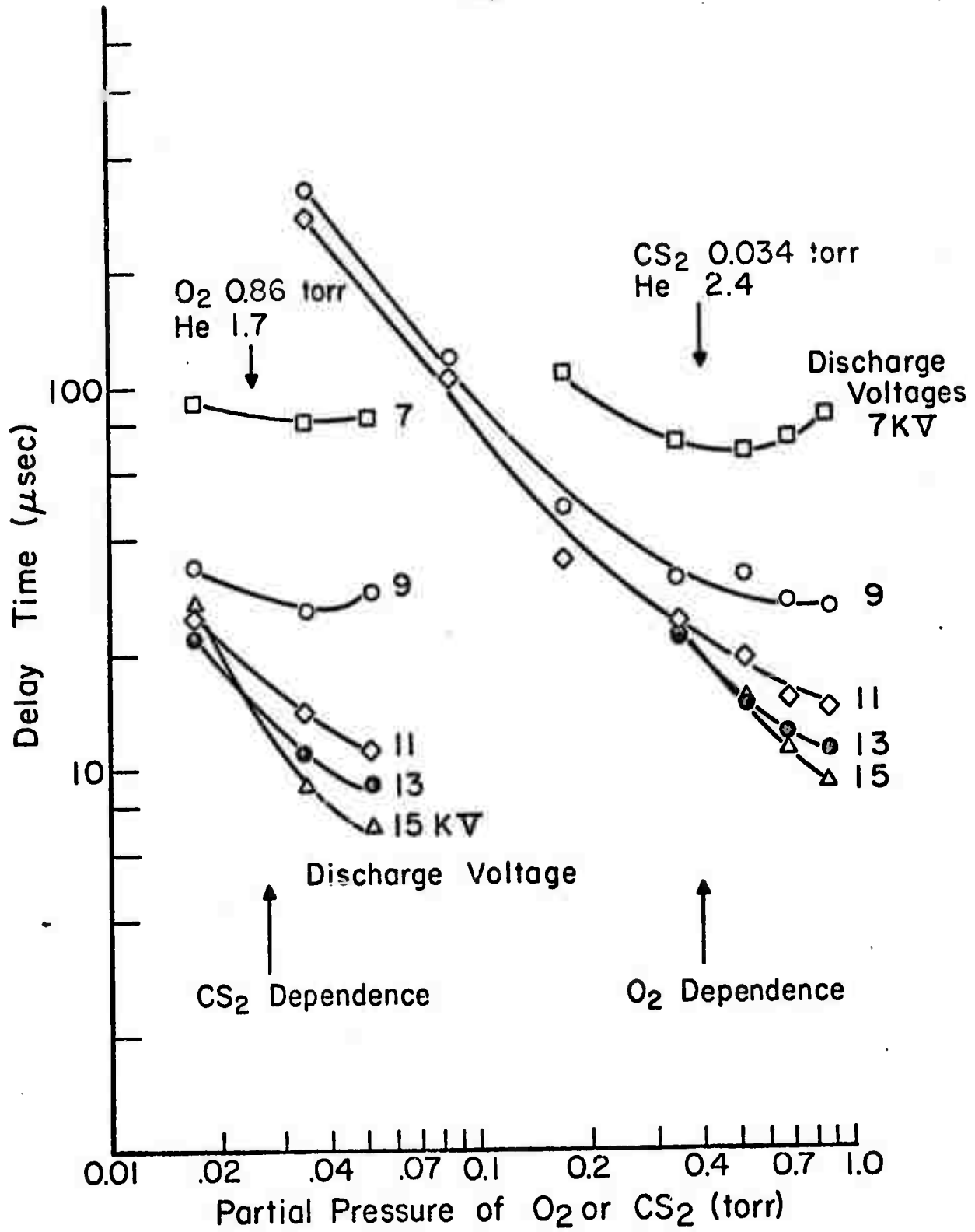


Fig. 5 Dependence of delay times on operating conditions.

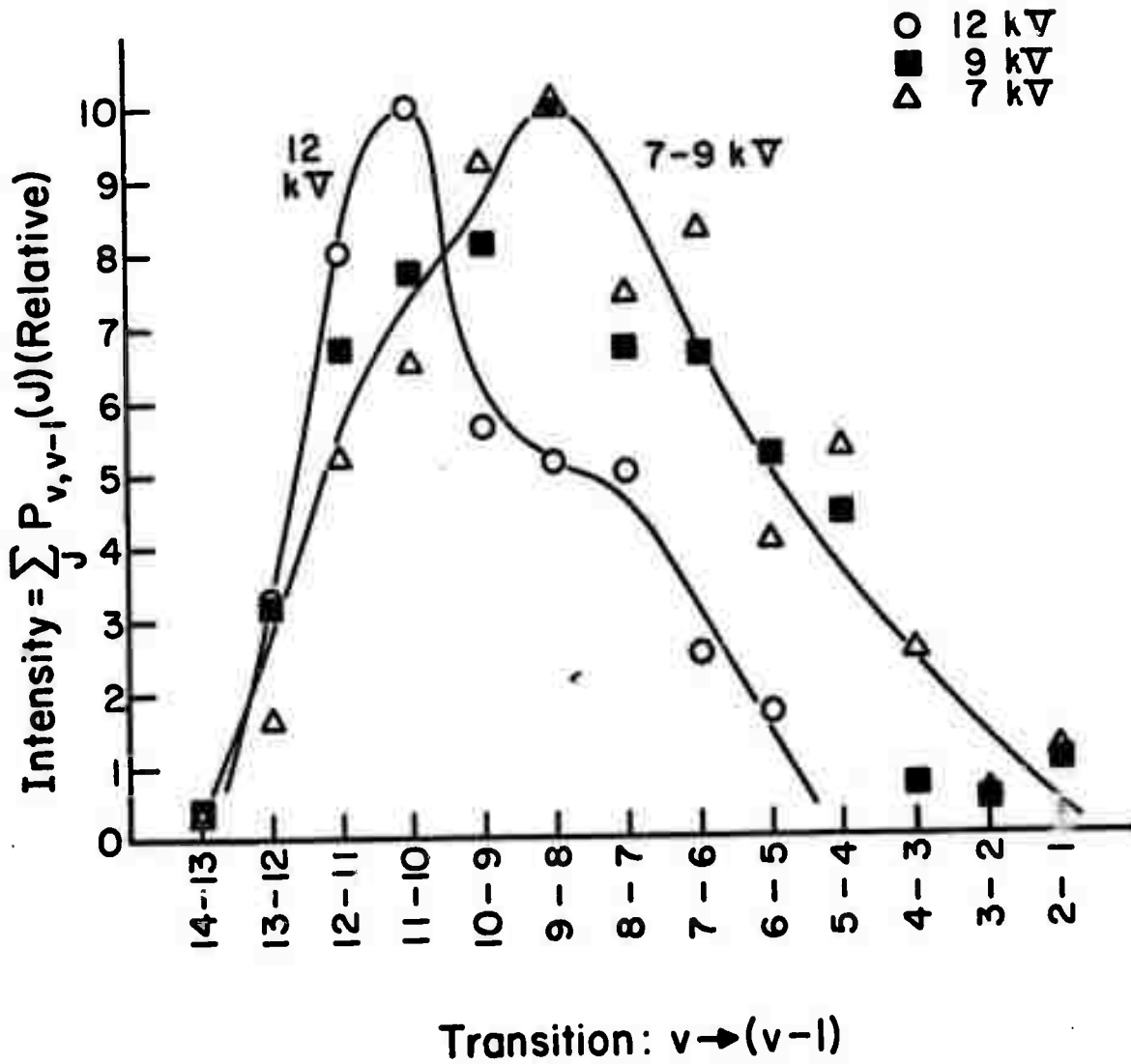


Fig. 6 Integrated Laser power-output as a function of vibrational level, normalized to peak value; CS<sub>2</sub> 0.017 torr + O<sub>2</sub> 0.68 torr + He 1.7 torr.



**FIGURE 7.** Change of time delay for initiation of  $P(10)$  laser pulse, as a function of vibrational level (abscissa:  $20\mu\text{s}/\text{div}$ ; ordinate for  $v = 13 \rightarrow 12$  through  $v = 6 \rightarrow 5$  transitions:  $0.01, 0.05, 0.05, 0.02 \text{ v}/\text{div}$ ).

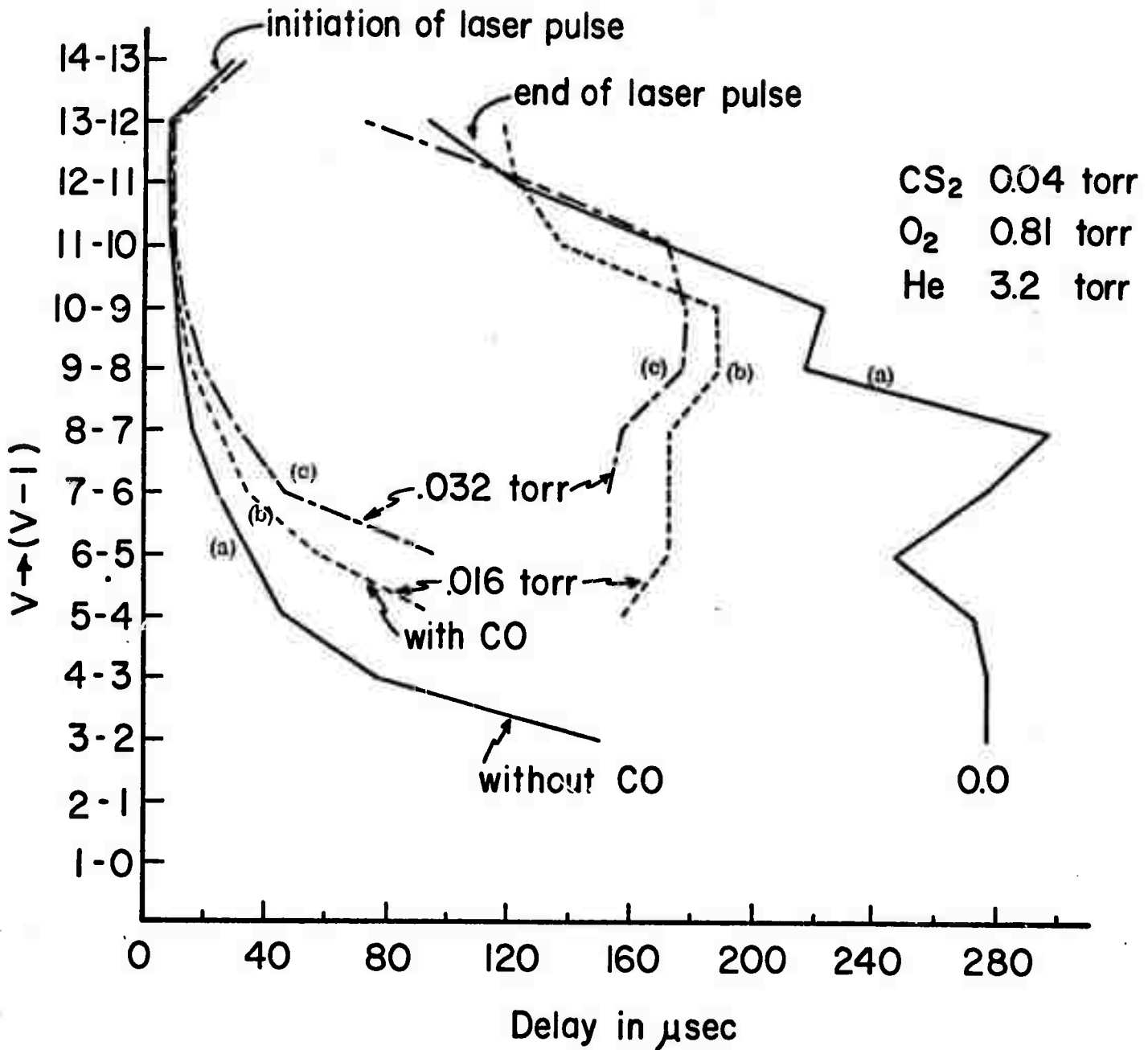


FIGURE 8. Time history of P(9) lasing line, for no added CO(a); 0.016 torr CO added (b); 0.032 torr CO added (c).

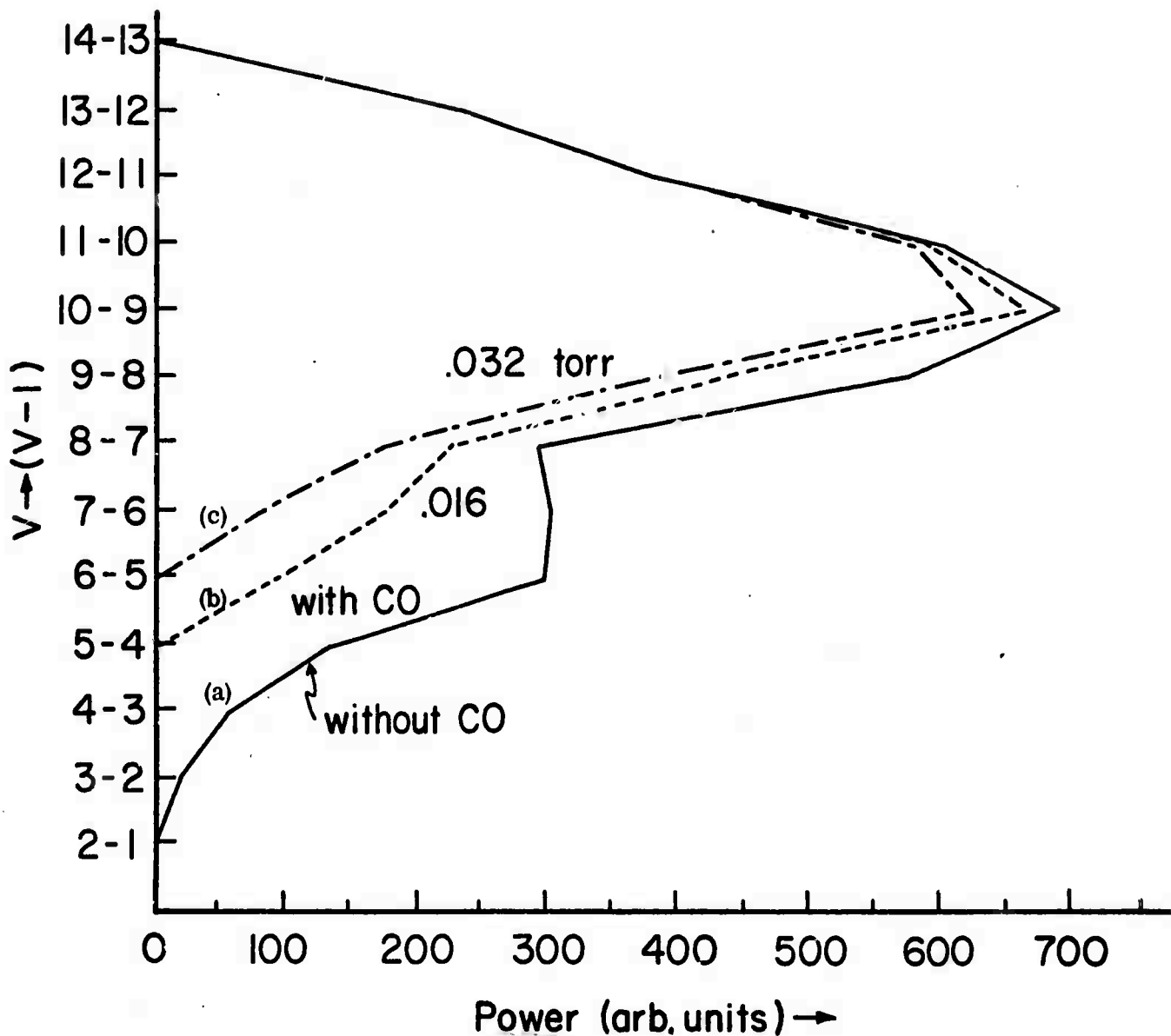
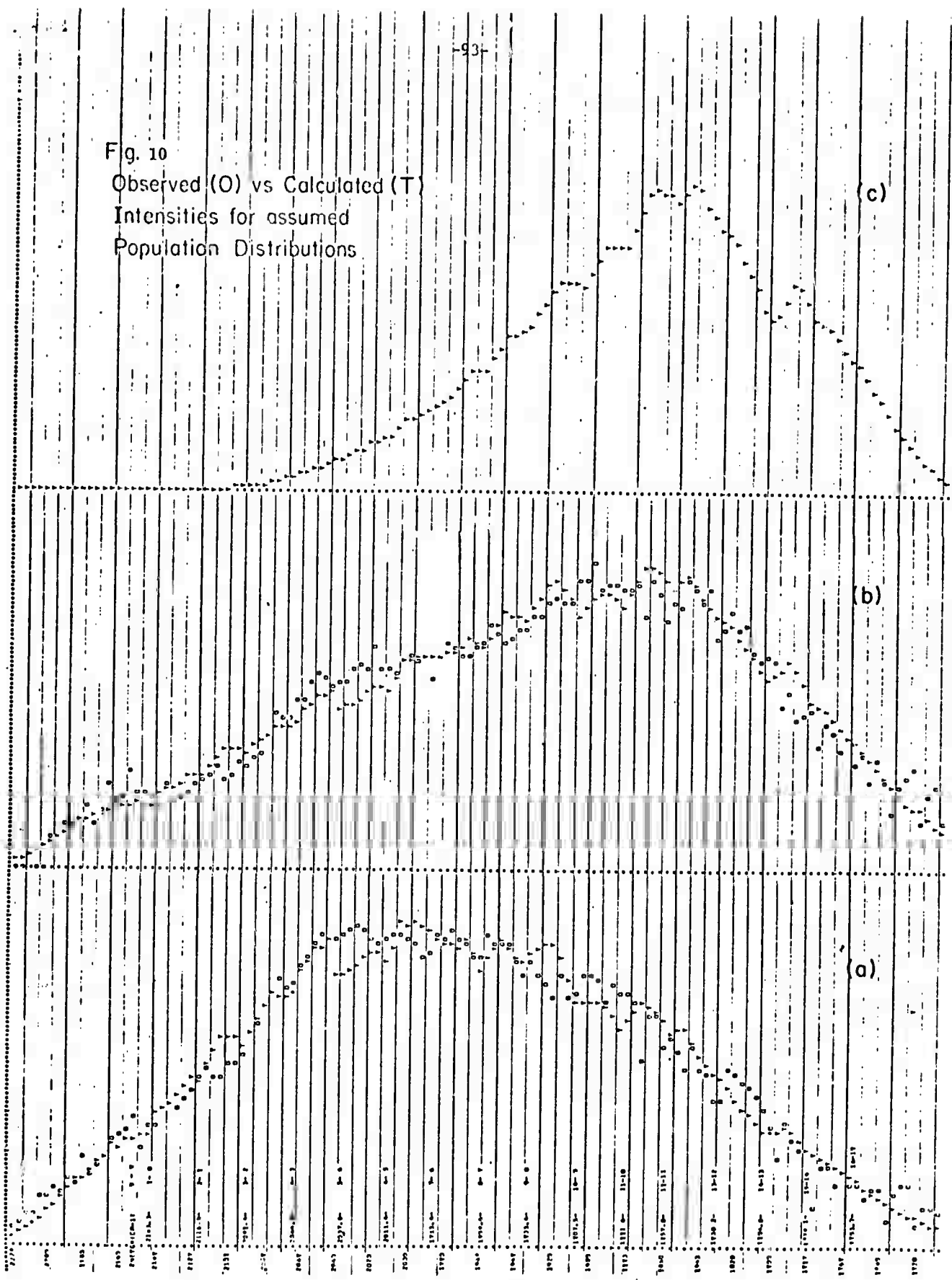


FIGURE 9. Dependence of integrated power for P(9) on vibrational transition and the amount of added CO. [Conditions same as in Figure 12].

Fig. 10  
Observed (O) vs Calculated (T)  
Intensities for assumed  
Population Distributions



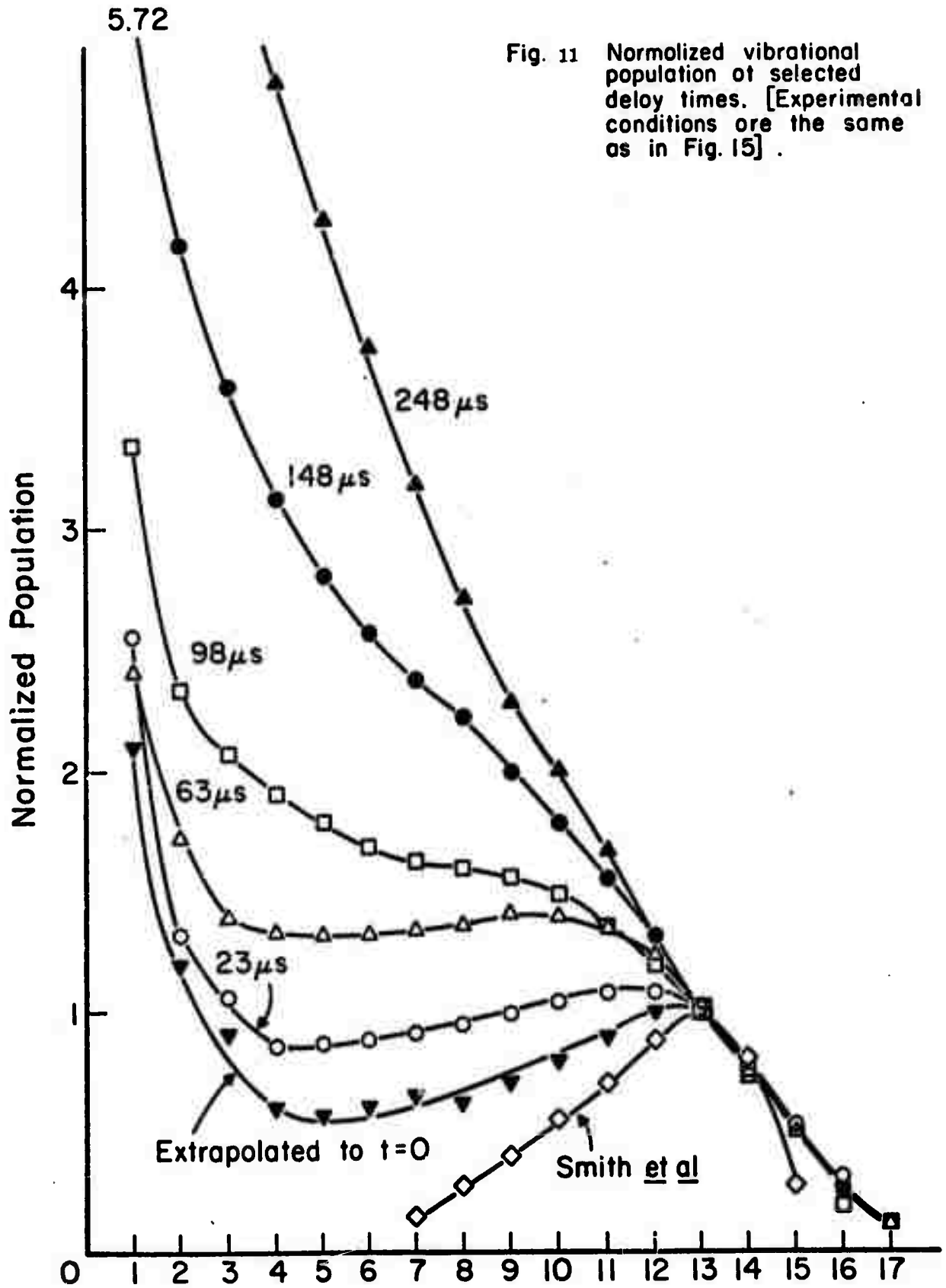


Fig. 11 Normalized vibrational population of selected delay times. [Experimental conditions are the same as in Fig. 15].

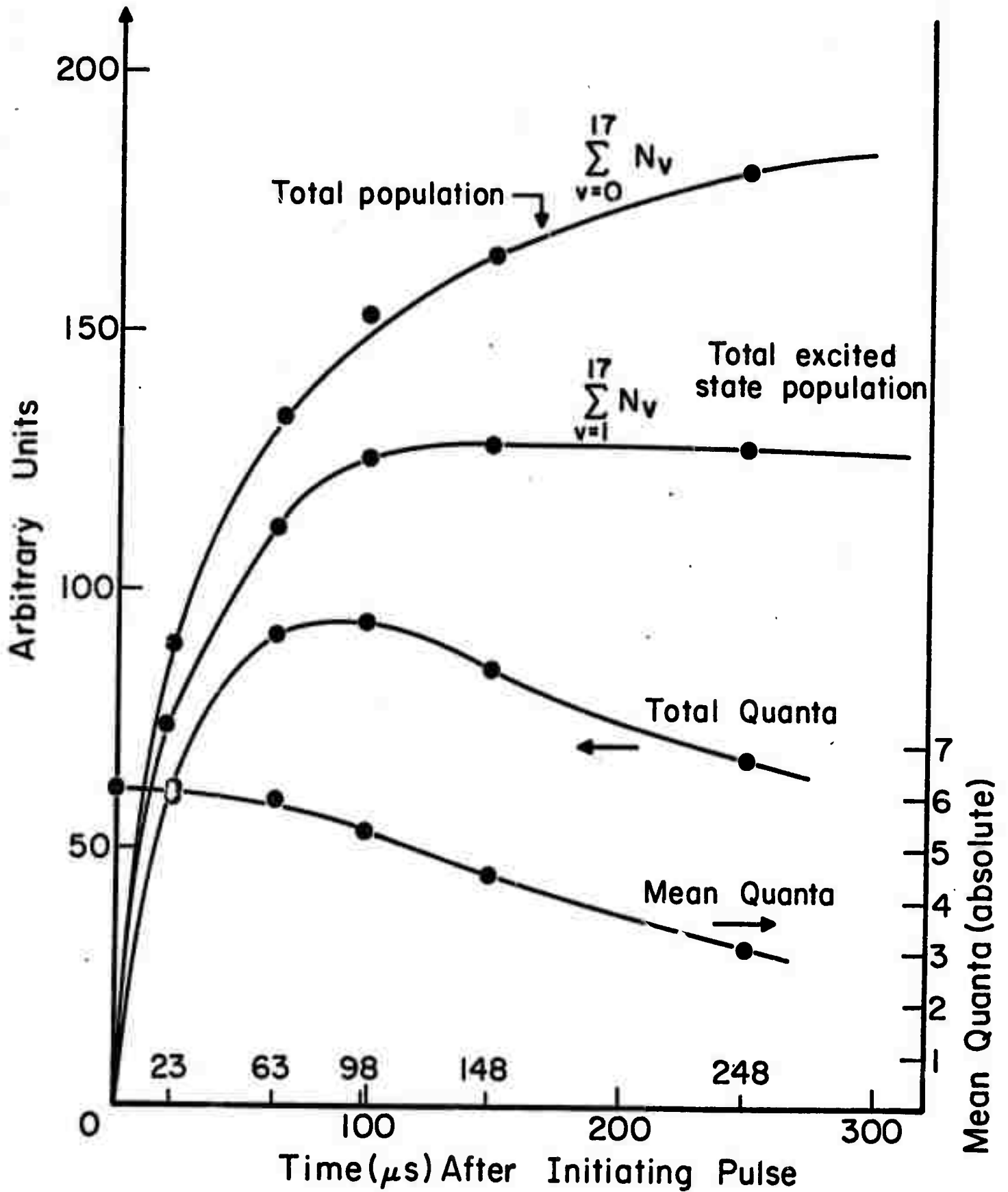


Fig.12 Experimental data from Fig.15

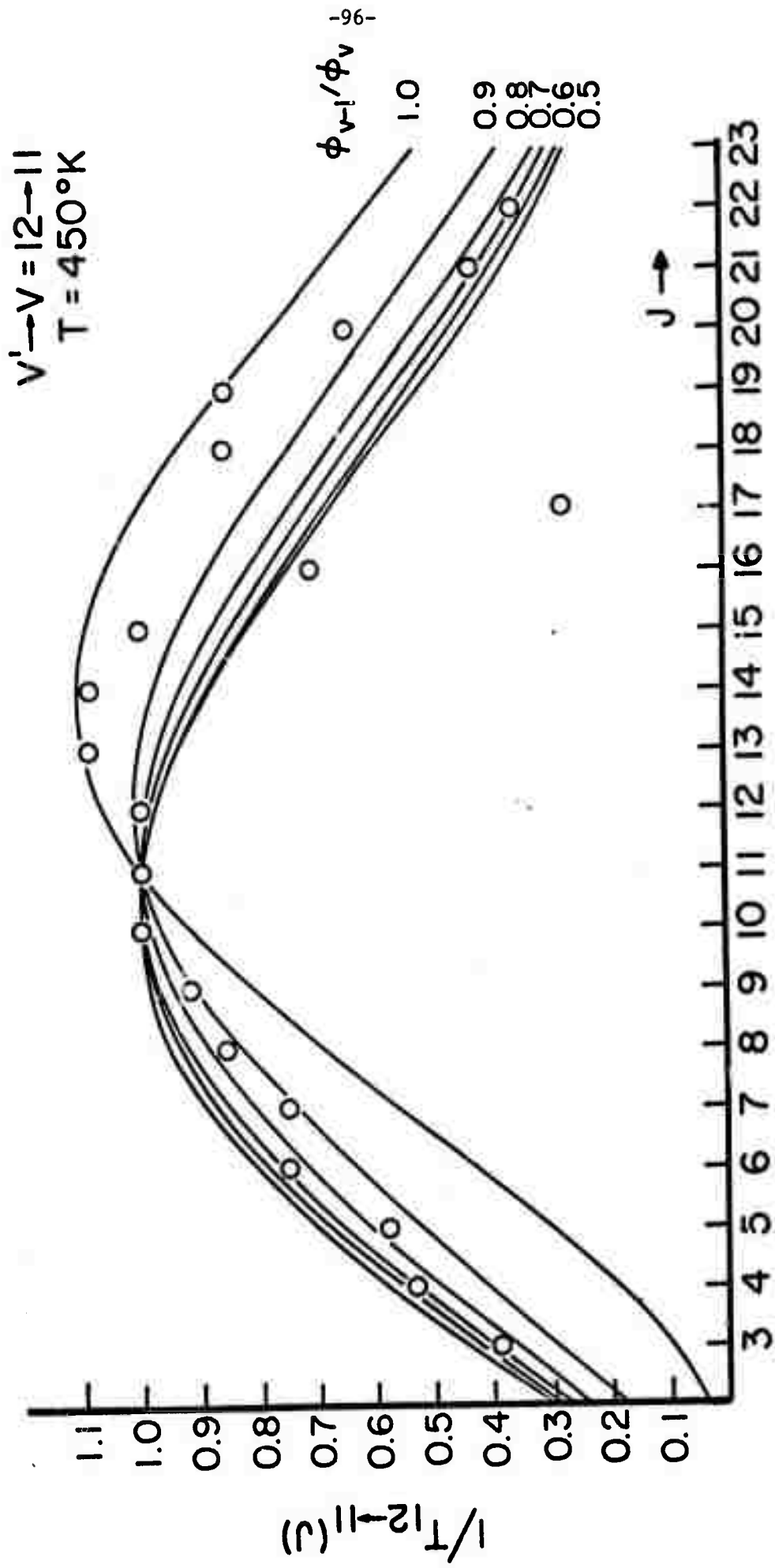


Fig. 13 Dependence of  $1/T_{12 \rightarrow 11}(J)$  on  $\phi$  ratio. The observed points (O) were normalized to the calculated curves at P(11).

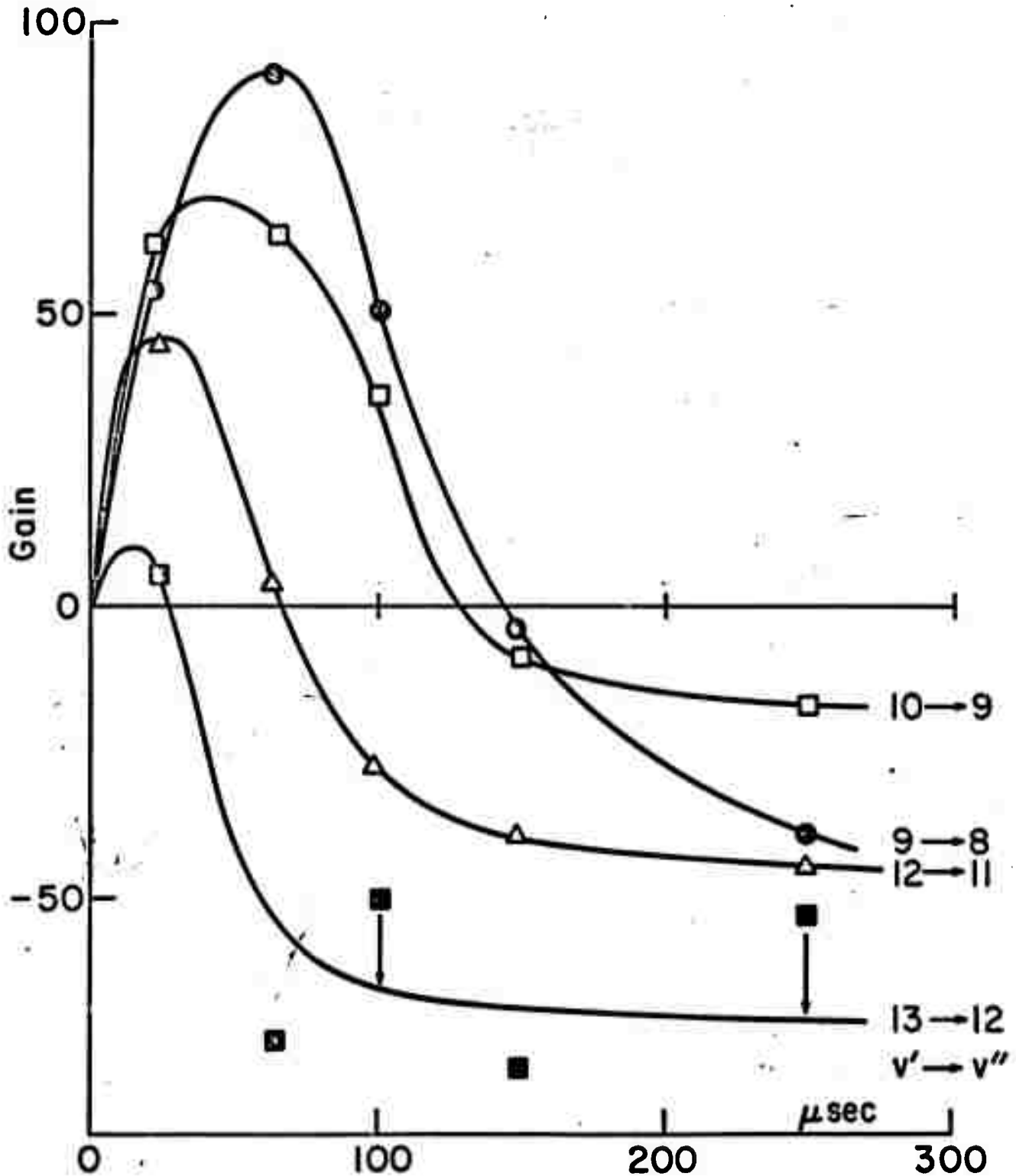


Fig. 14a Relative gain vs time after initiation, measured at P(9) for various  $v \rightarrow (v-1)$   
Derived from experimental data, Fig. 15

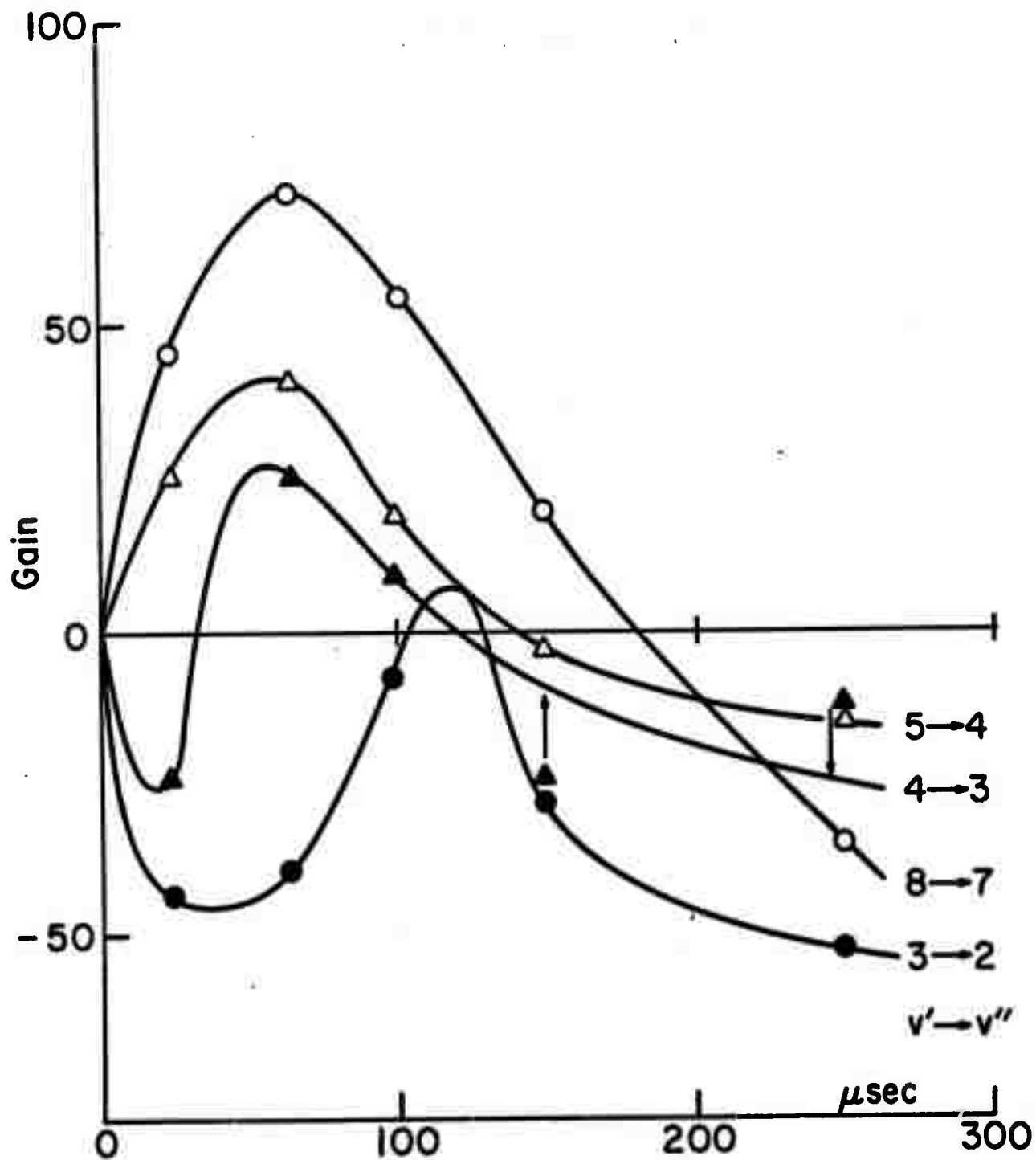


Fig. 14b Relative gain vs time after initiation, measured at P(9) for various  $v \rightarrow (v-1)$   
Derived from experimental data, Fig. 15

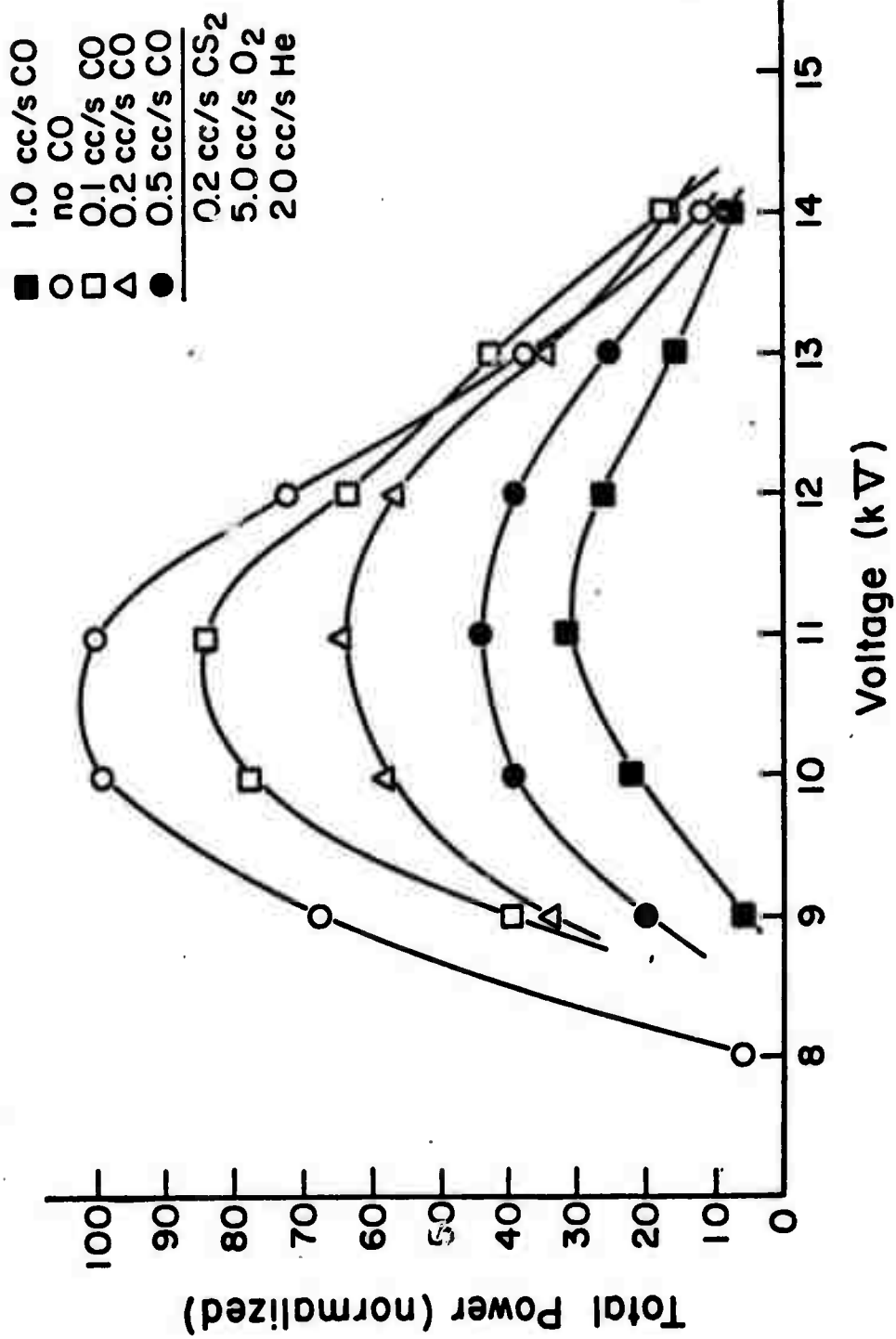


Fig. 15 Dependence of total integrated power on the amount of CO added, for various discharge voltages.

C. Studies of the O - C<sub>2</sub>H<sub>2</sub> Reaction (R. A. McFarlane)

The reaction of atomic oxygen with acetylene can lead to the production of vibrationally excited carbon monoxide via either or both of the following reactions.



It has been the purpose of our studies during the past period to determine whether as a result of the reactions a population inversion exists between vibrationally excited levels of the CO ground electronic state. A chemical laser based on this reaction and operating in the 5  $\mu$  spectral region would have significant advantages over present systems in regard to fuel costs and greatly simplified handling of both fuel and reaction products.

Our report for the previous period described the atomic oxygen source using a 1 kw, c.w. magnetron and described our measurements on atom concentration available for our studies of the above reactions. The accomplishments of the present period are discussed in detail in the accompanying papers which have been published or submitted for publication.

Measurements of Vibrational Population Distribution

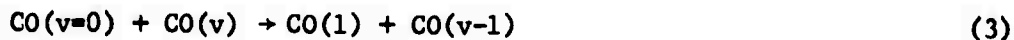
Following the injection of acetylene into the fast flowing stream of atomic oxygen (typically  $10^{-4}$  mole/sec) observation was made of the first overtone emission from the chemically formed carbon monoxide in the spectral range 2.3 - 2.8 microns. Scans were made using a one-half

meter monochrometer equipped with a room temperature PbS cell and the system sensitivity was measured using a 600°K blackbody source.

A computer program was set up to produce a synthetic spectrum using as input parameters the vibrational populations and the rotational temperature. The program included the spectroscopic constants of the CO molecule, the system sensitivity and the spectroscopic slit function. The input parameters were adjusted to give a synthetic spectrum which matched the observed scan and by this means it was possible to determine the relative populations of levels  $v = 2$  to  $v = 14$  under a wide variety of reaction conditions. With the large amount of Helium diluent used the rotational temperature was typically though not always very close to 300°K.

At low fuel levels corresponding to low concentrations of chemically formed CO, a near Boltzman distribution of population was observed corresponding to a vibrational temperature of approximately 8000°K. As the fuel level was increased the effect of the Traanor pumping mechanism became apparent whereby low vibrational levels were found to have a local vibrational temperature of 3500°K and the higher vibrational levels,  $v = 5$  to  $v = 14$  a local vibrational temperature as high as 14000°K. This latter value is typical of that found in electrically excited CO lasers and is adequate to provide a partial inversion on P branch transitions of  $J > 20$ .

Studies were made of the affect on the vibrational population of adding cold CO premixed with the  $C_2H_2$  fuel. The process



can be expected to dramatically modify the distribution where the probability for this one quantum exchange is large. At a temperature of 300°K this probability is largest for small  $v$  and peaks near  $v = 3 - 4$ . The addition of 0.1 torr cold CO resulted in a very high but positive local vibrational temperature for levels  $v = 5$  and  $v = 6$  while the addition of 0.2 torr cold CO resulted in a total vibrational inversion for levels  $v = 5$  to  $v = 7$ .

There are therefore two different regimes in which the oxygen-acetylene reaction could be employed for laser purposes.

1. High fuel condition - taking advantage of Treanor pumping to populate high  $v$  levels.
2. Preferential V-V relaxation of lower vibrational levels in a time short compared with V-T processes.

## TOTALLY INVERTED VIBRATIONAL POPULATION OF CO FORMED IN THE REACTION OF OXYGEN WITH ACETYLENE †

Y.S. LIU, R.A. McFARLANE and G.J. WOLGA

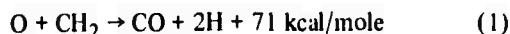
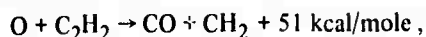
*School of Electrical Engineering, Laboratory of Plasma Studies and Materials Science Center, Cornell University, Ithaca, New York 14850, USA*

Received 15 March 1972

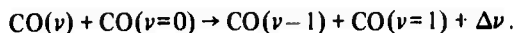
Infrared chemiluminescence from the reaction of atomic oxygen with acetylene was studied for CO laser application. A totally inverted vibrational population between  $\nu = 5$  and  $\nu = 7$  was obtained by preferentially relaxing the lower vibrational levels with added cold CO. Treanor pumping at high fuel flows was also observed.

In this letter we report the first observation of a totally inverted vibrational population distribution in carbon monoxide formed in the chemical reaction of oxygen with acetylene. It is apparent from the results that this reaction is potentially valuable for use in CO laser applications.

The primary reactions are [1]



for low fuel flows. These reactions are sufficiently energetic to permit the excitation of vibrational levels in CO up to  $\nu = 14$ . Previous studies [2] have found that as a consequence of the anharmonic nature of the molecular potential the relative populations in higher vibrational levels can be increased through intramolecular V-V energy transfer, producing a highly non-Boltzmann distribution. In the present work, advantage is taken of the V-V energy-transfer process



Calculations [2, 3] of the probability of this process

† Research supported by the Advanced Research Projects Agency and monitored by ONR under Contract N00014-67-A-0077-0006, and also through the Materials Science Center, Cornell University.

show that it peaks between  $\nu=4$  and  $\nu=6$  for temperatures between 300 and 700°K, decreasing only slightly as resonance is approached with decreasing  $\nu$  and falling off much more rapidly at higher values of  $\nu$ . It has been possible therefore with the addition of cold CO to the reaction to significantly depress the populations of levels  $\nu \leq 5$  and provide a total vibrational inversion between  $\nu=5$  and  $\nu=7$ .

Using a fast flow system, IR chemiluminescence of CO\* was measured in the fundamental and the first overtone emission regions. Atomic oxygen at flow rates in excess of  $10^{-4}$  mole/sec was produced in a microwave discharge, the concentration being established by titration with NO<sub>2</sub>. Acetylene was injected radially into a teflon reaction tube 3/8 inch i.d. and 18 inches long. The system was pumped with a 100 c.f.m. blower backed by a model 1397B Welch mechanical pump. A linear flow speed of greater than 80 m/sec in the mixing zone was measured under typical conditions.

Emission from the reaction products was monitored through NaCl windows in the side wall of the reaction tube. A silicon lens focused the light from a small region in the reaction zone, through a chopper, onto the entrance slit of a 1/2 meter Jarrell-Ash Ebert monochromator, equipped with a 105 l/mm grating blazed at 8.6 microns in first order. A room-temperature PbS photoconductive detector was used for the overtone measurements and a liquid-nitrogen cooled Au-Ge detector for observations in the fundamental region. The

detector output signal was amplified by a Keithley Model 103 low-noise amplifier and a Princeton Applied Research Model JB-5 lock-in amplifier. Spectra were recorded on a linear strip chart recorder. The entire optical path was flushed with dry nitrogen to minimize absorption by atmospheric carbon dioxide and water vapour.

A broad-band emission of substantial intensity throughout the region of the CO fundamental made it difficult to determine the vibrational populations from the fundamental emission. The first overtone emission spectrum between 2.3 and 2.8 microns was distinct however and permitted the determination of the relative population distribution by a method described by Karl et al. [4]. A computer is used to generate a simulated spectrum to compare with the experimental scans. It accounts for the instrumental sensitivity variation as a function of wavelength, the spectral slit width, the Einstein  $A$  coefficient of each upper level and the molecular spectroscopic constants. The rotational temperature and the relative population of each vibrational level are adjusted to obtain a match between the synthetic spectrum and the experimental scan.

Fig. 1 shows the vibrational population distribution of CO\* at a time approximately 100 microseconds after injection of the acetylene. The distribution did not alter appreciably for observations made several centimeters downstream. An addition of cold CO [5] to the fuel dramatically modifies the vibrational distribution leading to a total vibrational inversion with 0.2 torr CO added to the acetylene. The data have been plotted taking account of relative signal levels under different conditions of added cold CO. The data is clearly consistent with the peak in the V-V exchange probability predicted to be near  $\nu=5$  although no attempt has yet been made to set up a comprehensive model which includes reactant mixing, the detailed chemistry, V-V and V-T relaxation and radiative decay. Our observations at fuel flows six times that of fig. 1 but without the addition of cold CO show clearly the effects of V-V pumping predicted by Treanor et al. [2]. The vibrational temperature of approximately 8000°K which characterizes the Boltzmann distribution of population at very low fuel levels becomes modified at high fuel levels. A local vibrational temperature of approximately 3500°K was determined for levels  $\nu=2$ , to  $\nu=4$ , while for levels  $\nu=6$  to  $\nu=14$  populations were characteristic of a 14000°K vibrational temperature. This latter value is typical of electrically

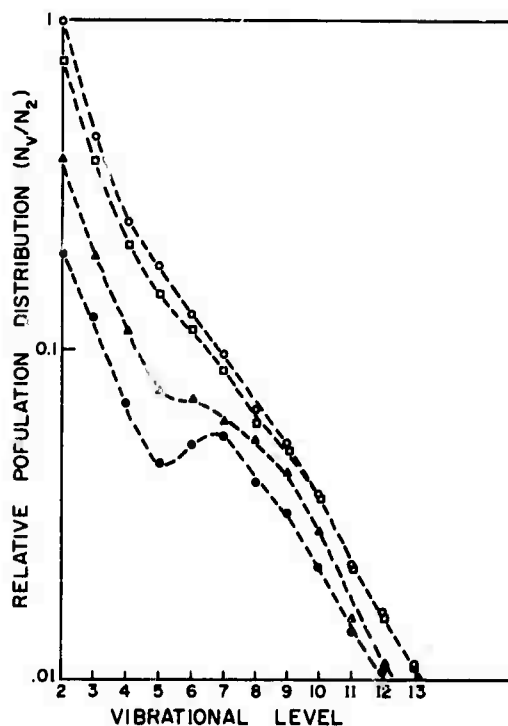


Fig. 1. Relative vibrational population distribution of CO\*. Pressures: C<sub>2</sub>H<sub>2</sub> 0.05 torr, O<sub>2</sub> 0.68 torr, He 1.67 torr. Temperature  $T_{rot} = 350^\circ\text{K}$ . [C<sub>2</sub>H<sub>2</sub>] =  $0.25 \times 10^{-4}$  mole/sec, [O] =  $1.7 \times 10^{-4}$  mole/sec.  $\circ$  Without additional cold CO,  $\square$  0.05 torr additional cold CO,  $\triangle$  0.1 torr additional cold CO,  $\diamond$  0.2 torr additional cold CO.

excited CO lasers which operate under conditions of partial inversion.

It is apparent that both modes of operation are potentially useful for CO laser application. Since the reaction rate of oxygen with acetylene is greater than that for the reaction of oxygen with carbon monoxide the above results also suggest a free burning flame laser in which a mixture of acetylene and carbon monoxide is burned in an oxygen atmosphere.

## References

- [1] D.M. Creek, C.M. Melliar-Smith and N. Jonathan, *J. Chem. Soc. A* (1970) 646.
- [2] C.E. Treanor, J.W. Rich and R.G. Rehn, *J. Chem. Phys.* 48 (1968) 1728.
- [3] W.Q. Jeffers and J.D. Kelley, *J. Chem. Phys.* 55 (1971) 4433.
- [4] G. Karl, P. Kraus and J.C. Polanyi, *J. Chem. Phys.* 46 (1967) 224.
- [5] G. Hancock and I.W.M. Smith, *Appl. Opt.* 10 (1971) 1827.

### Measurement of V-V Energy Transfer Probabilities in CO-CO Collisions

The population data obtained upon the addition of cold CO to the system were used to determine the V-V energy exchange probabilities of process (3) for excited vibrational levels  $v = 3$  to  $v = 9$ . Under the conditions of the experiment the volumetric pumping rate greatly exceeded all other loss processes for a given vibrational level population. This permits the series of coupled steady state equations describing the population densities to be uncoupled and the collisional deactivation rate due to added cold CO to be determined separately for each vibrational level. The detailed analysis is discussed in an appended paper.

Reasonably good agreement is obtained with data reported by Hancock and Smith in studies of the  $\text{CS}_2\text{-O}_2$  reaction and under very different flow conditions. The "Fast Flow Approximation" used in the present study substantially simplifies the analysis of the data and avoids uncontrolled wall effects and others which would complicate the interpretation.

Calculations were made, following the work of Caledonia and Geater, of the V-V exchange probabilities for single quantum exchange in collision. Both long and short range interactions are included in the calculation and data is now available over a sufficiently wide range of vibrational levels to indicate that both contributions are required to correctly describe the collisional process. Good agreement was obtained with our experimental measurements and those of Hancock and Smith.

### A Time-Dependent Solution of the Kinetic Equations for the Vibrational Populations

For the system under study it is necessary to provide some redistribution of vibrational energy in the carbon monoxide before conditions of total or

partial inversion maintain. This process is a dynamic one and for laser applications it is necessary to know at what time optimum population conditions occur. A computer solution was obtained for the coupled equations describing the population densities for each vibrational level as a function of time. This is discussed in detail in an appended paper. The mixing and chemistry are assumed to be very rapid and the model includes all single quantum V-V energy exchanges, V-T energy exchange and spontaneous radiative decay.

The results of calculations demonstrate the preferential deactivation of low  $v$  levels discussed above as well as the Treanor pumping of high  $v$  levels. In general it is found that the populations relax through a series of non Boltzmann distributions and at long times the populations do indeed approach a Boltzmann distribution.

Using as initial conditions those for the experiments on the effect of adding cold CO to the fuel, it was possible to reproduce the observations that 0.1 torr added cold CO gives an increased but positive local vibrational temperature while 0.2 torr leads to a total vibrational inversion.

The computation was used to study the time development of CO population using results for the initial population distribution from the  $\text{CS}_2\text{-O}_2$  reaction determined by Hancock and Smith and by Tsuchiya, Nielsen and Bauer. Only preliminary calculations have been made to date but it is clear from comparing them with the experimental time development data reported by the Cornell group, that substantial populations in  $v = 0$  and  $v = 1$  are needed to reasonably simulate the time development found. The modeling for this system described in the appended paper shows an overall time development which is somewhat too slow compared to experiment and appears to underestimate the magnitude of Treanor pumping which is operative.

To accurately describe any of the systems where the computation might be applied it is clearly desirable to include chemical reactions as time dependent contributors to the populations. Using known or estimated reaction rates this represents a trivial extension of the present program. Recent calculations of multiple quantum V-V processes by Dillon and Stephenson will be included in future computations.

#### Continuing Activity

In addition to the elaboration of the computation discussed above work is in progress to set up a laser based on the  $O-C_2H_2$  reaction and to carry out parametric studies of its performance. To this end we have:

- a) Begun the installation of a 2000 cfm. blower system to provide an order of magnitude increase in pumping capacity over that now being used. This will be used to permit operation of a transverse flow laser system.
- b) Constructed a c.w., grating tuned CO laser for diagnostic studies of both the present linear flow system and the planned transverse flow system.
- c) Constructed an electronic system for differential gain and loss measurements on any chemical laser system of interest. Two pyroelectric detectors are employed and normalization circuitry is provided to eliminate errors resulting from probe laser power fluctuations.

Measurement of V-V Energy Transfer Probabilities  
in CO-CO Collisions Following the Reaction  
of Oxygen with Acetylene.

Y. S. Liu\*  
Department of Applied Physics and Materials  
Science Center, Cornell University  
Ithaca, NY 14850

R. A. McFarlane and G. J. Wolga  
School of Electrical Engineering and Materials  
Science Center, Cornell University  
Ithaca, NY 14850

\* Now at General Electric Research and Development Center,  
Schenectady, N.Y., 12301.

Research supported by the Advanced Research Projects Agency and  
monitored by ONR under Contract N00014-67-A-0077-00006 and also  
through the Materials Science Center, Cornell University.

Measurement of V-V Energy Transfer Probabilities  
in CO-CO Collisions Following the Reaction  
of Oxygen with Acetylene.

Y. S. Liu, R. A. McFarlane and G. J. Wolga

Abstract

Infrared chemiluminescence has been studied from vibrationally excited CO formed in the reaction of oxygen with acetylene. By monitoring the first overtone emission at various levels of added cold CO in a fast-flow system, we were able to determine the V-V energy transfer probabilities  $p_{v,v-1}^{0,1}$  for  $3 \leq v \leq 9$ . The analysis is greatly simplified by using a fast-flow approximation in which the volumetric pumping rate greatly exceeds the removal rate for other loss processes. The results are compared with previously reported data and with the probabilities determined theoretically where both long and short range interaction potentials are included.

## INTRODUCTION

In recent years studies of inter- and intra- molecular energy transfer in diatomic molecules have been motivated by interest in chemical lasers. Various experimental methods have been employed to measure the rates of vibrational energy transfer which occur upon collision. Among them I.R. chemiluminescence has been exploited most extensively. The method has been successfully applied by Polanyi and his co-workers<sup>(1)</sup> to determine the relative rate constants for the production of specific energy levels of the product molecule in hydrogen halide reactions and many others. More recently, the quenching of I.R. chemiluminescence has been used by Hancock and Smith<sup>(2)</sup> to measure the rates of de-excitation of vibrationally excited CO by ground state CO and other molecules. They observed the I.R. chemiluminescence from vibrationally excited CO formed in the reaction of oxygen and carbon disulfide and studied the quenching of the CO first overtone spectrum upon the addition of various gases.

There are two times that have to be considered in I.R. chemiluminescence experiments: the spontaneous radiative lifetime  $\tau_{\text{spont}}$  and the collisional de-activation time  $\tau_{\text{collision}}$  of the molecule. The former is characterized by the spontaneous transition probabilities  $A_{v',v}$ ; the latter depends on the collisional de-activation probability and on the density. For the vibrationally excited CO molecule, the spontaneous radiative lifetime is on the order of  $10^{-3}$  seconds. A pressure of a few Torr is required for the collisional de-activation time to be of the same order.

Chemiluminescence experiments are frequently carried out using a low flow condition set by a relatively small capacity pump. The low pressure required is established by moving only a small amount of material. In the low flow system, however, undesirable and unavoidable experimental problems such as the de-excitation due to surface effects, the cascading process from the vibrationally excited states and the spatial inhomogeneity of the species have to be taken into account. These can greatly affect the accuracy of rate determinations based on

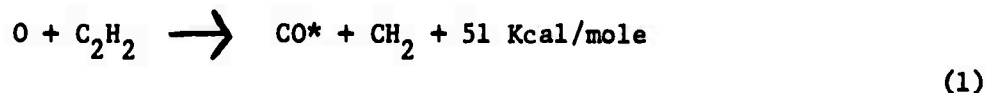
I.R. measurements and can lengthen the analysis of the experimental results.

In view of these difficulties encountered in the conventional I.R. chemiluminescence experiments using the low flow condition, it appears more appropriate to operate I.R. chemiluminescence experiments at a high flow rate. The pressure can be reduced by increasing the volumetric pumping rate. The "Fast Flow" condition is satisfied by carefully choosing the experimental parameters such that the volumetric pumping rate is made much faster than the spontaneous radiative rate and collisional deactivation rates. Under these conditions, using the appropriate approximations, the master rate equations can be de-coupled and solved in a very simple way. The approach is hence called the "Fast Flow Approximation".

The vibrational energy exchange probabilities measured in the present work are compared with those obtained by Hancock and Smith<sup>(2)</sup> in an I.R. quenching chemiluminescence experiment and with theoretical values calculated by including both long-range dipole-dipole interactions and the short range repulsive interactions. Reasonably good agreement is obtained between the present values and those reported by Hancock and Smith. This is particularly satisfying in view of the very great experimental differences in the two determinations. Both sets of data are also in good agreement with the calculated V-V energy exchange probabilities.

#### THE EXPERIMENT

Vibrationally excited CO is produced in the primary reactions:<sup>(3)</sup>

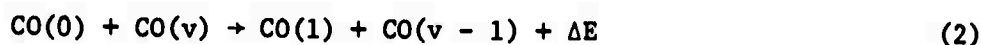


The exothermicity of the reactions is sufficient to produce vibrationally excited  $\text{CO}^*$  up to  $v = 14$ . In the present work chemiluminescence of  $\text{CO}^*$  was measured in the first overtone emission bands between 2.3 and 2.8 microns as shown in Figure 1(a). The spectra were monitored as different amounts of cold CO were added to the acetylene and injected into the mixing zone. The addition of cold CO affects not only the overall intensity of the spectrum but changes the intensity distribution as well. This latter effect is caused by the preferential deactivation of the lower vibrational levels of the vibrationally excited CO molecules. Figures 1(b) and 1(c) show two spectra recorded at different levels of added cold CO.

The experimental apparatus is shown in Figure 2. Atomic oxygen at a flow rate of  $10^{-4}$  mole/sec was produced in a microwave discharge. The oxygen concentration was determined by titration with  $\text{NO}_2$ . Acetylene was injected radially through small orifices into a teflon reaction tube 3/8 inch i.d. and 18 inches long. Precautions were taken in choosing the dimensions to assure that the low pressure and fast flow conditions were satisfied. The system was pumped with a 100 cfm blower backed by a moder 1397B Welch pump. A linear flow speed of 83 m/sec in the mixing zone was measured under normal operating condition.

The infrared emission was observed in a direction transverse to the flow. The observations were made through a side window at various positions along the flow downstream from the mixing point. The infrared emission was focussed with a silicon lens through a chopper onto the entrance slit of a Jarrell-Ash 1/2 meter Ebert monochromator. A room temperature PbS detector was used. The signal was amplified by a Keithley Model 103 low noise amplifier and processed through a Princeton Applied Research Model JB-5 lock-in-amplifier phase locked at a reference frequency set by the light chopper. The spectra were recorded on a Hewlett-Packard dual-pen strip chart recorder. The spectrometer employed a grating with 105 lines/mm blazed at 8.6 microns in first order. The optical path internal and external to the spectrometer was flushed with dry nitrogen to avoid the atmospheric water vapor absorption which overlaps strongly with the CO fundamental and somewhat less with the overtone.

The vibrational population distributions were determined by a computer simulation method introduced by Karl, Kruss and Polanyi<sup>(4)</sup>. A spectrum can be synthesized to match the experimental scan with vibrational populations and the rotational temperature as the input parameters and using the molecular and spectroscopic constants, the frequencies of transition and the instrumental characteristics. A preliminary discussion of the determination of the vibrational populations for the present system has been reported<sup>(5)</sup>. In the present work we will describe the determination of the V-V energy exchange probability for the process



using the vibrational population data of reference (5).

A STEADY STATE SOLUTION FOR VIBRATIONAL POPULATIONS USING THE FAST-FLOW APPROXIMATION

The steady state master equation for the population densities  $N_v$  of the vibrational level  $v$  can be expressed as

$$0 = \frac{d}{dt} N_v = R_v + \sum_{n=1}^{\max} \{A_{v+n,v} + K_{v+n,v}[X]\} N_{v+n} - \left\{ \sum_{n=1}^v [A_{v,v-n} + K_{v,v-n}[X]] + K_w + K_p \right\} N_v \quad (3)$$

The positive term represents the total production rate of the population density into vibrational level  $v$ . The negative term describes the rate of removal of molecules from the vibrational level  $v$ . The notation is as follows:

- $R_v$  is the chemical production rate that produces population in the vibrational level  $v$ .
- $A_{v',v}$  is the spontaneous radiative rate of the transition from  $v'$  to  $v$ .

- $K_{v',v}$  is the collisional deactivation rate at which a molecule is moved from the state  $v'$  to the state  $v$ .
- $[X]$  is the concentration of molecule  $X$  that causes deactivation. Only CO is included in the following analysis.
- $K_w$  is the total rate of deactivation by surface recombination and diffusion.
- $K_p$  is the volumetric pumping rate.

The master equation can be simplified with the following approximations.

- (1) The Fast Flow Approximation

$$K_{v+n,v}[X] + A_{v+n,v} + K_w \ll K_p$$

$$(2) \quad \sum_{n=1} A_{v+n,v} = A_{v+1,v} + A_{v+2,v}$$

$$(3) \quad \sum_{n=1} K_{v+n,v} = K_{v+1,v}$$

$$(4) \quad R_v = \text{constant}$$

The first approximation is valid if the volumetric pumping rate is much faster than the spontaneous radiative rate, the collisional deactivation rate and diffusion rate. The second and the third assumptions imply that the spontaneous radiation is confined in the fundamental and the first overtone emissions and collisional energy transfer is a single quantum exchange process. Further, we assume that the reaction rate is not affected by the addition of another gas.

With these approximations, the steady state master equation without and with cold CO can be written as,

$$0 = \frac{\partial}{\partial t} N_v^0 = R_v + \{A_{v+1,v} + K_{v+1,v} [q]\} N_{v+1}^0 + A_{v+2,v} N_{v+2}^0 - \{A_{v,v-1} + A_{v,v-2} + K_{v,v-1} [q] + K_p + K_w\} N_v^0$$

$$0 = \frac{\partial}{\partial t} N_v = R_v + \{A_{v+1,v} + K_{v+1,v} [Q]\} N_{v+1} + A_{v+2,v} N_{v+2} - \{A_{v,v-1} + A_{v,v-2} + K_{v,v-1} [Q] + K_p + K_w\} N_v$$

where

[q] is the concentration of CO formed in the reaction.

[Q] is the concentration of CO added. [Q] >> [q].

$N_v^0$  is the concentration of vibrational population in level v without additional cold CO.

$N_v$  is the concentration of vibrational population in level v with the additional cold CO.

If we subtract and rearrange the two equations and keep the significant terms, we obtain

$$\left\{ \frac{N_v^0}{N_v} + \frac{A_{v+1,v}}{K_p} \left[ \frac{N_{v+1} - N_{v+1}^0}{N_v} \right] \right\} = 1 + \frac{K_{v+1,v}}{K_p} \left\{ \frac{[q] N_{v+1}^0 - [Q] N_{v+1}}{N_v} \right\} \quad (7)$$

If the left-hand side is plotted against the magnitude of the bracket on the right-hand side using the measured values of  $N_v$  and  $N_v^0$  and the values [Q] of the additional cold CO,  $K_{v+1,v}$  can be determined. The concentration of CO formed in the reaction [q], is determined using the known reaction rate constant and the known concentrations of oxygen and acetylene. It is estimated as  $[q] = 5.4 \times 10^{-10}$  mole/cm<sup>3</sup>. Together with the values of  $K_p$  and  $A_{v+1,v}$ , the values of the brackets in Equation (7) can be determined for each vibrational level v. The results are shown in Figure 3 for the vibrational levels v = 2, 4, and 8. The deactivation rate constant  $K_{v+1,v}$  can be determined from the slope.

The V-V energy transfer probabilities of the process (I) can be determined from the measured values of the de-activation rate constants.

$$P_{v,v-1}^{0,1} + \frac{K_{v,v-1}}{Z_{CO-CO}}$$

The CO-CO collision frequency is calculated to be  $1.86 \times 10^{14} \text{ mole}^{-1} \text{ cm}^{-3} \text{ sec}^{-1}$  at a temperature of 300°K.

Our determinations of  $K_{v,v-1}$  and  $P_{v,v-1}^{0,1}$  are summarized in Table 1. Also shown are the data reported by Hancock and Smith<sup>(2)</sup> from their measurements on the quenching of CO chemiluminescence resulting from the reaction of oxygen and carbon disulfide.

#### CALCULATION OF THE VIBRATIONAL ENERGY TRANSFER PROBABILITIES

The V-V energy transfer probabilities for the process



must be calculated including both long range and short range interaction potentials. In general the V-V energy transfer in CO-CO collisions can be resonant or highly non-resonant depending on the energy levels involved. No single theory can adequately explain the energy transfer mechanism. The short range interaction from the molecular repulsive potential has been treated by Rapp et al.<sup>(7)</sup> and the long range interaction due to molecular multipole moments has been treated by Sharma and Brau<sup>(6)</sup>. Detailed calculations including both contributions to the transition probability have been reported by Jeffers and Kelly<sup>(8)</sup> and by Caledonia and Center<sup>(9)</sup>.

Figure 4 shows the measured V-V exchange probabilities compared to our calculated values based on the formulation of Caledonia and Center. The experimental data supports the notion that both long and short range interactions must be part of an accurate description of the V-V energy exchange process.

#### DISCUSSION AND CONCLUSION

The "Fast-Flow" approximation used in the determination of V-V energy exchange probabilities results in a substantial simplification of the system of simultaneous equations which describe the steady state

vibrational population distribution. Diffusion and wall deactivation processes can be made insignificant compared to the volumetric pumping rate as can collisional processes other than those of interest. For example under the conditions of the experiment deactivation of vibrationally excited CO by oxygen or helium is estimated to be  $10^4$  times smaller than by the added cold CO. Deactivation by water formed during the combustion of acetylene is difficult to estimate. Since the formation of water probably occurs in a reaction step subsequent to the primary steps leading to CO\* it appears likely that V-V and to some extent V-T equilibration will take place before the appearance of a substantial amount of water.

Knowledge of the time development of the vibrational populations, particularly a population inversion, is critical for the application of this reaction in a chemical laser. A time-dependent solution of the kinetic equations of the vibrational populations has been carried out and will be discussed in another paper<sup>(10)</sup>. The solution includes all single vibrational quantum exchange collisions between levels  $v = 0$  to  $v = 14$ , V-T and spontaneous radiative processes. The computation agrees with the data of reference (5) that under the conditions of the experiment 0.2 Torr added cold CO can give rise to a total vibrational population inversion while 0.1 Torr added cold CO can increase local vibrational temperatures but fails to produce an inversion. The computation also indicates that for the CS<sub>2</sub>-O system a substantial amount of CO in the  $v = 0$  level is required in addition to the initial distributions reported<sup>(2)</sup> <sup>(11)</sup> in order to approximate the observed time dependence of the distributions for this system<sup>(11)</sup>.

REFERENCES

- (1) Polanyi, J.C., J. Chem. Phys. 34, 347, 1961.
- (2) Hancock, G., and Smith I.W.M., App. Opt. 10, 1827, 1971.
- (3) Clough, P.N., Schwartz, S.E. and Thrush, B.A., Proc. Roy. Soc. London, A 317, 575, 1970.
- (4) Kari, G., Kruss, P., and Polanyi, J.C., J. Chem. Phys. 46, 224, 1967.
- (5) Liu, Y.S., McFarlane, R.A. and Wolga, G.J., Chem. Phys. Letter 14, 559, 1972.
- (6) Sharma, R.D. and Brau, C.A., J. Chem. Phys. 50, 924, 1969.
- (7) Rapp, D. and Englander-Gordon, P., J. Chem. Phys. 40, 573, 1964.
- (8) Jeffers, W.Q. and Kelly, J.D., J. Chem. Phys. 55, 4433, 1971.
- (9) Caledonia, G.E. and Center, R.E., AVCO Research Report 364, September 1971.
- (10) Liu, Y.S. , McFarlane, R.A., and Wolga, G.J. (in preparation).
- (11) Tsuchiya, S., Nielsen, N. and Bauer, S.H., Third Conference on Chemical and Molecular Lasers, St. Louis, Mo., May 1-3, 1972.

FIGURE CAPTIONS

FIGURE 1 CO first overtone spectrum showing the effect of adding cold CO.

FIGURE 2 A schematic diagram of the experimental setup.

TABLE 1. V-V energy transfer probabilities  $P_{v,v-1}^{0,1}$  and the values of the de-activation rate constants  $K_{v,v-1}$  of CO-CO collisions.

FIGURE 3 Determination of the de-activation rate constant  $K_{v,v-1}$ .

FIGURE 4. Collisional V-V energy transfer probabilities of CO. The measured data is compared with a theoretical calculation which includes both long range and short range interactions at  $T = 300^{\circ}\text{K}$ .

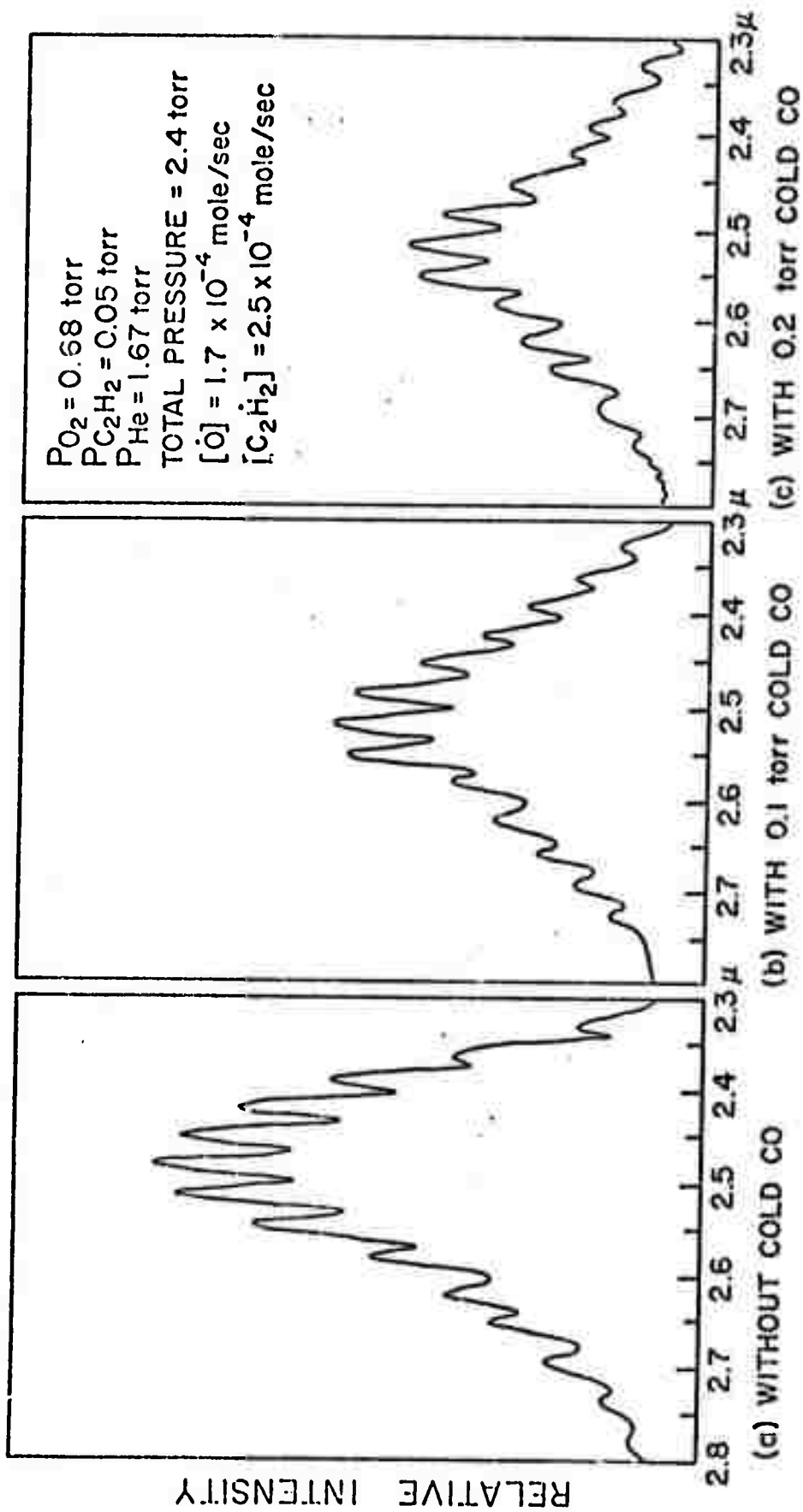


Figure 1X CO FIRST OVERTONE EMISSION SPECTRUM SHOWS THE EFFECT OF ADDING COLD CO

A SCHEMATIC DIAGRAM OF THE EXPERIMENTAL SET UP:

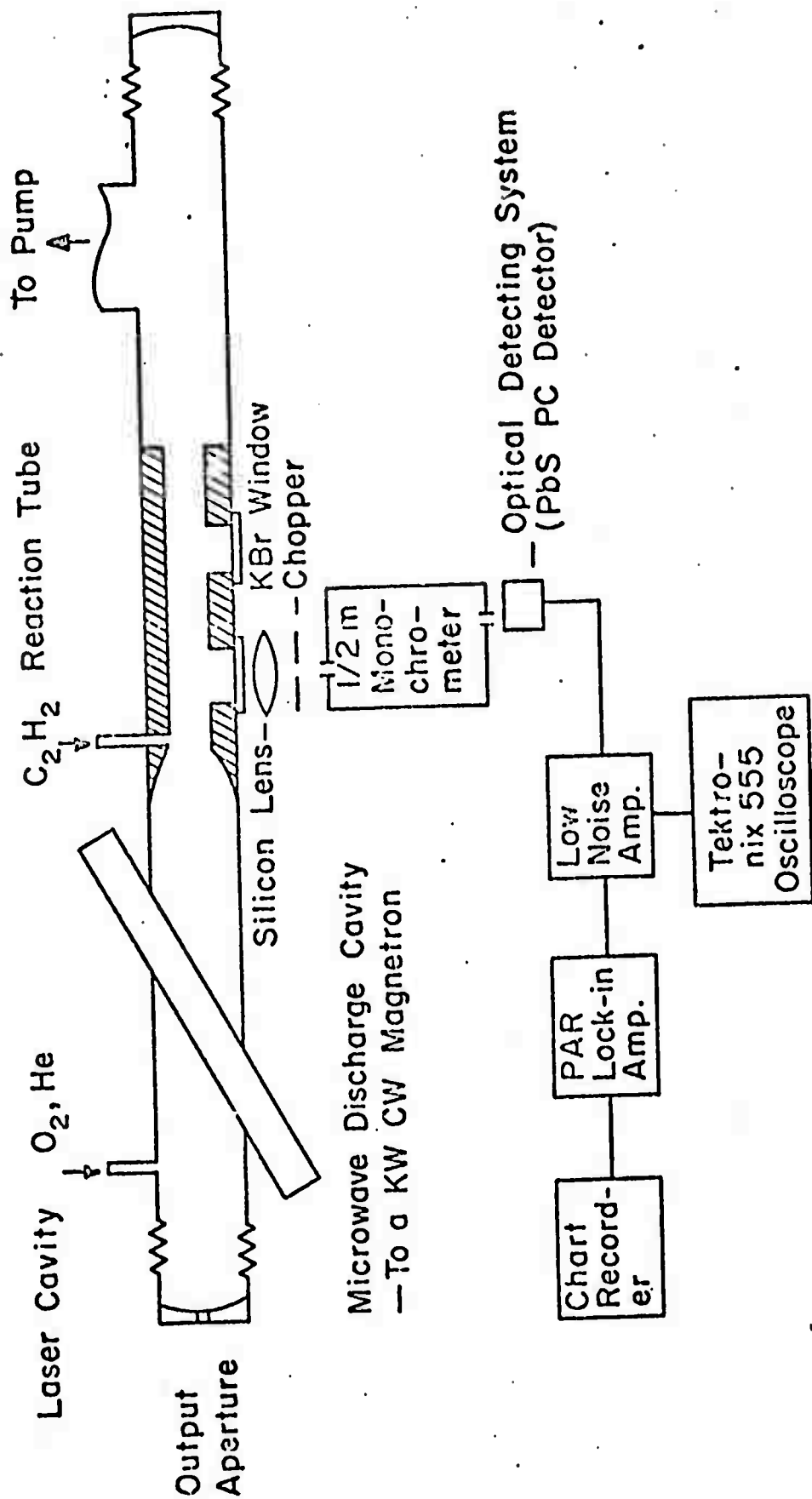


Figure 5.

Table 1

V-V ENERGY TRANSFER PROBABILITIES  $P_{V,V-1}^{0,1}$  AND VALUES OF  
THE DE-ACTIVATION RATE CONSTANTS  $K_{V,V-1}$  OF



RESULTS

VIBRATIONAL LEVEL	PRESENT RESULTS		HANCOCK & SMITH'S <sup>1</sup>	
	$K_{V,V-1}$	$P_{V,V-1}^{0,1}$	$K_{V,V-1}$	$P_{V,V-1}^{0,1}$
3	2.43(-12)	8.5(-3)	-	-
4	1.84(-12)	6.2(-3)	2.0(-12)*	6.7(-3)
5	1.19(-12)	4.0(-3)	1.3(-12)	4.3(-3)
6	8.67(-13)	2.9(-3)	6.3(-13)	2.1(-3)
7	5.2(-13)	1.74(-3)	3.4(-13)	1.15(-3)
8	3.62(-13)	1.21(-3)	1.77(-13)	5.9(-4)
9	2.38(-13)	8.06(-4)	1.13(-13)	3.8(-4)

<sup>1</sup> G. HANCOCK & I.W.M. SMITH, APPL. OPT., 10, 1827, 1971

\* 2.0(-12) =  $2.0 \times 10^{-12} \text{ cm}^3 - \text{MOLECULE}^{-1} - \text{SEC}^{-1}$

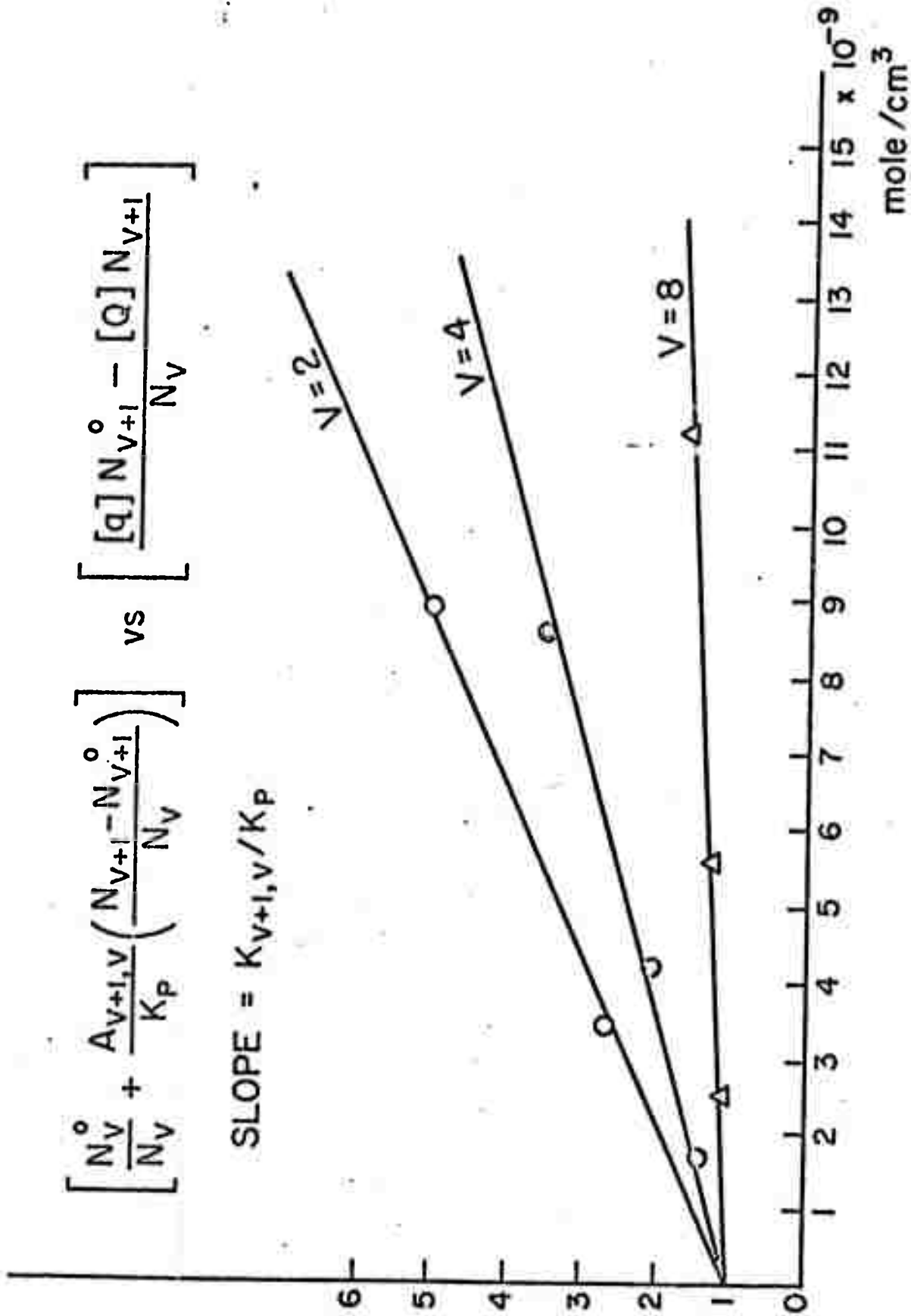


Figure 3 DETERMINATION OF  $K_{V+1,V}$

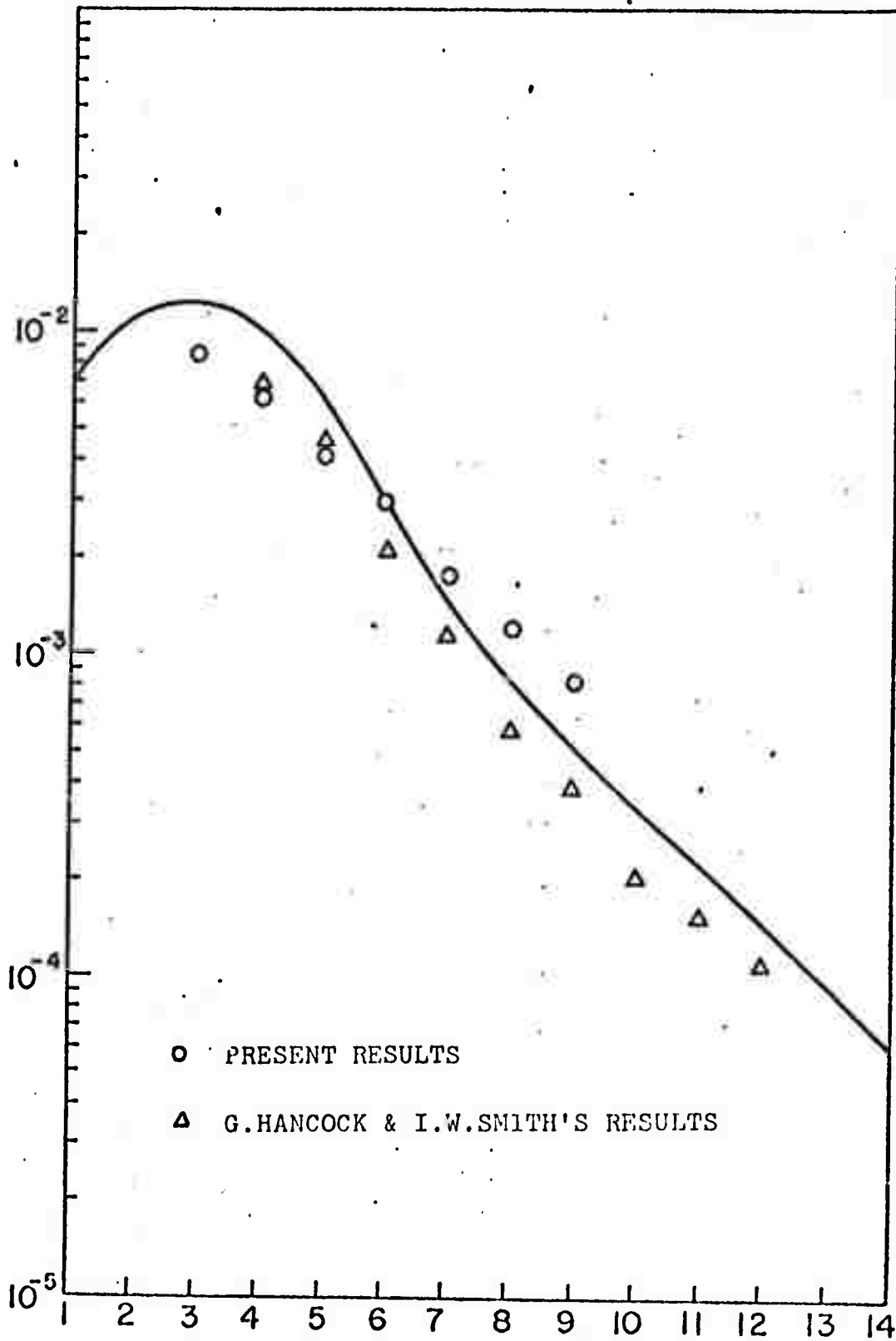


Figure 4 COLLISIONAL V-V ENERGY TRANSFER PROBABILITIES OF CO.  
THE SOLID LINE IS THE THEORETICAL CALCULATION INCLUDING  
BOTH LONG RANGE AND SHORT RANGE INTERACTIONS AT  $T = 300^{\circ}\text{K}$

**A Study of the Dynamic Behavior of the Vibrational  
Population Relaxation in Carbon Monoxide**

by

**Yung S. Liu\***

**Department of Applied Physics and  
Materials Science Center  
Cornell University, Ithaca, NY 14850**

and

**R. A. McFarlane and G. J. Wolga  
School of Electrical Engineering and  
Materials Science Center  
Cornell University, Ithaca, NY 14850**

---

\* Now at General Electric Research and Development Center,  
Schenectady, NY 12301.

Research supported by the Advanced Research Projects Agency and  
Monitored by ONR under Contract N00014-67-A-0077-00006, and  
also through the Materials Science Center, Cornell University.

ABSTRACT

The dynamic behavior of a relaxing CO-He mixture has been studied. The time evolution of the non-equilibrium vibrational population distribution was obtained by numerically integrating the master equations for the vibrational population including Vibrational-Vibrational, (V-V), Vibrational-Translational, (V-T), and the spontaneous decay processes. The result shows the characteristic relaxation through the V-V energy transfer of an anharmonic molecule. The results show good agreement with the experimental data from chemiluminescence experiments in the following two reactions  
(i)  $O + C_2H_2 \rightarrow CO^* + CH_2 + 51 \text{ Kcal/mole}$ ;  $O + CH_2 \rightarrow CO^* + 2H + 71 \text{ Kcal/mole}$ ; and (ii)  $O + CS_2 \rightarrow CO + CS$ ,  $O + CS \rightarrow CO + S + 75 \text{ Kcal/mole}$ .

## INTRODUCTION:

Studies of the vibrational energy distribution of an anharmonic molecule in non-equilibrium states have received increasing attention in recent years. This is true not only because of the relative simplicity of the system for the study of the relaxation mechanisms in a diatomic molecule, but also because of its importance of the understanding of the molecular kinetics in a chemical or molecular laser system, and for the improvement of the performance of such laser systems.

Recently, the I. R. chemiluminescence method has been successfully applied to study the vibrational population distribution of the product molecules in exothermic reactions.<sup>(1, 2, 3)</sup> It has been observed that the products are frequently in highly vibrationally excited states following the reaction, and then relax through a rapid V-V energy transfer process. Studies of I. R. chemiluminescence provide information on the vibrational energy distribution at various stages of the relaxation during a kinetic process. However, due to the complexity of the kinetics involved, there has not been a comprehensive study of the dynamic behavior of the vibrational relaxation mechanism in a diatomic molecular system.

## MODELING OF THE RELAXATION PROCESS

In this work, we report a successful modeling scheme for study of the time-dependent behavior of the vibrational energy transfer in a relaxing CO-He mixture. The set of master equations for the vibrational population has been numerically integrated by the Runge-Kutta-Treanor method.<sup>(4)</sup> The time evolution of the vibrational population thus obtained shows good agreement with our data measured experimentally from the I. R. chemiluminescence of the excited CO produced in the exothermic reaction of oxygen with acetylene.<sup>(5)</sup> We have been able both experimentally and computationally to demonstrate that a total inversion of the vibrational population occurs as a consequence of the preferential de-activation of low vibrational levels due to the presence of an excess amount of ground state CO. We have also applied this modeling method to examine the vibrational population data recently

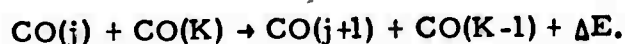
reported by Tsuchiya et al. (6) in a chemiluminescence experiment on a pulse-discharged  $CS_2/O_2/He$  system. The results show a reasonably satisfactory agreement although some discrepancy exists as to the overall relaxation rate. The time-dependent solution of the vibrational population was obtained numerically by solving the set of master equations for the vibrational population including V-V, V-T and the spontaneous radiative process with a given set of the initial populations experimentally determined from chemiluminescence data.

The master equation we have used for the vibrational population of the level V is:

$$\begin{aligned} \frac{\partial}{\partial t} N_K(t) = & Z_{CO-CO} \left\{ \sum_{j=0}^{13} \left[ P_{j+1,j}^{K-1,K} N_{K-1} N_{j+1} - P_{j,j+1}^{K,K-1} N_K N_j \right] \right. \\ & + \sum_{j=1}^{14} \left[ P_{j-1,j}^{K+1,K} N_{K+1} N_{j-1} - P_{j,j-1}^{K,K+1} N_K N_j \right] + N_{CO}(t) \left[ Y_{K-1,K} N_{K-1} \right. \\ & \left. - Y_{K,K-1} N_K + Y_{K+1,K} N_{K+1} - Y_{K,K+1} N_K \right] \left. \right\} + Z_{CO-He} N_{HE} \left[ U_{K-1,K} N_{K-1} \right. \\ & \left. - U_{K,K-1} N_K + U_{K+1,K} N_{K+1} - U_{K,K+1} N_K \right] + A_{K+2,K} N_{K+2} + A_{K+1,K} N_{K+1} \\ & - A_{K,K-1} N_K - A_{K,K-2} N_K, \end{aligned} \quad (1)$$

where  $N_K, N_j$  are the population densities for levels K and j at time t.

$P_{j,j+1}^{K,K-1}$  is the V-V energy transfer probability in the CO-CO collisional process;



This probability was calculated by combining the Sharma-Brau theory<sup>(7)</sup> and that of Rapp<sup>(8)</sup> to include both long-range and short-range interactions. The measured probability has recently been reported<sup>(9,10,11)</sup> by several workers and the results show good agreement with the calculated values thus obtained for the room temperature case.<sup>(12,13)</sup>  $Y_{K,K-1}$  and  $U_{K,K-1}$  are the V-T energy transfer probabilities in CO-CO and CO-He collisions at room temperature, and the values employed were calculated from SSH theory.<sup>(14)</sup>  $Z_{CO-CO}$  and  $Z_{CO-He}$  are the collisional frequencies for CO-CO and CO-He collisions.  $N_{CO}(t)$  is the concentration of CO at time  $t$ .  $N_{He}$  is that of He.  $A_{K,K-1}$  and  $A_{K,K-2}$  are the spontaneous radiative rates of the level K to levels K-1 and K-2 respectively. In the above equation, only a single quantum exchange is included in the V-V exchange process. The set of equations (1) for the vibrational levels  $V = 0$  to  $V = 14$  has been integrated numerically by the Runge-Kutta-Treanor method.<sup>(4)</sup> This numerical integration technique has been widely applied for solving coupled non-linear differential equations such as are found in modeling coupled chemical reactions.

Figure (1) shows the vibrational population distribution of CO\* measured experimentally from the chemiluminescence data from excited CO formed in the oxygen-acetylene reaction.<sup>(5,10)</sup> The vibrational population was determined from the first overtone chemiluminescence spectrum between 2.3 and 2.8 microns by using a computer simulation method first described by Karl, et al.<sup>(15)</sup> A numerical method is used to generate a simulated spectrum to compare with the experimental scans. It takes into account the instrumental sensitivity variation as a function of wavelength, the spectral slit width, the Einstein A coefficient of each upper level and the molecular and spectroscopic constants. The rotational temperature and the relative population of each vibrational level are adjusted to obtain a match between the synthetic spectrum and the experimental scan. More detailed discussion of this procedure was reported previously.<sup>(5)</sup> The figure shows the non-equilibrium relative vibrational population distribution of CO\* at a time approximately 100 microseconds after the injection of the acetylene into the atomic

oxygen stream. The addition of cold CO to the fuel dramatically modified the vibrational distribution. Preferential de-activation of the lower vibrational levels leads to a total inversion of the vibrational population with 0.2 Torr CO added to the acetylene. The data have been plotted taking account of the relative signal levels under different conditions of added cold CO. It is seen from the curve that as a consequence of the anharmonic nature of the molecular potential, the process



has a maximum transfer probability between  $V = 4$  and  $V = 6$  and decreases rapidly at higher values of  $V$ . With the addition of cold CO to the reaction, it has therefore been possible to significantly depress the populations of levels  $V \leq 5$  and produce a vibrational population inversion.

Figure 2(a) shows the calculated time-evolution of the vibrational population model for the conditions shown in Figure 1 in the presence of 0.2 Torr cold CO. The initial vibrational population was taken from the experimental data<sup>(5,16)</sup> and was a nearly-Boltzmann distribution similar to the top curve shown in Figure 1. The system was assumed to be isothermal at a temperature 300°K and no attempt was made to model the mixing mechanism in the flow. The populations are seen to be changing more rapidly for vibrational levels  $V \leq 8$  and a total inversion occurs at a time about 150 microseconds after the collisional relaxation begins. The populations relax through a series of non-Boltzmann distributions with the high vibrational levels over-populated. As the relaxation time reaches 1 millisecond, a Boltzmann distribution appears for level  $V \leq 8$ . This is shown in Figure 2(b).

Figure 3(a) shows the time-evolution of the vibrational population with the same conditions except the added cold CO was changed to 0.1 Torr. It is seen from the curves that the vibrational population changes moderately during the relaxation process but a total inversion does not appear in this case. The population curve corresponding to 162.9  $\mu\text{sec}$  after the start of relaxation shows very good agreement with the curve ( $\Delta$ )

in Figure 1. Figure 3(b) shows the long-time behavior for this case

Figure 4 shows the experimental results of a study of the relative populations of vibrationally excited CO produced in a pulse-discharged  $\text{CS}_2 + \text{O}_2 + \text{He}$  mixture as reported recently by Tsuchiya et al.<sup>(6)</sup> They deduced the relative populations from the chemiluminescence of  $\text{CO}^*$  at selected delay times after the discharge pulse which initiated the reaction and established the time dependence of the population for each level. A modeled time-evolution of the vibrational populations for this case is shown in Figure 5. The two figures show a similarity of the time-dependent behavior of the relative vibrational populations. However, some discrepancies exist. First, the computed relaxation process appears slower than that determined experimentally. Since in our model, only V-V exchange by CO-CO collisions, V-T exchange by CO-CO, and CO-He collisions and the spontaneous radiative decay were considered, any other de-activation processes will speed the relaxation. However, our modeling scheme does provide a method to verify some experimental conditions assumed. Second, in our model, initial populations for the ground level and the first level must be determined by extrapolating from the populations in the adjacent levels assuming that a nearly Boltzmann distribution exists for these low levels. Since it is not possible to determine the population for the lowest level by a chemiluminescence experiment, the question of how these lowest levels are populated in the nascent species in these two types of reaction has not yet been solved. Failure to include a substantial  $V = 0$  population from the  $\text{CS} - \text{O}$  reaction in the calculation resulted in a time development very different from that observed experimentally.

#### DISCUSSION:

Our results for the time-dependent behavior of the vibrational populations have shown a rather satisfactory agreement with the experimental data presently available from chemiluminescence experiments. The model includes V-V and V-T processes and radiative decay in a relaxing CO-He mixture. It is a rather simple one, and the numerical

integration technique we employed is straightforward. The agreement with the experimental data suggests that this modeling scheme is widely applicable to general kinetic problems in other diatomic molecular laser systems. It can be elaborated with more complicated relaxation mechanisms, namely, multiquantum vibrational exchange, chemical reactions, fluid mixing, and stimulated emission to model the kinetics of a transverse-flow chemical laser system which is of particular current interest.

ACKNOWLEDGMENT:

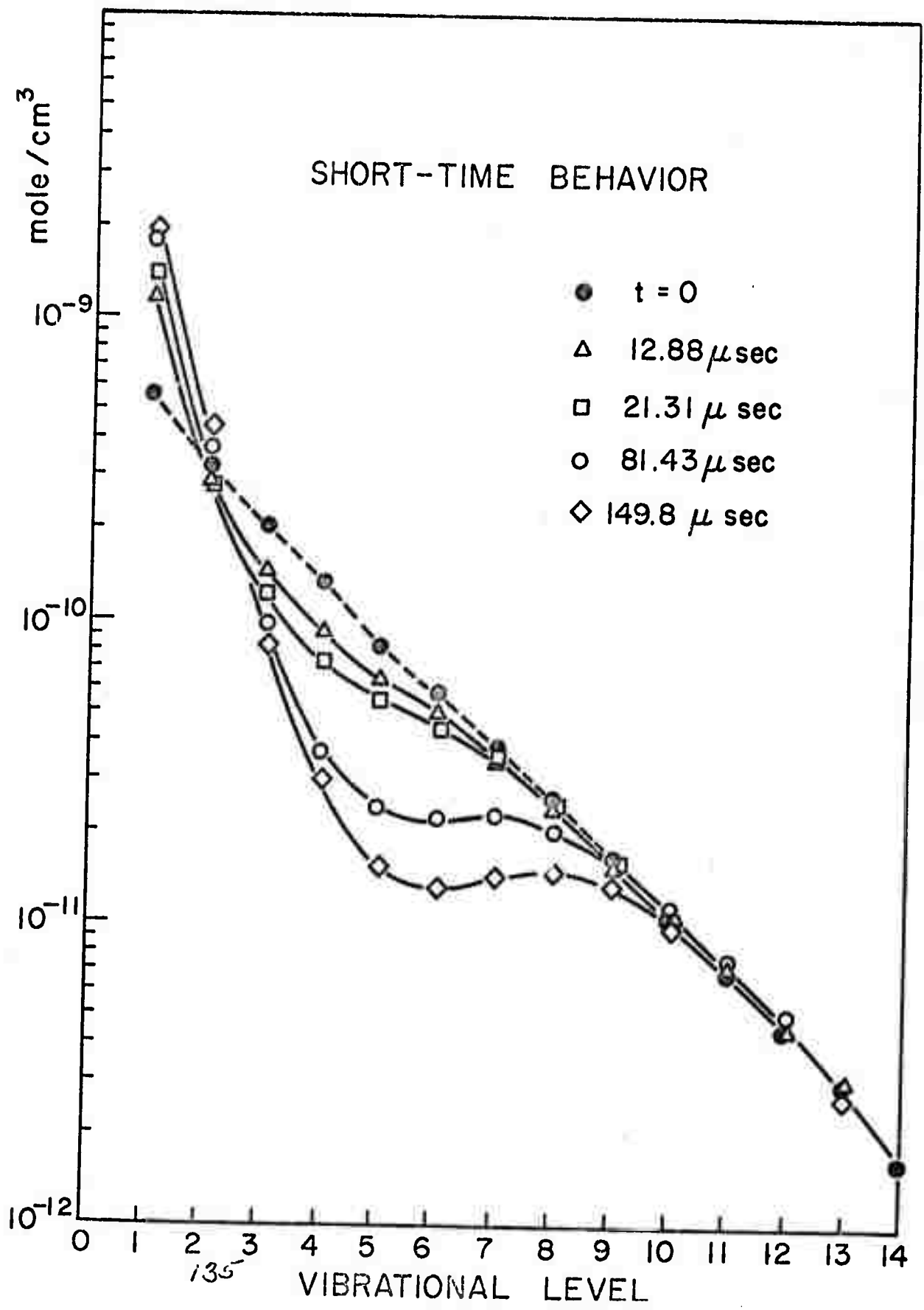
The authors wish to thank Dr. S. H. Bauer for providing the experimental data of the time-dependent vibrational population of CO\* produced in a pulse-discharged CS<sub>2</sub>+O<sub>2</sub>+ He mixture. We wish to thank Dr. D. Edelson of the Bell Telephone Laboratories for valuable discussions on the numerical integration problem. The program was initially provided by D. Cameron, and his able assistance is also acknowledged.

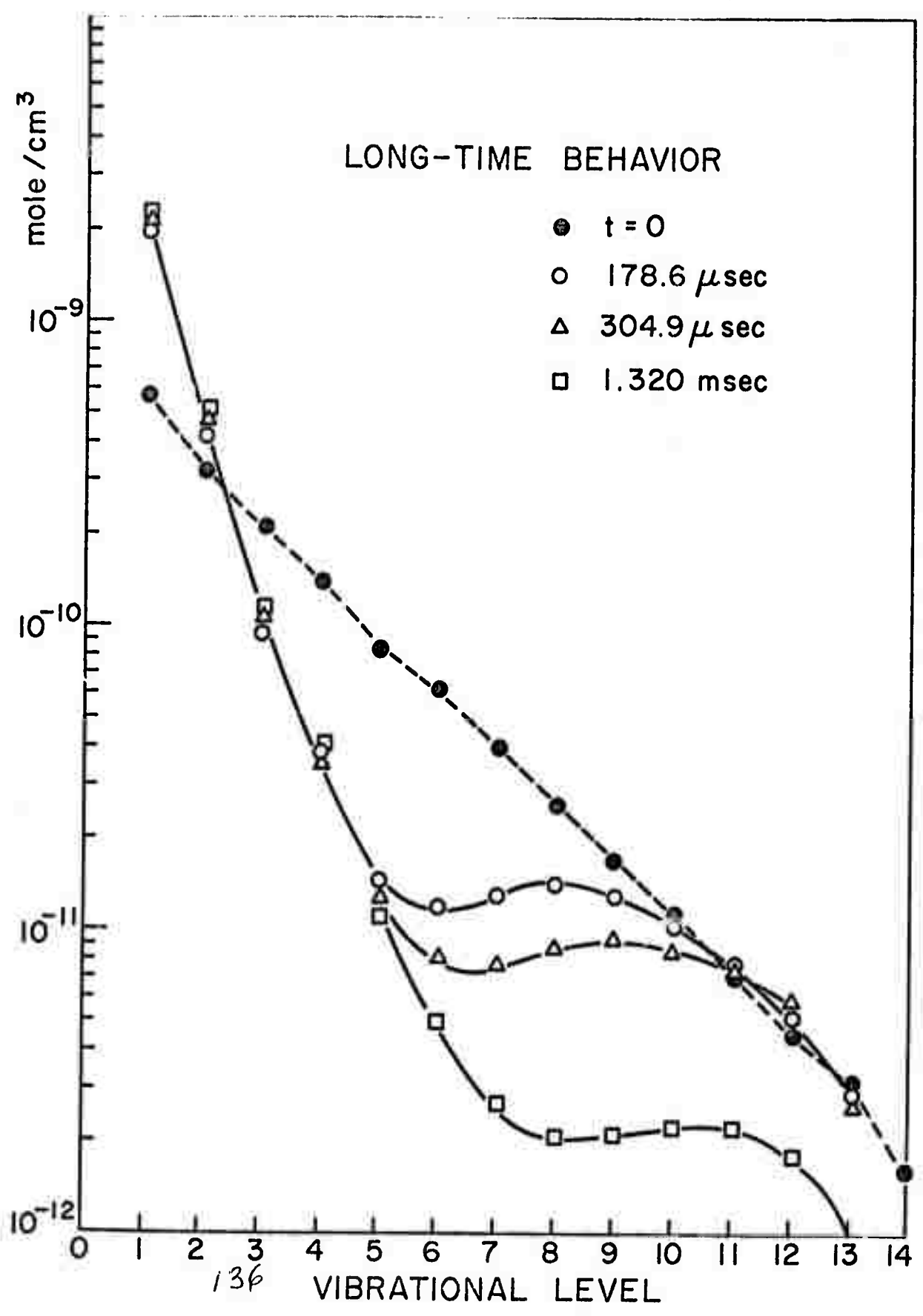
REFERENCES:

1. Polanyi, J.C., J. Chem. Phy. 31, 1388, 1959.
2. Polanyi, J.C., and Charters, P.E., Dis. Faraday. Soc., 33, 107, 1962.
3. Polanyi, J.C., App. Opt. 10, 1717, 1971.
4. Treanor, C.E., Cornell Aeronautical Lab. Report No. AG-1729-A-4, 1964.
5. Liu, Y.S., McFarlane, R.A., and Wolga, G.J., Chem. Phys. Letters 14, 559, 1972.
6. Tsuchiya, S., Nielson, N., and Bauer, S.H. - to be published.
7. Sharma, R.D. and Brau, C.A., J. Chem. Phys. 50, 924, 1969.
8. Rapp, D. and Englander-Gordon, P., J. Chem. Phys. 40, 573, 1964.
9. Liu, Y.S., McFarlane, R.A. and Wolga, G.J., presented to 3rd Conference on Chemical and Molecular Lasers, St. Louis, U.S.A. 1972.
10. Liu, Y.S., McFarlane, R.A. and Wolga, G.J. - to be published.
11. Hancock, G. and Smith, I.W.M., App. Opt. 10, 1827, 1971.
12. Jeffers, W.Q. and Kelly, J.D., J. Chem. Phys. 55, 4433, 1971.
13. Liu, Y.S., Ph.D. Thesis, Cornell University, 1972.
14. Schwartz, R.N., Slawsky, Z. and Herzfeld, K., J. Chem. Phys. 20, 1951, 1952.
15. Karl, G., Kruss, P. and Polanyi, J.C., J. Chem. Phys. 46, 224, 1967.
16. Creek, D.M., Melliar-Smith, C.M. and Jonathan, N., J. Chem. Soc. (A) 646, 1970.

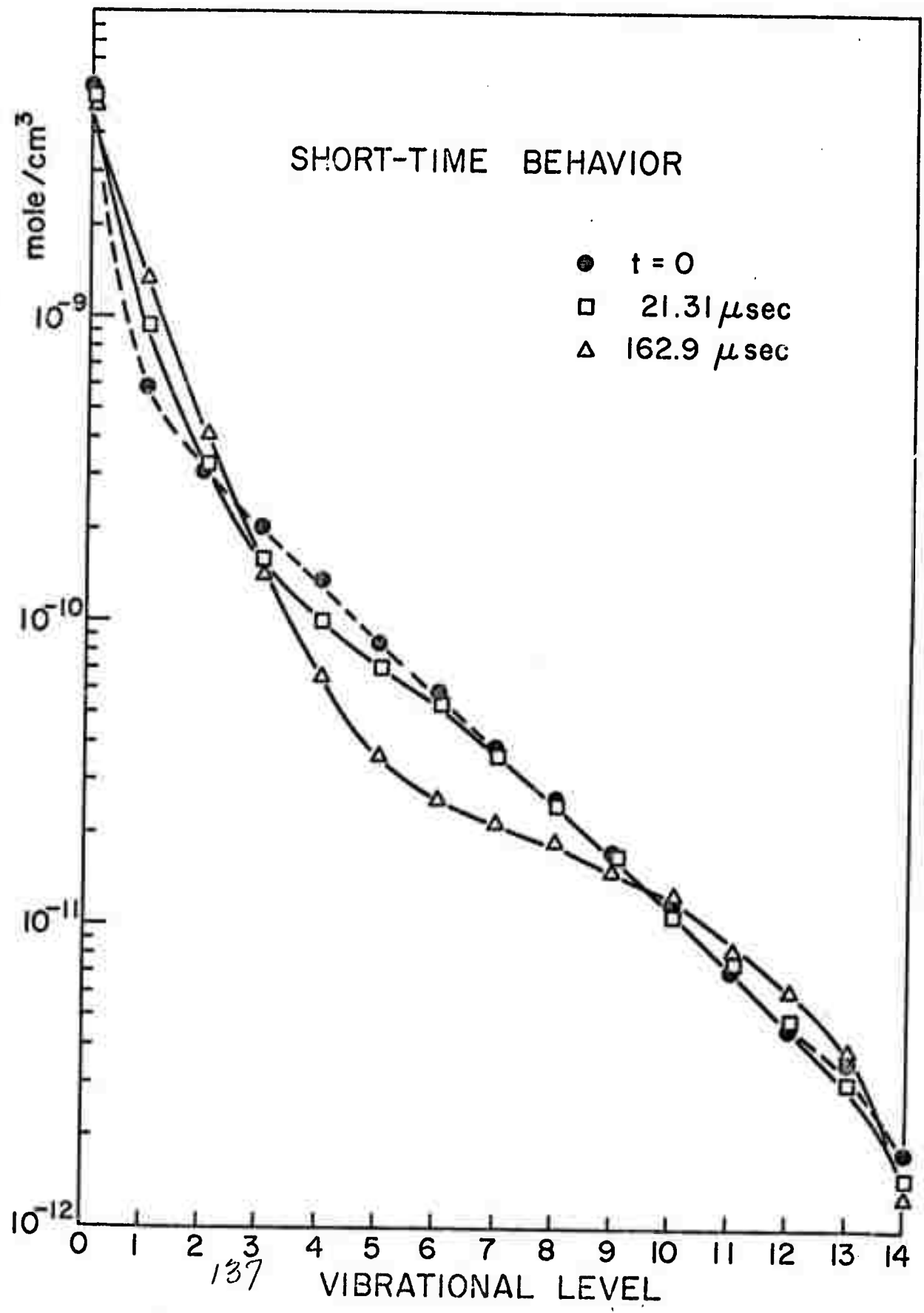
FIGURE CAPTIONS:

- FIGURE 1      Relative vibrational population distribution of CO\*.  
Pressures: C<sub>2</sub>H<sub>2</sub> 0.05 Torr, O<sub>2</sub> 0.68 Torr. He 1.67 Torr. Temperature T<sub>rot</sub> = 300°K. [C<sub>2</sub>H<sub>2</sub>·] = 0.25 x 10<sup>-4</sup> mole/sec. [O·] = 1.7 x 10<sup>-4</sup> mole/sec. o without additional cold CO. □ 0.05 Torr additional cold CO. Δ 0.1 Torr additional cold CO. ● 0.2 Torr additional cold CO.
- FIGURE 2(a)    The time evolution of the vibrational population of a relaxing CO-He mixture in the presence of 0.2 Torr cold CO. The partial pressure of He is 1.70 Torr; that of CO is 0.25 Torr. T = 300°K. The calculation includes V-V, V-T and radiative decay processes.
- FIGURE 2(b)    The long-time behavior of 2(a).
- FIGURE 3(a)    The time evolution of the vibrational population of a relaxing CO-He mixture in the presence of 0.1 Torr cold CO. The partial pressure of He is 1.70 Torr; that of CO is 0.15 Torr. T = 300°K. The calculation includes V-V, V-T and radiative decay processes.
- FIGURE (b)    The long-time behavior of 3(a).
- FIGURE 4      Vibration population distribution of CO\* produced in pulsed-discharged CS<sub>2</sub> + O<sub>2</sub> + He mixtures. The time-dependence of the population is determined by the delay time. The partial pressure of CS<sub>2</sub> is 0.045 Torr; that of O<sub>2</sub> is 0.76 Torr and He is 3.0 Torr. 15 KV discharge. Data taken from Tsuchiya, et al. (6)
- FIGURE 5.      Calculated time-evolution of the vibrational populations for the experiment of Figure 4.

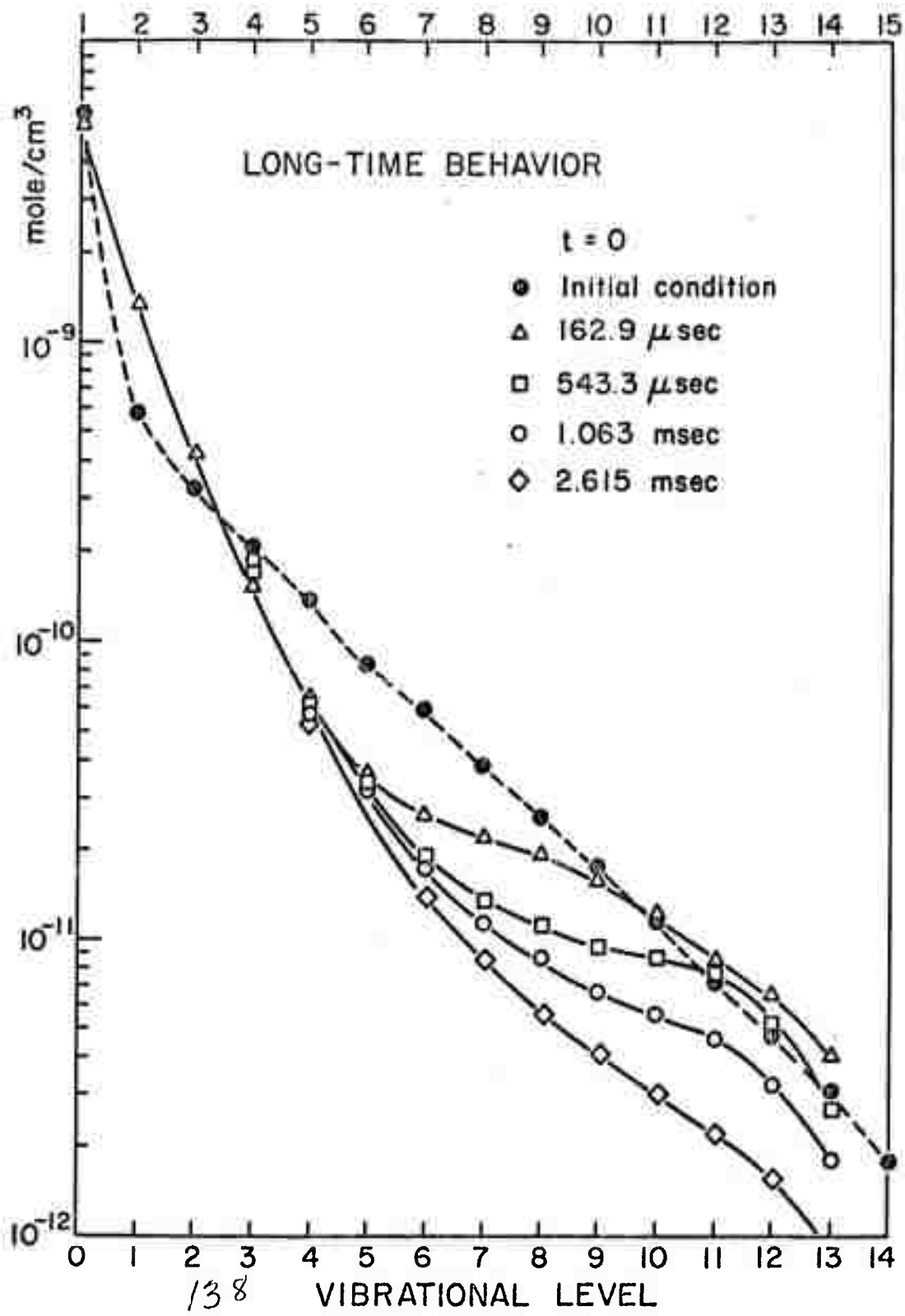


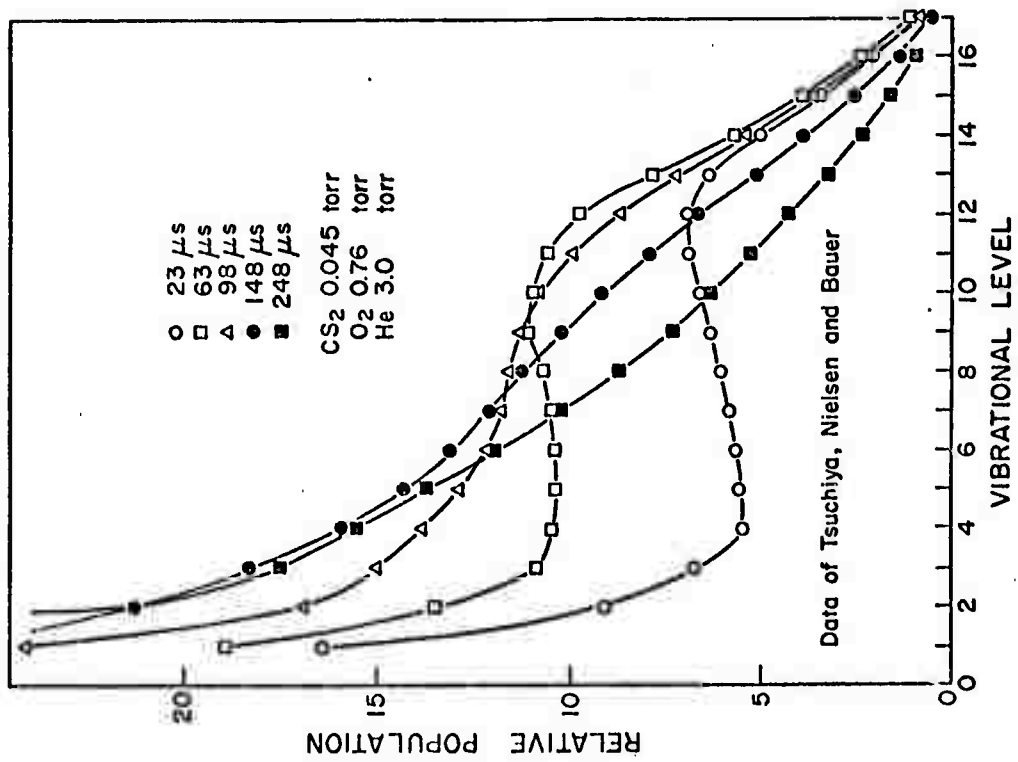
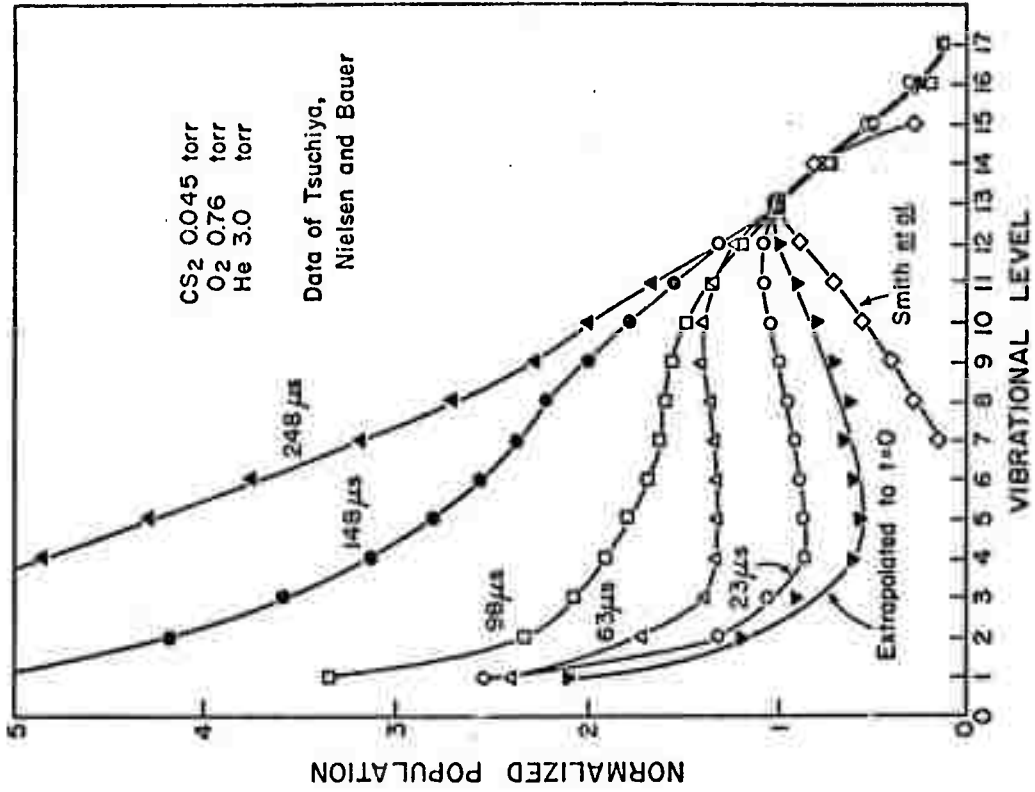


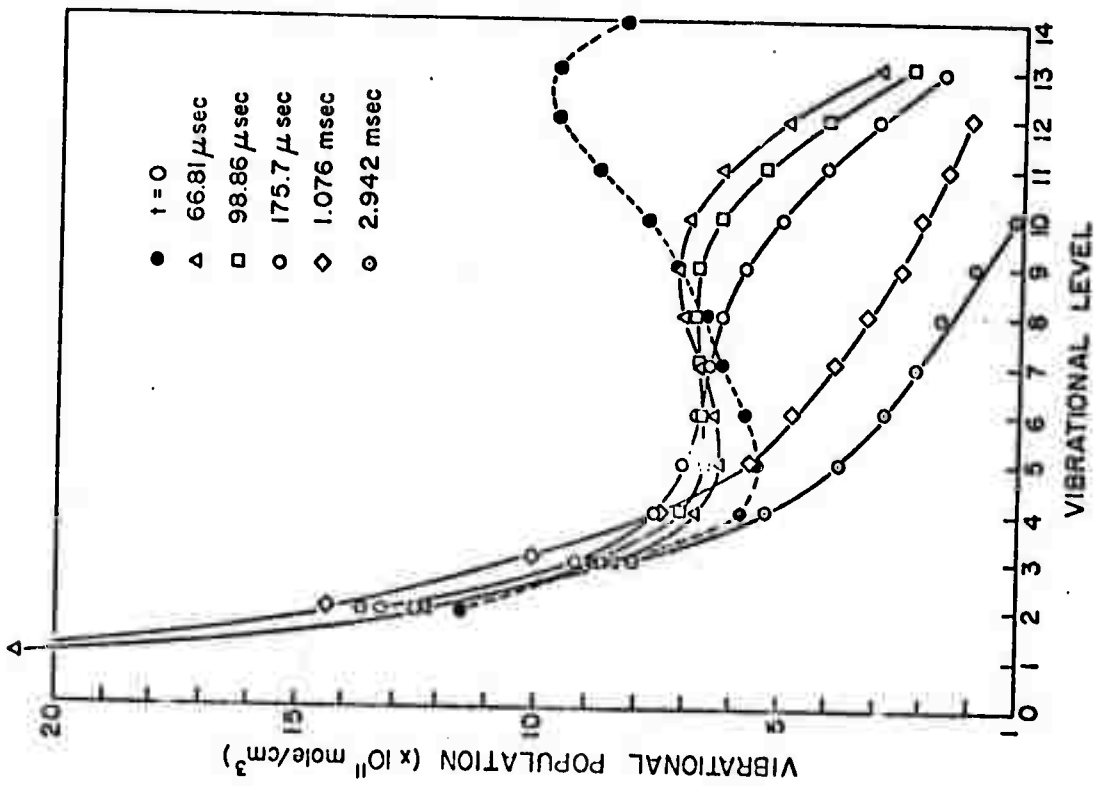
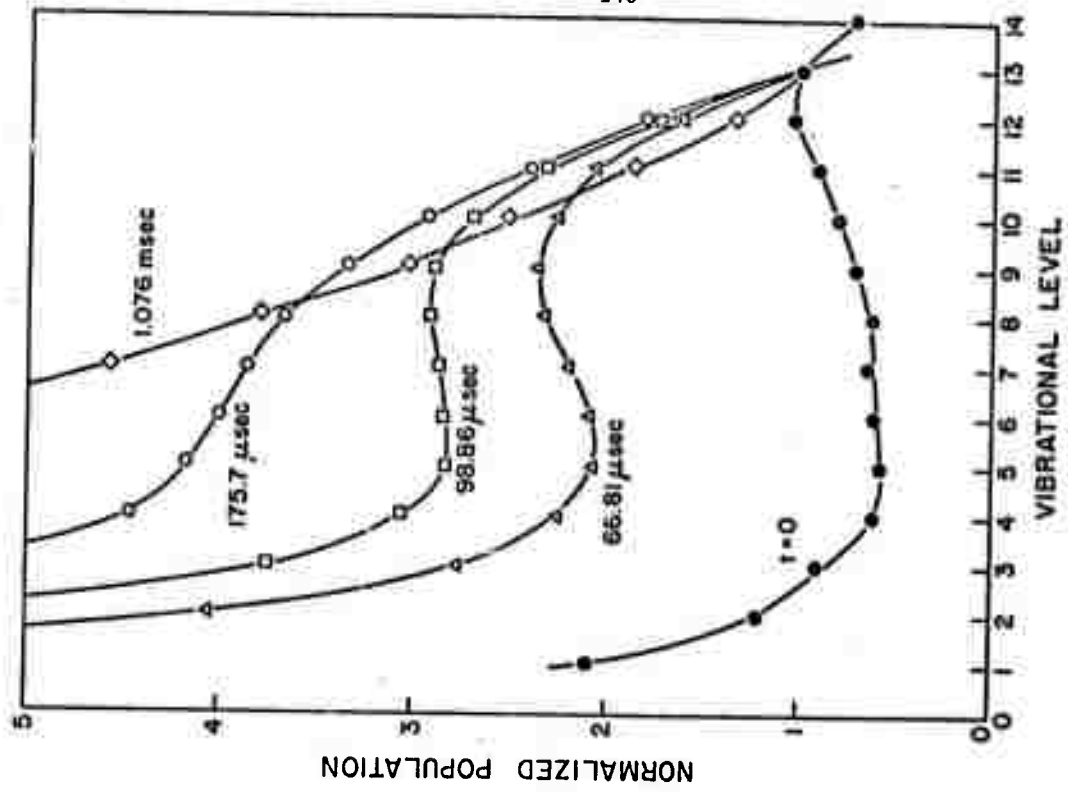
136



137



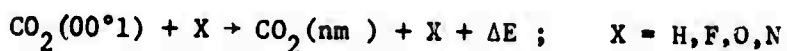
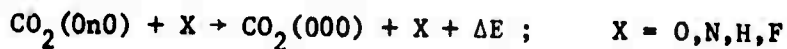
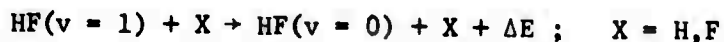




V. Molecular Relaxation via Atomic Collisions

Three studies are currently in progress to measure atomic collision induced vibrational relaxation in important molecular laser systems.

The collisional processes being studied are:



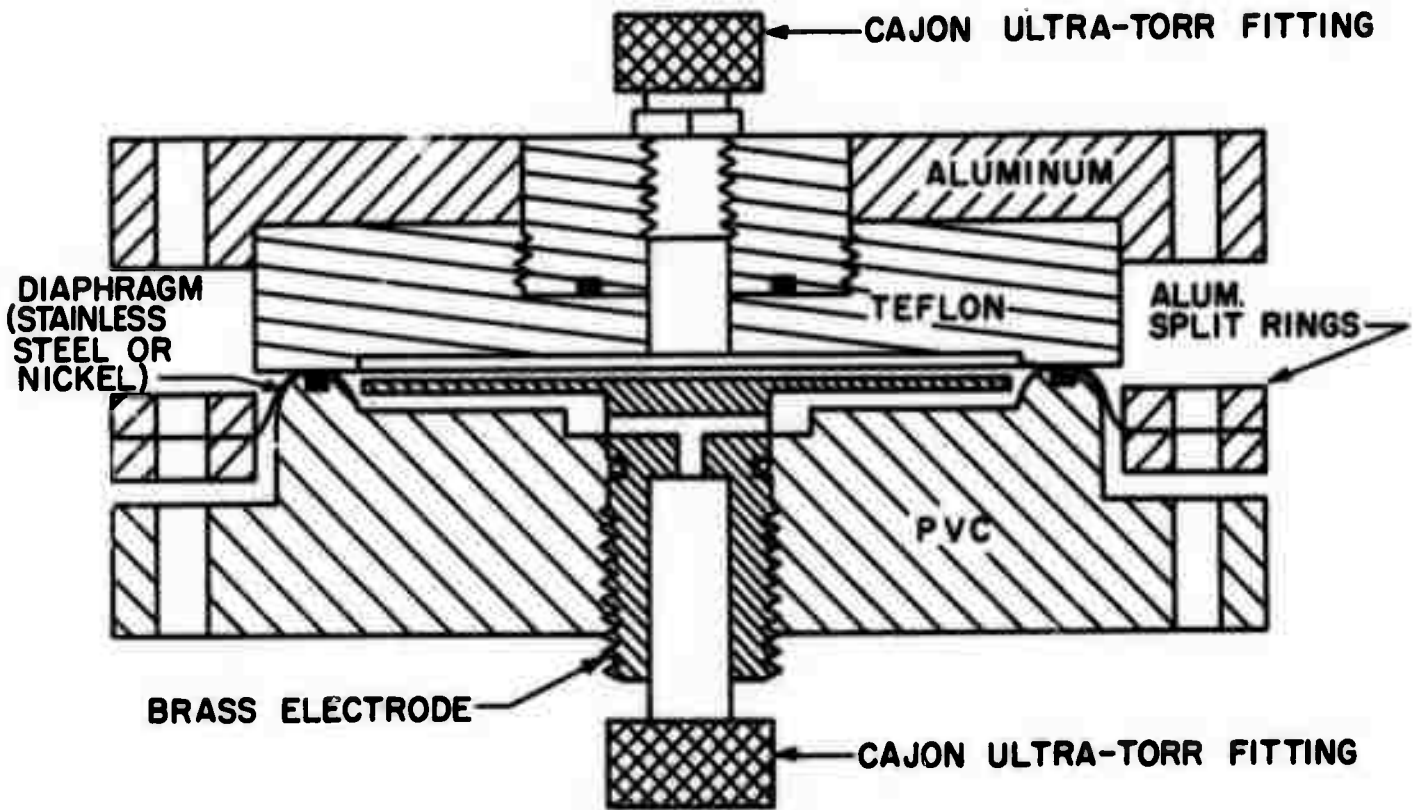
A. Atomic Relaxation of HF(v = 1) (G. J. Wolga)

At the time of submission of our Semi-Annual Report for 1972 we discussed the status of this experiment. In this report we shall complete the description of the experiment which is now in progress.

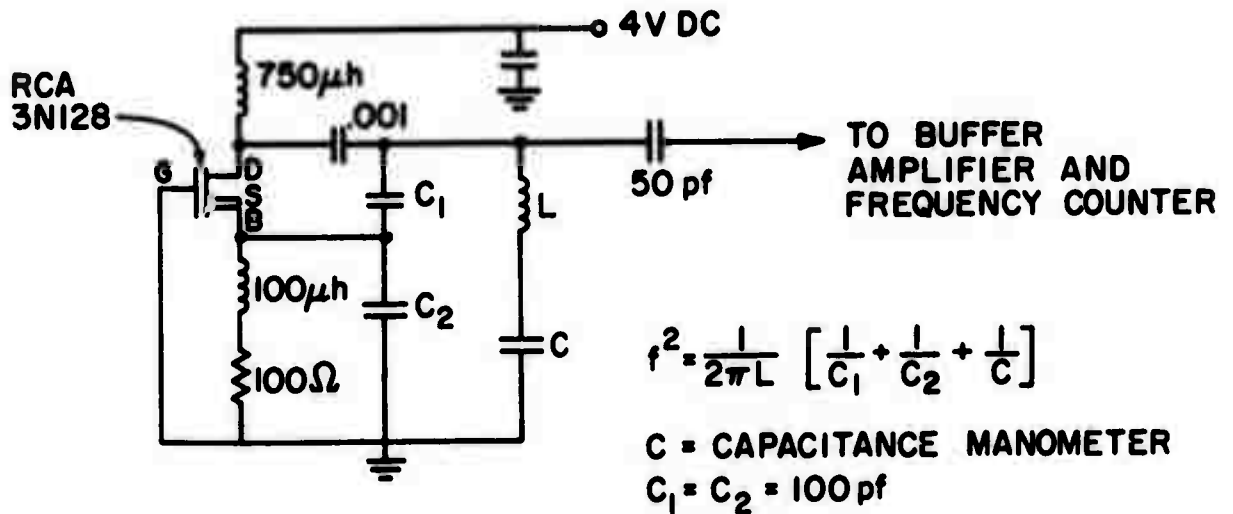
The capacitance diaphragm pressure gauge has proven to be very useful and reliable. In the following figures we show a schematic drawing of the gauge and typical calibration runs. The gauge is constructed from materials (Teflon, PVC, Monel) that are corrosion resistant and no difficulty is anticipated in applying it to our work with HF, F<sub>2</sub>, etc.

The HF, v = 1 → 0 pump laser was redesigned and significantly improved. We now obtain approximately 20-30 milli joules/pulse on the v = 1 → 0 transition. This will be more than adequate for our experimental needs.

The fluorescence cell was designed and constructed. A schematic drawing of the cell is attached as a figure. The cell design stressed use of construction materials that could withstand the corrosive gases and maintenance of a good filling factor for the pump radiation and good optical coupling for



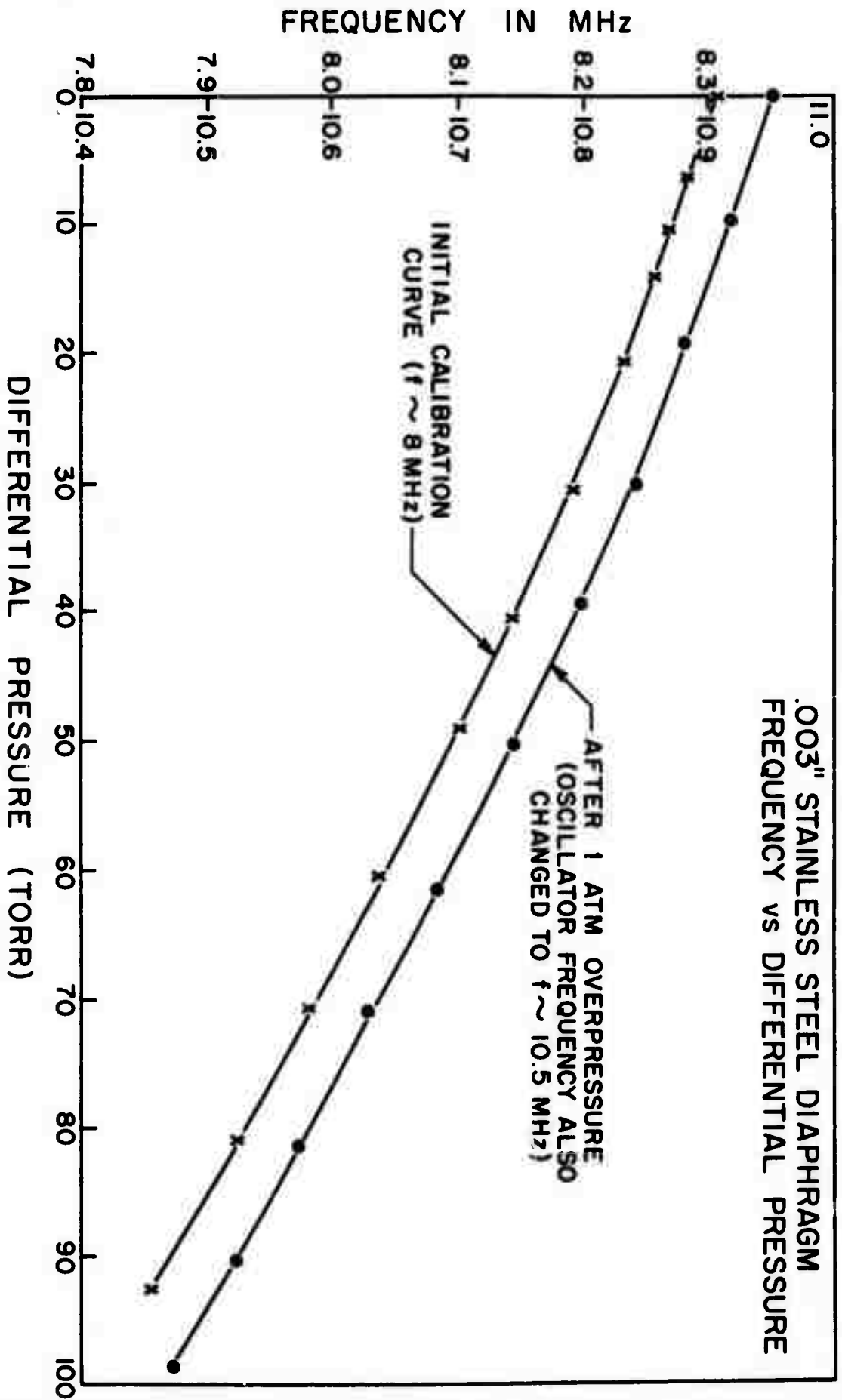
CAPACITANCE MANOMETER

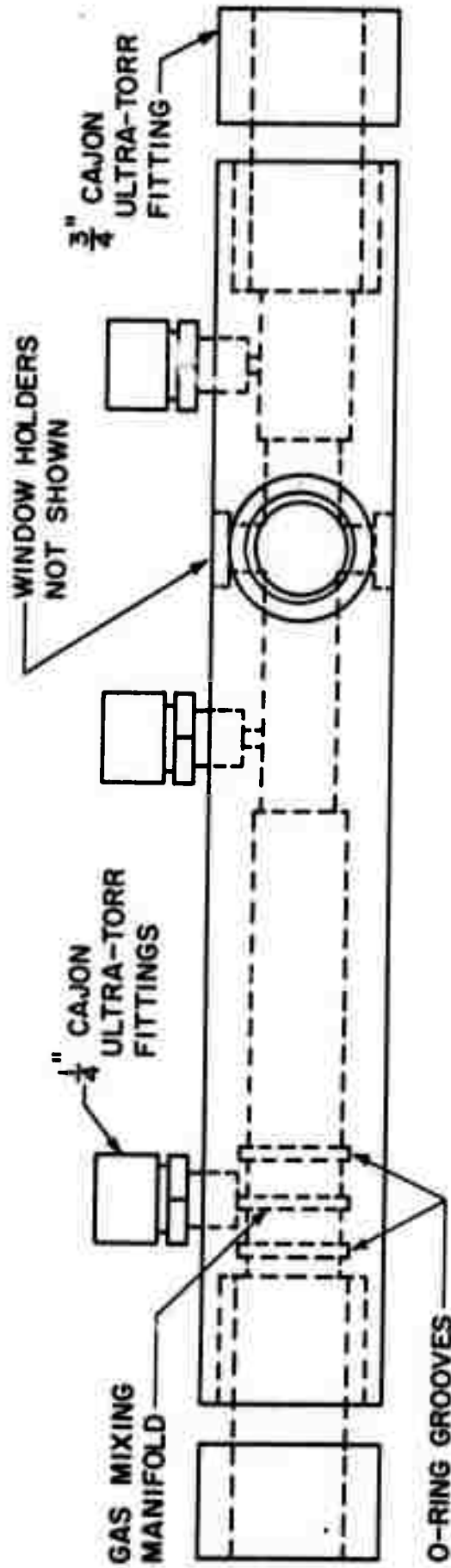


$$f^2 = \frac{1}{2\pi L} \left[ \frac{1}{C_1} + \frac{1}{C_2} + \frac{1}{C} \right]$$

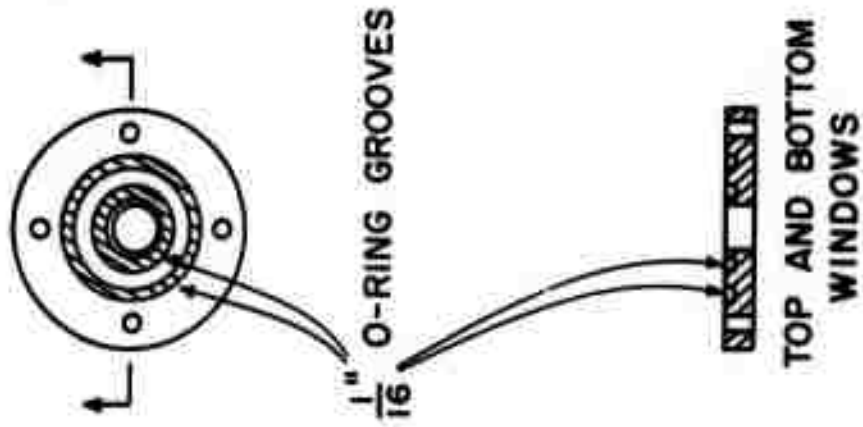
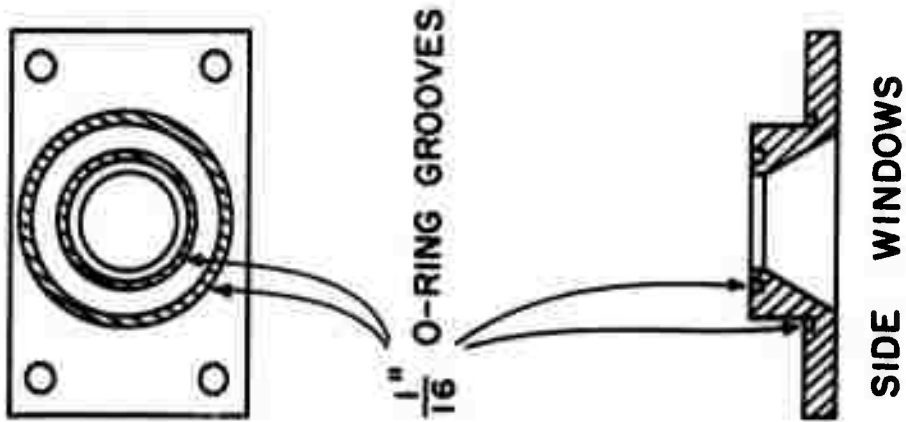
C = CAPACITANCE MANOMETER  
C<sub>1</sub> = C<sub>2</sub> = 100 pf

CLAPP OSCILLATOR





MONEL FLUORESCENCE CELL  
(to scale)



WINDOW HOLDERS (to scale)

detection of fluorescence.

We have made studies of the atom wall recombination rate for H atoms in our flow system. Knowledge of this loss mode for H is essential to the quantitative studies we have undertaken.

At the time of preparation of this report, experiments studying the process  $\text{HF}(v = 1) + \text{H} \rightarrow \text{HF}(v = 0) + \text{H} + \Delta E$  were in progress.

B. Atomic Relaxation of  $\text{CO}_2(0n0)$  (S. H. Bauer)

Construction of a high power TEA  $\text{CO}_2$  laser is nearly completed. We plan to use this unit for simultaneous irradiation of  $\text{CO}_2$ -M mixtures with 4.2  $\mu\text{m}$  (HBr laser) and 10.6 or 9.6  $\mu\text{m}$  ( $\text{CO}_2$  laser) pulses in order to obtain (concurrently) substantial populations of  $\text{CO}_2$  molecules in the  $(00^01)$  and  $(02^00)$  or  $(10^00)$  states and to measure the fluorescence lifetimes at 4.2  $\mu\text{m}$  and 15.5-16.5  $\mu\text{m}$ . These decay times will permit us to obtain transition probabilities for the various collisional vibrational deexcitation steps, at selected cell temperatures, with specified colliders (M). Indeed, we anticipate eventually to go over to flow cells for measuring the relative efficiencies of atomic relaxers.

C. Atomic Relaxation of  $\text{CO}_2(00^01)$  (G. J. Wolga)

A parallel experiment to that of part A has been set up to study the process  $\text{CO}_2(00^01) + \text{X} \rightarrow \text{CO}_2(nm) + \text{X} + \Delta E$ ;  $\text{X} = \text{H}, \text{F}, \text{O}, \text{N}$ . A second EPR apparatus for measuring atom concentrations is in operation. The pump laser for the laser induced fluorescence studies will be shared with the HF deactivation experiment except that it will be operated as an HBr chemical